Real-Time Monitoring and Robust Control of Offshore De-oiling Processes

Durdevic, Petar

Publication date:
2017

Document Version
Publisher's PDF, also known as Version of record

REAL-TIME MONITORING AND ROBUST CONTROL OF OFFSHORE DE-OILING PROCESSES

BY
PETAR DURDEVIC LØHNDORF

DISSERTATION SUBMITTED 2017

AALBORG UNIVERSITY
DENMARK

Real-Time Monitoring and Robust Control of Offshore De-oiling Processes

Ph.D. Dissertation
Petar Durdevic Løhndorf

Dissertation submitted March 22, 2017

Dissertation submitted: March 22, 2017

PhD supervisor: Assoc. Prof. Zhenyu Yang
Aalborg University

PhD committee: Professor (mso) Henrik C. Pedersen (chairman)
Aalborg University

Emeritus Prof. Morten Lind
Technical University of Denmark

Dr. Ming Yang
Environmental Consultancy Services Manager NEL

PhD Series: Faculty of Engineering and Science, Aalborg University

ISSN (online): 2446-1636
ISBN (online): 978-87-7112-930-4

Published by:
Aalborg University Press
Skjernvej 4A, 2nd floor
DK – 9220 Aalborg Ø
Phone: +45 99407140
aauf@forlag.aau.dk
forlag.aau.dk

Printed in Denmark by Rosendahls, 2017

Abstract

De-oiling facilities in the offshore Oil and Gas industry are vital in ensuring reduced discharge of oil into the ocean, where in addition to fulfilling regulatory requirements they minimize oceanic pollution. Several aspects of the de-oiling facilities have been investigated in this Ph.D. study, aiming to improve the current systems efficiency.

At present, de-oiling efficiency is neither measured continuously nor is it in real-time in offshore installations and thereby a major part of this work was to investigate this aspect. A reliable real-time and on-line efficiency measurement, could provide a strong basis for evaluating the performance of the de-oiling system and could pave the way to improvements in its performance. Efficiency measurement would also aid in understanding the effect of different operating conditions on the de-oiling process, an understanding of which would help in improving the current control strategies.

After an initial survey of several monitoring technologies and the evaluation of three selected technologies, a fluorescence based Oil in Water (OiW) monitor was eventually employed to measure the oil concentrations on the inlet and the outlet of the de-oiling hydrocyclone. The efficiency of the hydrocyclone was thereby calculated based on these on-line measurements, and the dynamic changes in the efficiency under varied operating conditions were observed. These experiments on monitoring also revealed that the efficiency depended more on the inlet flow rate than on the pressure drop ratio (PDR), which is the basis for current control solutions.

Clearly, it is useful to develop a model of the system that is under consideration to facilitate the design of advanced controllers. However, until now there has been limited work in control oriented models and modelling methods of the de-oiling hydrocyclone. This challenge was thus another focus of this Ph.D. study. By regarding the PDR of the de-oiling hydrocyclone as the system output and the opening degree of the control valves as the system input, a set of linear system models were obtained using black-box system identification techniques. A scaled pilot plant was used to acquire the data used for the model estimation. Furthermore by coupling this hydrocyclone model with the upstream three phase gravity separator model, a MIMO

structured model was obtained for the entire de-oiling process. By limiting the entire de-oiling process nearby an operating point, a linear MIMO process model could be obtained and it served as the primary model for control design.

A robust control solution using H_∞ control design is proposed in this work, with two objectives; to increase the system's robustness with respect to disturbances and secondly to handle the coupling of system's dynamics. The H_∞ control solution that was developed was implemented onto the scaled pilot plant and its performance was compared to a benchmark PID control solution. The H_∞ control solution had a improved performance in terms of robustness towards disturbances, and demonstrated a superior performance in handling the influence of severe fluctuating flows which often occur at the gravity separator inlet during production operations in the offshore industry.

Resumé

Olieudskilleranlæg i offshore olie og gasindustrien er vigtige for at sikre en reducering af udledningen af olie ud i havet, hvilket bærer en lavere forurening af verdenshavene samt opfyldelse af myndighedskravene med sig. Flere aspekter af olieudskilleranlæg er blevet undersøgt i denne PhD opgave, med mål om at forbedre de nuværende systemers effektivitet. På nuværende offshore installationer, måles effektivitet af olieudskilleranlægene hverken kontinuerligt eller i real-tid, og derfor var en undersøgelsen af dette aspekt en væsentlig del af denne opgave. En pålidelig real-tids og on-line effektivitetsmåling kunne give et solidt grundlag for evalueringen af olieudskilleranlæget og dette kunne bane vej til at forbedre dens præstationer. En pålidelig effektivitetsmåling ville også hjælpe med at forstå effekten af forskellige driftsforholds påvirking af olieudskilleranlæget, sådan en indsigt kunne forbedre de nuværende kontrol strategier. Efter en indledende undersøgelse af flere forskellige overvågningsteknologier og en evaluering af tre udvalgte teknologier, en olie i vand (OiV) monitor baseret på fluorescerende teknologi var i sidste ende anvendt til at måle olie koncetrtaionedn på hydrocyclonknens ind og udgang. Hydrocyklonernes effektivitet var dermed beregnet baseret på disse on-line målinger, og dynamiske ændringer i effektiviteten under varierende forhold var observeret. Disse eksperimenter afslørede også at hydrocyklonernes effektivitet afhang mere af indløbs strømning raten end af trykfalds forholdet (PDR) , som er basis for nuværende kontrol strategier. Det er en klar fordel ved at udvikle en model af det pågældende system, for at fremme design af avancerede kontrollerer. Indtil nu er arbejdet med kontrol orienterede modeller af olieudskiller hydrocykloner været begrænset. Denne udfordring var derfor endnu et fokuspunkt af denne PhD opgave. Ved at betragte PDR af olieudskiller hydrocykloner som systemets output og åbningsgraden af styreventilerne som systemets input, blev et sæt af lineære systemmodeller opnået ved at anvende black-box system identifikation teknikker. Erhvervelse af data som var anvendt til model estimationen, blev udført på et skaleret pilotanlæg. Ved at koble hydrocyklon modellen med en model af opstrøms trefaset gravitationsudskiller, blev en MIMO struktureret model endvidere opnået for hele olieudskiller pro-

cessen. Ved at begrænse olieudskiller processen i nærheden af et driftspunkt, var en lineær MIMO procesmodel opnået og den tjente som den primære model for videre kontrol design. En robust kontrol løsning som gør brug af robust suboptimal H_∞ control er foreslået i dette værk, med følgende to mål; at øge systemets robusthed overfor forstyrrelser og at håndtere koblingen af systemets dynamik. Den udviklede H_∞ kontrol løsning var implementeret på en skaleret pilotanlæg og dens præstation blev sammenlignet med en reference PID kontrol løsning. H_∞ kontrol løsningen have den mere tilfredsstillende ydelse med hensyn til robusthed overfor forstyrrelser, og den viste en overlegen ydelse i håndtering af alvorlige svingende flow som ofte forekommer ved gravitationsudskillers indløb under produktionen i offshore industrien.

Contents

List of Figures

Thesis Details

Thesis Title:	Real-Time Monitoring and Robust Control of Offshore De-oiling Processes
Ph.D. Student:	Petar Durdevic Løhndorf
Supervisors:	Assoc. Prof. Zhenyu Yang, Aalborg University

The main body of this thesis consists of the following papers.

[A] P. Durdevic, S. Pedersen and Z. Yang, "Challenges in Modelling and Control of Offshore De-oiling Hydrocyclone Systems" *Presented at: Advanced Control and Diagnosis – 13th ACD 2016, 17 - 18 November 2016, Lille, France*, Journal of Physics: Conference Series 2017, Volume 783, conference 1; doi: 10.1088/1742-6596/783/1/012048

[B] P. Durdevic, S. Pedersen, M. Bram, D. Hansen, A. A. Hassan, Z. Yang, "Control Oriented Modeling of a De-oiling Hydrocyclone," *17th IFAC Symposium on System Identification SYSID 2015 – Beijing, China, 19–21 October 2015*, IFAC-PapersOnLine, vol. 48, no. 28, pp. 291–296, 2015; doi: 10.1016/j.ifacol.2015.12.141

[C] P. Durdevic and L. Hansen and C. Mai and S. Pedersen and Z. Yang, "Cost-Effective ERT Technique for Oil-in-Water Measurement for Offshore Hydrocyclone Installations," *2nd IFAC Workshop on Automatic Control in Offshore Oil and Gas Production OOGP 2015 – Florianópolis, Brazil, 27–29 May 2015*, IFAC-PapersOnLine, vol. 48, no. 6, pp. 147–153, 2015; doi:10.1016/j.ifacol.2015.08.023

[D] P. Durdevic and S. Pedersen and Z. Yang, "Evaluation of OiW Measurement Technologies for Deoiling Hydrocyclone Efficiency Estimation and Control," *Proceedings of OCEANS'16 MTS/IEEE Shanghai*, 2016; doi: 10.1109/OCEANSAP.2016.7485361

[E] P. Durdevic and C. S. Raju and M. V. Bram and D. S. Hansen and Z. Yang, "Dynamic Oil-in-Water Concentration Acquisition on a Pilot-Scaled Offshore Water-Oil Separation Facility," *Journal of Sensors (MDPI)*, Sensors 2017, 17(1), 124; doi: 10.3390/s17010124

[F] P. Durdevic and S. Pedersen and Z. Yang, "Application of H_∞ Robust Control on a Scaled Oil&Gas De-Oiling Facility," *Submitted to: IEEE Transactions on Control Systems Technology*, 2017.

In addition to the main papers, the following publications have also been made.

[1] S. Pedersen and P. Durdevic and Z. Yang, "Influence of riser-induced slugs on the downstream separation processes," *Submitted to: Journal of Petroleum Science and Engineering*, 2016.

[2] S. Pedersen and P. Durdevic and Z. Yang, "Challenges in Slug Modeling and Control for Offshore Oil and Gas Productions: A Review Study," *International Journal of Multiphase Flow*, vol. 88, pp. 270–284, 2017.

[3] S. Pedersen and P. Durdevic and K. Stampe and S. L. Pedersen and Z. Yang, "Experimental Study of Stable Surfaces for Anti-Slug Control in Multi-phase Flow" *International Journal of Automation and Computing*, Vol. 13, No. 1, p. 81-88, 2016.

[4] Z. Yang and P. Durdevic and S. Pedersen, "Optimization of Offshore De-oiling Hydrocyclone Performance: Plant-wide Control and Real-time OiW Measurement" *Proceedings of 2016 NEL Produced Water Workshop*, 2016.

[5] Z. Yang and S. Pedersen and P. Durdevic and C. Mai and L. Hansen and K. L. Jepsen and A. Aillos and A. Andreasen, "Plant-wide Control Strategy for Improving Produced Water Treatment" *Proceedings of 2016 International Field Exploration and Development Conference (IFEDC)*, 2016.

[6] M. V. Bram and A. A. Hassan and D. S. Hansen and P. Durdevic and S. Pedersen and Z. Yang, "Experimental modeling of a deoiling hydrocyclone system" *Proceedings of the 2015 20th International Conference on Methods and Models in Automation and Robotics (MMAR)*, p. 1080 - 1085, 2015.

[7] S. Pedersen and C. Mai and L. Hansen and P. Durdevic and Z. Yang, "Online Slug Detection in Multi-phase Transportation Pipelines Using Electrical Tomography" *2nd IFAC Workshop on Automatic Control in Offshore Oil and Gas Production OOGP 2015 – Florianópolis, Brazil, 27–29 May 2015*, IFAC-PapersOnLine, vol. 48, no. 6, pp. 159–164, 2015.

[8] S. Pedersen and P. Durdevic and Z. Yang, "Review of Slug Detection, Modeling and Control Techniques for Offshore Oil & Gas Production Processes" *2nd IFAC Workshop on Automatic Control in Offshore Oil and Gas Production OOGP 2015*, IFAC-PapersOnLine, Vol. 48, No. 6, p. 89–96, 2015.

[9] Z. Yang and S. Pedersen and P. Durdevic, "Cleaning the Produced Water in Offshore Oil Production by Using Plant-wide Optimal Control Strategy" *Proceedings of the OCEANS'14 MTS/IEEE Conference*, IEEE Press, 2014.

[10] S. Pedersen and P. Durdevic and Z. Yang, "Experimental Study of Stable Surfaces for Anti-Slug Control in Multi-phase Flow" *Proceedings of the 20th International Conference on Automation and Computing, ICAC 2014. Cranfield*, IEEE Press, p. 43-48, 2014.

[11] S. Pedersen and P. Durdevic and Z. Yang, "Learning control for riser-slug elimination and production-rate optimization for an offshore oil and gas production process" *Proceedings of the 19th World Congress of the International Federation of Automatic Control*, IFAC Proceedings Volumes, Vol. 47, No. 3, p. 8522–8527, 2014.

Published articles which are not directly related to the Ph.D. thesis:

[12] P. Durdevic and S. Pedersen and Z. Yang, "Modeling Separation Dynamics in a Multi-Tray Bio-Ethanol Distillation Column" *Proceedings of the 2015 IEEE International Conference on Mechatronics and Automation (ICMA). Beijing*, IEEE Press, p. 1349–1354, 2015.

[13] Z. Yang and S. Pedersen and P. Durdevic, "Control of Variable-Speed Pressurization Fan for an Offshore HVAC System" *Proceedings of the 2014 IEEE International Conference on Mechatronics and Automation (ICMA)*, IEEE Press, p. 458–463, 2014.

[14] P. Durdevic and Z. Yang, "Hybrid Control of a Two-Wheeled Automatic-Balancing Robot with Backlash Feature" *Proceedings of the 2013 IEEE International Symposium on Safety, Security, and Rescue Robotics (SSRR), Linkoping*, IEEE Press, p. 1–6, 2013.

Preface

This thesis is submitted as a collection of papers in fulfilment of the requirements for the degree of Doctor of Philosophy at the Department of Energy Technology, Aalborg University, Denmark. The work has been carried out in the Department of Energy Technology, Aalborg University, Esbjerg Campus, in the period from October 2013 to March 2016 under the supervision of Associate Professor Zhenyu Yang.

This work has been partially supported by the Innovation Fund Denmark, Mærsk Oil and Rambøll Oil & Gas through the "Plant-wide De-oiling of Produced Water using Advanced Control (PDPWAC)" Project (No. 95-2012-3).

I greatefully acknowledge the contribution of My Supervisor: Zhenyu Yang and my AAU colleagues: Simon Pedersen, Kasper Lund Jepsen, Christian Mai, Leif Hansen, Mads V. Bram, Dennis Hansen, and to my industrial partners: J.P. Stigkær, A. Aillos, K. G. Nielsen and T. I. Bruun from Mærsk Oil A/S, colleagues P. Sørensen, A. Andreasen and Jakob Biltoft from Ramboll Oil & Gas A/S.

In addition I would like to place a special thanks to my parents for support and guidance. Finally the support from my wife is greatly appreciated, both with respect to my work and to bear with me during stressful times of which there were plenty throughout the period of the Ph.D.

Petar Durdevic Løhndorf
Aalborg University, March 22, 2017

Part I

Introduction

Chapter 1

Introduction

1 Context

The north sea oil and gas industry has roots dating back to the 1960*s*, where the first petroleum rig, called the Sea Gem, operated by BP, started producing gas in June 1965 (8). Since then, the Oil and Gas industry has been growing in the North Sea, increasingly pumping oil until the oil production reached its peak around the early 2000*s* and from then onwards the production has been slowly decreasing, refer to figure 1.1 and (51). The increased oil and gas production has had a number of impacts on the reservoirs. In the primary extraction phase the reservoir pressure is sufficient for extraction, but through time as the oil and gas are extracted, the pressures in the reservoirs decrease and to keep it high enough for further extraction the pressure is artificially maintained (100). This is done through injection of water (secondary recovery phase), while tertiary recovery phases use enhanced oil recovery (EOR) methods such as chemical flooding, steam flooding and in-situ combustion, (47), (98) and (75). Water injection has been extensively used in the North Sea, and was adopted by Denmark in 1985 as can be seen in figure 1.2. Reinjection of produced water, which is water produced together with the oil and gas from the reservoir (21), has become an increasingly popular form of pressure maintenance in reservoirs since the 2000s in the North Sea, (50), (64) and (61). The reduction in the oil fraction due to extraction and due to the injection of water into the reservoirs has resulted in a constantly increasing water concentration in the wells and has led to an increase in the water fraction of the extracted oil, in some cases up to 98%, (89) and (99). A similar example of such an increase, in the Danish oil and gas sector in the North Sea can be seen figure 1.2 where the dotted line represents the water to oil ratio.

The large quantities of water in the reservoirs and the requirement for

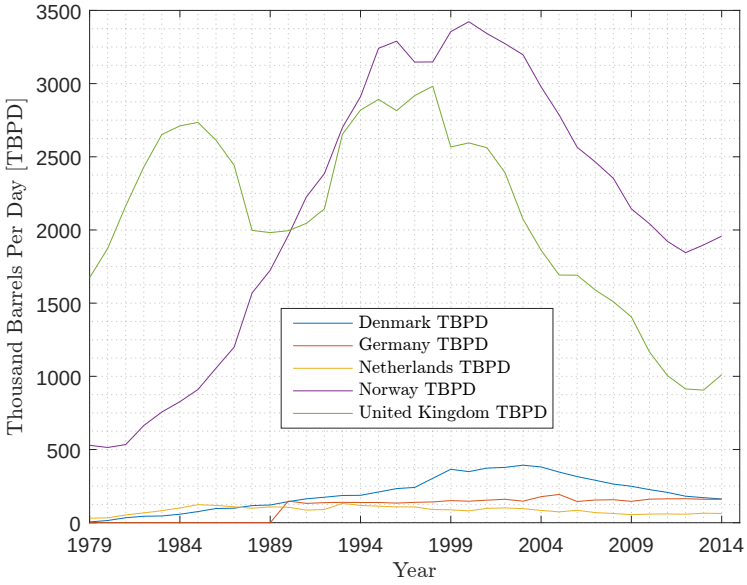

Fig. 1.1: Production of oil in the North Sea, per producing country, between the years 1979 - 2014, data adapted from (2).

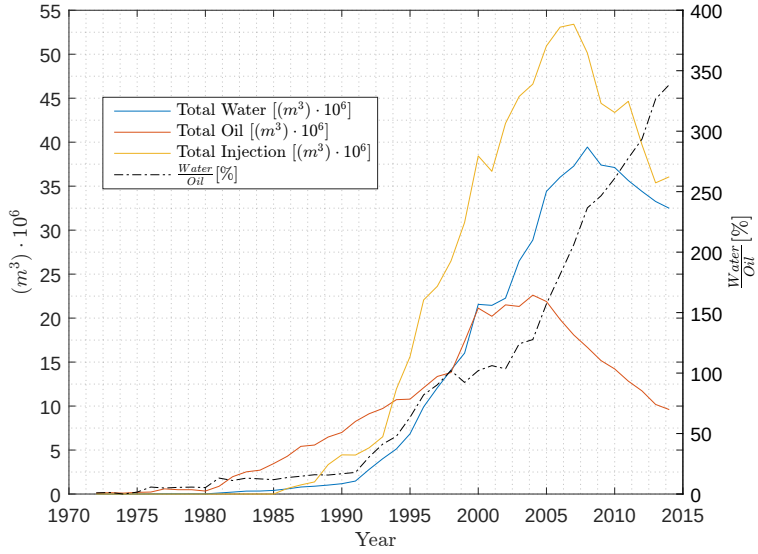

Fig. 1.2: Comparison of oil and water production in the Danish sector of the North Sea, data adapted from (1).

increased production of oil leads to an increasing strain on the production facilities, especially on the de-oiling and water treatment processes. Thus, even though the oil and gas production has been declining since the early 2000s, the amount of produced water has been increasing, which results in an increased total oil discharge into the oceans. The discharge limit of oil in the North Sea is 30 mg/l, (50). In article (24), it has been stated that 250 million barrels of produced water are produced on a daily basis, and if it is assumed that the discharged amount of oil averages around 30 mg/l under ideal circumstances, this roughly equals to around 1.2 tons of oil discharged into the ocean per day. The oil discharged, has been linked to adverse impacts on the surrounding marine life, (12), where even small oil concentrations in the ocean have been found to affect the development of fish. Alkylphenols (AP), naphtenic acids and polyaromatic hydrocarbons (PAH) which can be found in produced water, have been found to negatively affect the marine life, (31), (39), (96) and (60), for up to a 2 km radius of the producing platforms, and in some cases up to 5 km, (6). The produced water not only affects the environment but has a large impact on the economy of the offshore installations as well.

Due to the high cost of transportation of liquid to onshore separation facilities, the offshore plants are forced to process all the products on site, (5). In addition the presence of water in the transportation pipelines increases corrosion in the pipelines and the process equipment, and thus reduction of the water fraction is preferred before the oil is transported over long distances, (9). With the inherent space and weight restrictions and high operational costs in offshore platforms, the separation prices increase when it is dealt with on site. For example, in USA, onshore prices range from (USD 0.05 to USD 0.30 per bbl) whereas in the North Sea the prices range from (USD 0.19 to USD 3.40 per bbl), (20). There are therefore significant gains in economy and to the environment with improvements in produced water treatment and oil recovery. Driven by these motivators, this research aims at optimising the de-oiling facilities, by employing advanced control and instrumentation technologies.

2 Background

A typical offshore Oil and Gas de-oiling facility, which is the focus of this work, consists of a three phase gravity separator (gravity separator) and a downstream hydrocyclone that is connected to the water outlet of the gravity separator, (4). The section of the de-oiling process that was the focus of this Ph.D. study, including the instrumentation and control loops, is shown in figure 1.3.

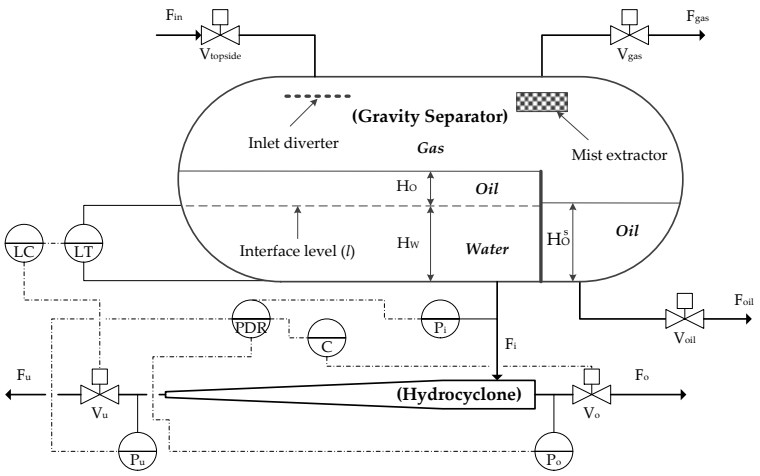

Fig. 1.3: Sketch of the de-oiling system under consideration, consisting of the gravity separator, the hydrocyclone and the control loops, figure from paper F.

2.1 Gravity Separator's Operation and Control

The liquid and gas mixture enters the gravity separator from the pipelines through the topside choke-valve, $V_{topside}$. Here, an inlet diverter reduces some of the kinetic energy from the inlet flow which would otherwise have disturbed the oil/water interface in the gravity separator (3). The mixture of liquid and gas are separated in the gravity separator through the principle of buoyancy, where the separated gas collects in the head-space of the gravity separator. The water and oil phase flow into the left hand side chamber of the gravity separator, the remaining gas separates from the water and the oil droplets surface to the top creating a water/oil interface, as seen in figure 1.3. The surfaced oil floats on the water/oil interface and flows over the weir into the right hand side chamber which contains the separated oil. The gas and oil are let out of the gravity separator through valves located at the top and the bottom of the right hand side of the gravity separator, V_{gas} and V_{oil} for the gas and oil respectively, refer to the sketch in figure 1.3. The separation of the oil and water in the left hand side of the gravity separator is governed by the residence time of the liquid, as the surfacing of oil droplets takes time, (4) and (3). This time is determined by equation 1.1, which describes the terminal velocity of a sphere in creeping flow, (13).

$$V_t = \frac{D^2 \cdot (\rho_{droplet} - \rho_{water}) \cdot g}{18\mu} \tag{1.1}$$

In equation 1.1 the terminal velocity V_t of the oil droplets is defined based on the droplet diameter D, the densities of the oil and the water, $\rho_{droplet}$ and ρ_{water}, the gravity g and the viscosity of the continuous phase, μ, which in this case is water, (13). If the desired separation is to be achieved, the residence time t_r must allow for the oil droplets to surface to the oil pad. In addition, a sufficient residence time ensures that the oil droplets have sufficient time to coalesce, which results in the formation of larger oil droplets thus ensuring a faster surfacing of the oil droplets according to equation 1.1, (44). The design of a gravity separator is a trade-off optimisation between the t_r and the D100, where D100 represents the minimum droplet size to be separated 100%, (49), (65) and (102).

This leads to the control of the gravity separator, which aims at maintaining a specific residence time by controlling the oil-water interface level l. The separators operation will be affected by several aspects such as fluctuating flow rates, oil types from different fields and added chemicals (34). Mechanical and chemical improvements to the gravity separator can be introduced to improve its operation, although this introduces negative economical and environmental aspects, (34), which is undesirable. Instead the operator can alter the reference point for the l control loop, to account for alterations in the operating conditions. The operator, however, cannot change the reference point beyond the physical limits of the gravity separator and the gravity separator is equipped with alarms which are triggered if l approaches a maximum or a minimum state, (43) and (76). The maximum level state prevents the oil-water interface from skimming over the weir and resulting in the water entering the separated oil chamber. The minimum level state prevents the interface level from reaching the water outlet in the bottom of the oil/water chamber and resulting in the oil exiting with the water phase, (53).

Offshore gravity separators have size and weight constraints due to the physical construction of the installations, and this does not allow for an indefinite residence time. Thus the effluent from the gravity separator will have residual oil droplets that are smaller than the size specified by the D100 criterion. This oil residue is removed in the downstream hydrocyclone unit.

2.2 Hydrocyclone's Operation and Control

The gravity separator and the hydrocyclone both separate based on density difference of the different phases, however the hydrocyclone utilises the enhanced gravity separation principle as it uses centrifugal/centripetal forces to generate the necessary forces required for separation, (71) and (91). The gravitational acceleration is negligible in the hydrocyclone, and the separation is facilitated by the centripetal/centrifugal force created by converting the tangential velocity V of the inlet flow into a vortex flow. The centripetal/centrifugal forces inside the hydrocyclone can reach an acceleration

up to 2-3000 times the gravitational acceleration, (83). Due to these large forces, the oil droplets inside the hydrocyclone travel faster than they do in the gravity separator, which yields a larger oil droplet settling velocity V_d. This reduces the residence time significantly, and a residence time of approximately 2 seconds is common in a de-oiling hydrocyclone, (95). The result is that smaller oil droplets can be separated from the water phase in a smaller space within a shorter time period. V_d, can be defined by Stokes law from equation 1.1, where the gravitational acceleration is replaced by the centrifugal acceleration which yields the equation 1.2.

$$V_d = \frac{\Delta\rho \cdot D^2 \cdot (V^2/r)}{18\mu} \tag{1.2}$$

Where V_d is the settling velocity of the droplet, ρ is the specific gravity, D is the oil droplet diameter, V is the tangential velocity of the droplet or the velocity of F_i (where F_i is the inlet volumetric flow rate to the hydrocyclone), μ is the viscosity of the continuous phase (water) and the r is the radial length between the droplet and the hydrocyclone axis, (102) and (73). The mixture of water and oil droplets entering the hydrocyclone start with a tangential motion and transition into a cyclic motion due to the vortices created inside the hydrocyclone, as seen in figure 1.4. The centripetal/centrifugal forces act on the oil/water mixture, and a balance between the centripetal/centrifugal forces and the drag force acting on the oil droplets, pushes the oil droplets towards the centre of the hydrocyclone and the water towards the wall of the hydrocyclone. Here the droplet diameter has an exponentially proportional relationship to the settling velocity, where larger droplets will result in faster settling velocities thereby reducing the residence time required for the oil droplets to reach the oil core and exit through the overflow. The tangential velocity V is directly proportional to the inlet flow rate F_i, assuming that the cross-sectional area of the hydrocyclone inlet is constant and for incompressible flow, (55), and therefore F_i is exponentially proportional to the settling velocity and thus related to the separation of the droplets (73). A photograph of the oil-core created in a transparent hydrocyclone can be seen in figure F.5b in the Appendix part III. The geometry of the hydrocyclone aids the movement of the two phases, where the lighter oil droplets collect at the centre of the hydrocyclone forming the oil-core which exits through a narrow opening called the overflow and the water exits through a larger opening called the underflow.

In offshore de-oiling facilities the hydrocyclone is operated by controlling the pressure drop ratio (PDR) over the hydrocyclone. The PDR is calculated using three pressures, P_i, P_u and P_o, which are the inlet pressure, underflow pressure and the overflow pressure respectively as seen in figure 1.3, using

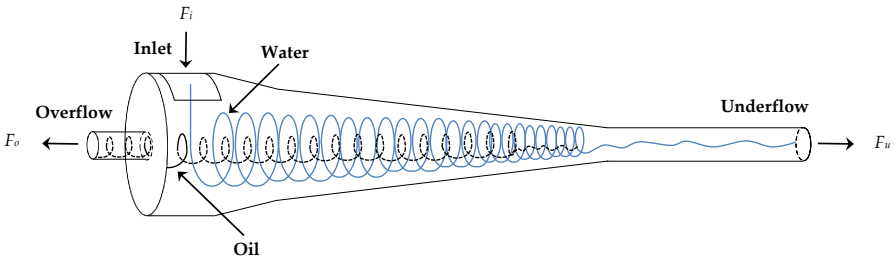

Fig. 1.4: A sketch of the hydrocyclone, showing the approximate trajectories of the water and the oil in the hydrocyclone. Adapted from figure [1], paper A

the equation 1.3, (106), (48), (38) and (36).

$$PDR = \frac{P_i - P_u}{P_i - P_o} \tag{1.3}$$

The PDR control solution is based on the principle of flow split, R_f, where the pressure drop ratio is related to the split of flow going from the inlet F_i to the underflow F_u and is defined by equation 1.4, (92). The steady state relationship between the PDR and the flow split have been experimentally investigated in previous studies, refer to articles (48), (106), (94), (92), (10) and (38).

$$R_f = \frac{F_u}{F_i} \tag{1.4}$$

Where F_u and F_i is the flow rate of the liquid through the underflow and the inlet respectively. If the cyclic flow inside the hydrocyclone is at nominal operation, i.e. ideal for all the oil droplets to reach the oil core and exit through the overflow; then a pre-set flow split will determine the amount of the oil to be sent through the overflow or the underflow and thus yields the efficiency of the hydrocyclone (ϵ) which is defined in equation 1.5, (87).

$$\epsilon = 1 - \left(\frac{C_u}{C_i}\right) \tag{1.5}$$

where C_u is the concentration of oil in the underflow of the hydrocyclone and C_i is the concentration of oil in the inlet of the hydrocyclone, (93). It is noteworthy that this equation only represents the de-oiling efficiency and not the de-watering efficiency. Therefore in order to satisfy a 100% ϵ the system could close V_u completely, saturating the valve which would send all the oil along with the water through the overflow, thus leading to 100% ϵ and 0% de-watering efficiency (E), where E is defined in equation 1.6.

$$E = \frac{F_u}{(1 - C_i) \cdot F_i} \tag{1.6}$$

In practical terms if E is low, then the water cut in the overflow could be high and the oil will be contaminated with water. This requires that the oil be recirculated and the separation process repeated in order to remove the unwanted water from the oil. Keeping the flow split within a certain range is thus a key operational parameter in order to channel the correct amount of oil through the overflow, while still keeping the flow through the overflow below the point where some of the water could contaminate it.

In the current offshore de-oiling facilities, the measurement of ϵ is neither on-line nor is it in real-time, which makes it impossible to apply it for control purposes. Due to this dearth of suitable ϵ measurements and the unavailability of control oriented hydrocyclone models, the dynamic behaviour of ϵ is not well understood both from the industrial and academic perspectives. Pressure measurements, however, are currently available and reliable, and hence the PDR is used as the control parameter for ϵ.

In literature, hydrocyclone control is mostly described with respect to the solid-liquid hydrocyclones used in the mining industry, (56), (79), (57), (58), (59) and (25). Although the control methodologies are extensive and appear to have good results, their implementation onto liquid-liquid hydrocyclone separators is not trivial.

2.3 Control of the De-oiling System

Current offshore installations commonly use PI/PID controllers to control the gravity separator's water/oil interface level l, (77), as well as for the control of the hydrocyclone's PDR according to a set of reference values, (16). To our knowledge the two controllers operate in an almost stand alone configuration in the North Sea installations, an example of their performance is presented in figure **[2]** in paper F. In some cases the two controllers do operate in a cooperative manner, but this structure is based on an ad-hoc empirical design.

The de-oiling system, however, is a heavily coupled system, and thus the downstream hydrocyclone's operating conditions are heavily dependent on that of the upstream gravity separator, which is dependent on the flow conditions in the pipeline systems which in turn are dependent on the reservoirs conditions, as discussed in paper (104) and (105). This coupling is due to the physical construction of the de-oiling facility, where the two control valves, the underflow valve V_u and the overflow valve V_o, which are used to control the gravity separator and the hydrocyclone, are both attached to the hydrocyclone, refer to figure 1.3. A block diagram of a typical control structure of the de-oiling process is illustrated in figure 1.5, where F_{in} is the inlet flow rate to the gravity separator. It illustrates the influence of each of the control valves on each of the two sub systems; where an actuation of either of the two valves will have a direct impact on both sub-systems. If fluctuating flow occurs upstream of the gravity separator and results in an oscillating F_{in}, it

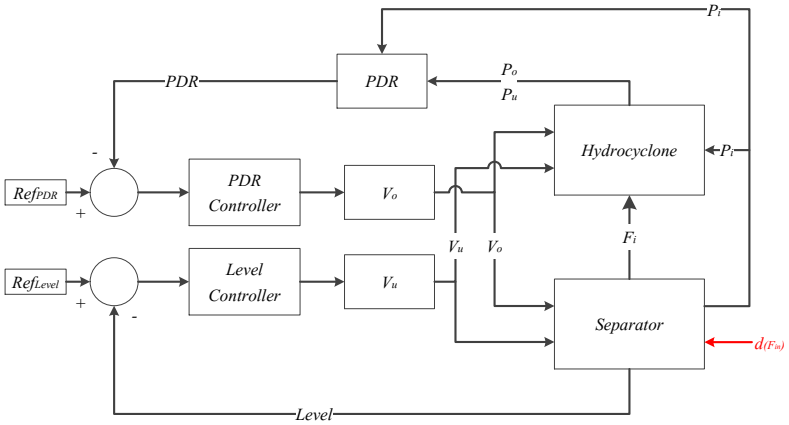

Fig. 1.5: Block diagram of the de-oiling separation system, including the feedback control loop; depicting the inherent coupling in the system. Addapted from figure [5], paper A.

will have an impact on the level inside the gravity separator, which in all cases is maintained at a given reference. To maintain the level at the given reference, the level controller will actuate V_u resulting in a fluctuating F_i. It has been shown in a study performed on an offshore facility that reducing the fluctuations in F_i can improve the de-oiling hydrocyclone's performance and thus the de-oiling efficiency, (37). In paper F the negative effects of the fluctuating flow as inferred from offshore data is discussed.

A fluctuating F_{in}, unfortunately, is a common occurrence in offshore Oil and Gas facilities (86), (53), (42) and (68). The fluctuating flow regimes are a product of transportation of multiphase mixtures in the pipelines from the reservoirs to the separation facilities, which can induce different flow regimes in the pipelines resulting in fluctuating flow rates, (78), (18), (41), (42), (70) and (67). Slugging flow is one type of of flow regime that has a severe impact on the de-oiling process and induces a fluctuating inflow to the de-oiling system,refer to (68), which is unfavourable for the de-oiling process, (37) and (38). In addition, the fluctuations of the level in the gravity separator can in severe cases trigger the safety alarm which then shuts down the process, (76). The influence of slugging flow on the riser top pressure based on offshore data has been illustrated in figure [3] in paper A. Where a fluctuating riser top pressure, caused by the slugging flow, will have an impact on the inlet flow to the gravity separator affecting the performance of the de-oiling system, unless it is explicitly handled using an anti-slug controller, although such

slug elimination is still a challenge, (66) and (37).

3 Problem Formulation

The physical construction of the deoiling system poses a disadvantage with respect to fluctuating flows into the system, and the current control solution of the de-oiling facilities in most cases does not account for the effects of such disturbances on the de-oiling performance. Thus the effect of the physical construction of the deoiling system on its performance especially during severe fluctuating flows needs to be investigated.

On-line dynamic measurement of the ϵ is not available as the methodology is still not matured. The ability to measure ϵ, will enable the investigation of the system, the evaluation of novel control solutions and enable the development of efficiency based models.

The current control solutions of the de-oiling facilities in most cases do not account for unmeasured disturbances caused by the fluctuating inlet flows. A novel control structure that has improved disturbance attenuation has the potential to improve the de-oiling system's efficiency.

Models of the hydrocyclone and the entire de-oiling system that can be used for control development are unavailable. Such models will enable the development of model based controllers and have certain advantages over model-free controllers, for example, with respect to tuning efforts and the option of using advanced control techniques.

4 Aim and Objectives

The aim of this research was to improve the performance of offshore de-oiling systems. The main focus was to investigate the de-oiling system during nominal and extreme conditions to identify latent issues and thereafter provide solutions that can readily be applied to de-oiling facilities. In order to evaluate the de-oiling process it was necessary to facilitate the use of a criterion to quantify the system's performance. Thus one of the objectives of the study was the measurement of the de-oiling efficiency ϵ by evaluating different approaches to measuring and monitoring the concentrations of oil in water. Another objective was to derive a control oriented model that represented the de-oiling process. The third objective was to develop a novel control solution that could, under various disturbances to the de-oiling process, be an improvement over the currently available control solution.

5 Thesis Outline

Chapter 1 started with a general introduction and a problem statement that led to the aim and objectives of this work. The process through which these objectives were investigated and met are documented as published articles and are collected in part II.

Paper A provides an overview of current control and operational issues affecting the de-oiling hydrocyclone, thus introducing several challenges which are part of the main aim of this work.

Based on the analysis in paper A, the lack of reliable real-time, on-line oil in water (OiW) measurement was addressed in chapter 2 and papers C, D and E. Initially a cost effective OiW measuring instrument based on Electrical Resistivity Tomography (ERT) was developed an its performance evaluated, this work has been published in paper C. Further analysis of commercially available equipment based on microscopy and fluorescence based technologies was done in paper D with the aim of investigating these equipments' ability to measure the hydrocyclone's efficiency on-line. As a continuation of this study the fluorescence based monitor was used for monitoring the dynamic behaviour of the hydrocyclone's efficiency, this study has been documented in paper E.

A lack of control oriented models for de-oiling hydrocyclones led to the derivation of such a model, which is documented in paper B and is further described in chapter 3. Further in this chapter and in paper F, an extended version of the hydrocyclone model was combined with a gravity separator model to yield a representative de-oiling process model. This model was used for designing the robust control solution described in chapter 4 and paper F.

A robust control solution was designed and compared to a conventional PID control solution to evaluate its abilities during fluctuating flows, this has been documented in paper F and chapter 4.

In addition to the papers, the thesis also includes summaries for each of the objectives, that include an overview of the work and the main findings, and these can be found in chapters 2, 3 and 4.

The experiments throughout this Ph.D. study were carried out on a scaled pilot plant located at Aalborg University, Esbjerg campus. The scaled pilot plant was custom designed and built specifically for emulating and evaluating the offshore Oil and Gas de-oiling system, details about this platform can be found in the Appendix part III.

Chapter 2

Oil in Water Monitoring

Efficiency measurement of the de-oiling hydrocyclone (ϵ) is important to evaluate the performance of the de-oiling system as can be inferred from paper A. This chapter describes the efforts made in this direction and the results thereof. Real-time, on-line measurement of efficiency ϵ is required for evaluating the dynamic performance of the de-oiling hydrocyclone. Currently ϵ is in most cases measured off-line and dynamic measurements are unavailable as stated in chapter 1 section 2.2 and in paper E. In order to measure ϵ, the concentration of Oil in Water (OiW) is required, as has been shown in equation 1.5 in chapter 1 section 2.2.

1 OiW monitoring equipment investigation

To begin with, an on-line instrument based on electric resistance tomography technology (ERT) was developed to measure OiW, this work has been published in paper C. The reason for choosing ERT technology was its ability to measure OiW with a high sampling rate thus satisfying the real-time requirement. The ERT also has the possibility to be placed in-line with the existing equipment thus eliminating the requirement for sampling points which induce delay in the sampling and increase droplet breakup. Another benefit of this instrument was its low cost in comparison to commercially available solutions as is stated in paper C. The low cost is due to its simple design, where the requirement is to equip a pipe with electrodes as shown in figure 2.1a, and transmit and receive electric signals, which can be done with relatively low cost data acquisition equipment.

An illustration of the instrument measuring a gas and water mixture can be seen in figure 2.1b, since oil and gas have a similar conductance, gas was used as an analogue to oil. The conductance is represented by the colour scale, where a darker red colour indicates an increase in conductance, which

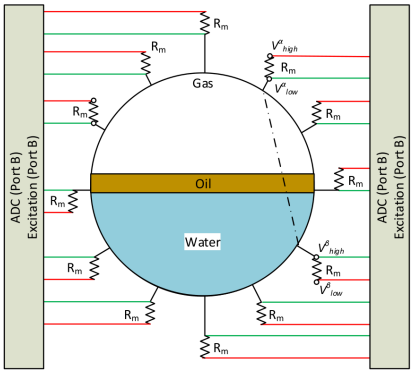

(a) Cross sectional sketch of the tomography transmitter, showing the position of the electrodes and the wiring to the I/O interface. Figure from paper C

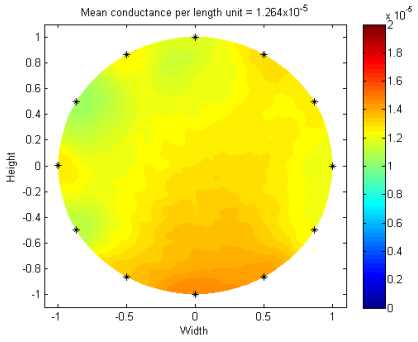

(b) Tomography results using the minimum distance algorithm, the experiment dealt with a high water concentration with small amounts of gas. Figure from paper C

Fig. 2.1: Sketch of the probe layout within the ERT instrument and one of the results from the ERT experiment from paper C.

is translated as a higher concentration of the conducting phase, in this case, water.

The ERT instrument was, however, found to be unsuitable for measuring the low OiW concentrations in the hydrocyclone effluent. The cause of this was its relatively low resolution and because the electrons take the path of least resistance instead of direct paths, (40). As the algorithms used to generate the tomography images rely on the distance between the electrodes for calculating the conductance per normalized length, it is crucial that the electrons travel a direct path, i.e. the same distance as is used to calculate the conductance per normalized length. If this path is altered the results may get skewed. The confinement of electric fields is applicable for all electric based tomography techniques, electrical capacitance tomography (ECT), electromagnetic tomography (EMT) and ERT, (40). In paper (45), ECT was combined with a γ-ray tomography, which could improve the accuracy of the equipment with the correct data processing. But in this Ph.D. work γ-ray tomography was not considered due to the safety issues involved in designing and operating such equipment as discussed in paper C.

Another drawback of the ERT technology was found to be corrosion, the electrodes were exposed to corrosive liquids which together with the current which was passed through them induced corrosion and significantly reduced the life span of the electrodes. Switching to a higher quality material could reduce the corrosion. Further study was aimed towards commercially available instruments and the ERT instrument was later utilised for slug detection

with good results, refer to the work done in (69).

Based on an investigation of commercially available equipment two instruments were chosen, of which one was based on fluorescence technology, Turner Designs' TD4100XDS (TD-4100), and one was based on microscopy technology, Jorin VIPA (VIPA). The fluorescence technology was chosen as it is widely used in the oil and gas industry for OiW measurements, and it benefits from high sensitivity and has no requirements for the use of solvents, (103). The aromatic compounds in oils have the ability to fluoresce. This occurs when the aromatic compounds absorb energy from incident photons, exciting them from a ground state to an upper excited singlet state. If the molecule returns to the singlet ground state without changing its spin state, it will emit a photon, (88) and (74). This light can then be detected by the instrument, and converted into a relative fluorescence unit which is used to calculate the concentration of OiW through proper calibration. One such calibration has been shown in 2.2, a line has been fitted to the data using simple linear regression and it indicates that the instrument has a linear response in the given range. The residuals plot indicated that the instrument has a tendency to deviate from its linear trend at lower concentrations. The observed offset is not to be blamed on the instrument alone, the calibration method could result in a higher offset towards the lower concentrations, as the lower concentrations are obtained by successive dilutions, increasing the scope for errors in the calibration solution. The conclusion of paper D was that the TD-

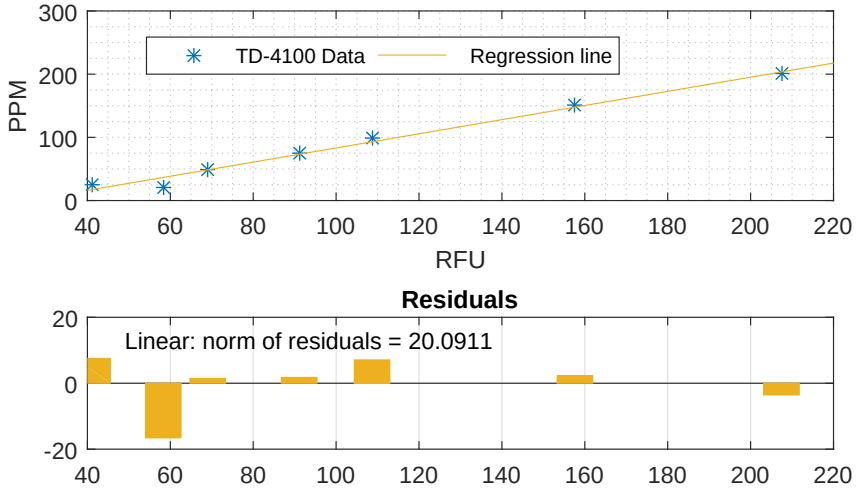

Fig. 2.2: Calibration of the TD-4100 in a Parts Per Million (PPM) range of [0 - 200], a regression line is fitted to the calibration data to illustrate the linearity of the instrument's measurements in the given range.

4100 showed promising results in steady state and in dynamic on-line OiW measurement.

The importance of a droplet size on the separation of oil from water in de-oiling hydrocyclones was discussed in chapter 1 section 2.2. Measurement of oil droplets was thus considered to provide a deeper understanding of the de-oiling systems efficiency. Thus the use of the microscopy based monitoring technique, the VIPA, was investigated. Here, the oil droplets can be visually analysed using advanced software which takes into consideration the shape and diameter of the detected particles (82), (103) and (46). Based on these readings the particles can be categorised as oil droplets or otherwise and based on their size and number, the relative concentration of OiW can be determined.

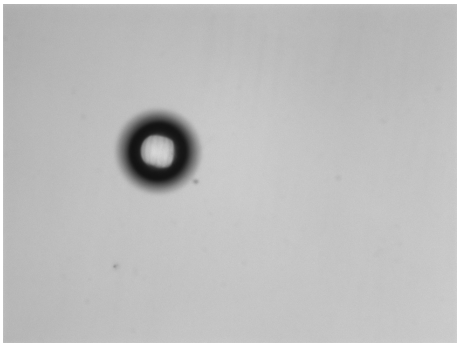

Fig. 2.3: One frame from the VIPA instrument showing a 75μm particle.

The instrument must be calibrated to detect the oil droplets correctly by following the manufacturers guidelines, making calibration a key objective for successful measurement. The VIPA instrument was calibrated using calibrated particles, commonly used for calibration of optical equipment, and then subjected to a stream of these particles to investigate the instruments repeatability and accuracy. Figure 2.3 shows one frame from the VIPA, here one of the particles that was used for calibration and validation can be seen, see paper D. In this experiment, the VIPA measured the particle sizes with high accuracy. However, the performance of the VIPA equipment was less satisfying when subjected to a continuous stream of oil.

An intensive investigation was performed on the two instruments (VIPA and TD-4100), and the preliminary analysis of the these two instruments is presented in paper D. The analysis involved an on-line investigation, where both instruments were compared with respect to their real-time on-line OiW concentration measuring capabilities, by applying the two instruments in series. In a direct comparison of the VIPA and the TD-4100, where both instruments were subjected to a OiW concentration of 90 mg/l, the TD-4100

measured a mean value of 90.818 Parts Per Million (PPM) with a standard deviation of 0.136PPM while the VIPA returned a mean value of 9.727 PPM and a standard deviation of 20.359. This led to the conclusion that the VIPA could not be used to measure the OiW concentration in real-time and on-line in an acceptable manner, the results are shown in figure [9] in paper D. The reason for the poor real-time measurement by the VIPA is believed to be due to the measurement methodology; where the image captured only represents a small sample of the entire flow and thus does not consistently show the distribution of all the particles in the flow line, as discussed in paper D. This in addition makes it difficult to validate the instrument, as the images captured by an instrument only represents a small sample of the entire sample space, which consists of randomly distributed droplets of random sizes.

The consistent measurement performed by the TD-4100 prompted further analysis to assess its ability to measure the dynamic behaviour of OiW changes in real-time. A feasibility study was made in paper D, where the TD-4100 was manually injected with different OiW concentrations, and its dynamic performance observed. The TD-4100 demonstrated a good dynamic response, but due to the manual injection of the oil-Isopropyl mixture, the dynamic performance could not be quantified.

In paper E the TD-4100 was tested on the scaled pilot plant. Two TD-4100 instruments were used to measure OiW concentrations, one on the inlet and one on the underflow of the hydrocyclone, and based on this ϵ was calculated based on equation (1.5) from chapter 1 section 2.2. The goal of this set of experiments was to investigate if this monitoring configuration could be used to measure the dynamic behaviour of ϵ, when subjected to variations in the inlet flow-rate F_i. Such a measurement has the potential to be used for system analysis, model development and as a feedback parameter for potential ϵ based de-oiling hydrocyclone control. To overcome the limitations that arose due to manual injections during dynamic measurement by the TD-4100, the scaled pilot plant used in paper E was upgraded with an oil and water injection system, described in paper E and in the Appendix part III, which ensured a consistent oil injection rate. To obtain a reliable and fast step input, the inlet flow rate was stepped as it had a fast dynamic and has a direct effect on ϵ as described in chapter 1 section 2.2. In paper E, increments of $\approx$ 0.06 l/s in F_i was applied and a dynamic change in ϵ was measured and it was observed that the rise-time of ϵ was consistent with F_i with a $\approx$ 10s delay at each step. From these results it was concluded that using the TD-4100 instrument the real-time dynamic on-line measurement of ϵ was feasible. In addition within the experiment's operating range, the PDR was discovered to have less impact on ϵ in comparison to that of F_i.

2 Dynamic response of ϵ when subjected to an increasing F_i.

The response of ϵ shown in paper E is for F_i within $[0.22 - 0.39]$l/s, the following investigation extends the range of the F_i to the maximum F_i achievable under the given operating conditions, to show how it effects the ϵ.

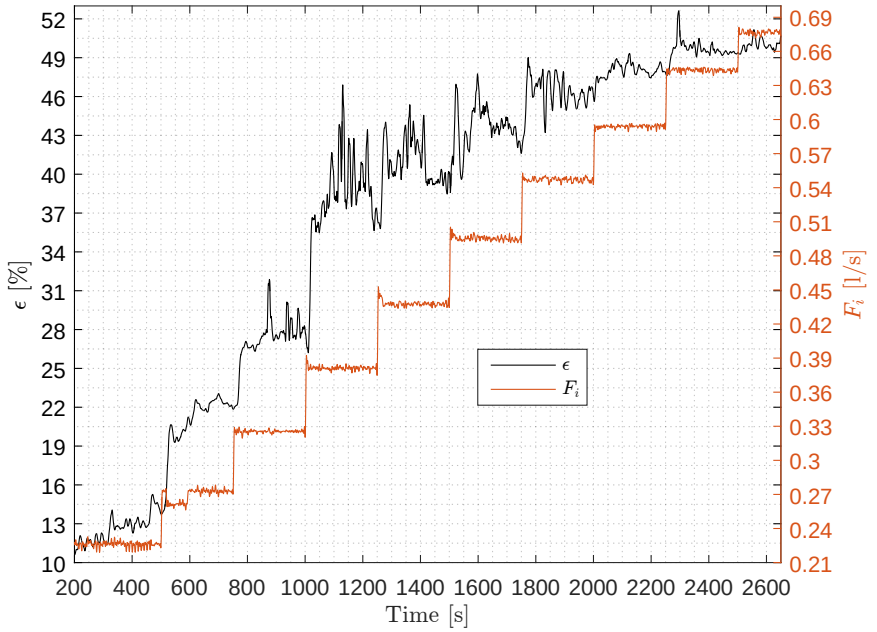

Fig. 2.4: Comparison of the F_i and ϵ. Operating conditions: $C_i \approx 400$mg/l.

Figure 2.4 illustrates the response of ϵ when subjected to steps in F_i, ranging from from 0.22 l/s to 0.68 l/s with steps of ≈ 0.05 l/s. The hydrocyclone is injected with a OiW concentration C_i of $\approx$ 400PPM. The resulting effect of larger F_i is an increase of ϵ from 40% to 50%. With increasing flows, the step gain of ϵ reduces and is negligible at the last step. The dynamic step response has the same trend, where at the larger ϵ the F_i steps have less impact on ϵ, and at the final step the step response is not observable. This result is similar to the results from steady state experiments performed in (32), (93) and (48), where the ϵ increases until it reaches a maximum value after which it remains at a plateau, and then begins decreasing when F_i reaches a certain point, as shown in (48). The ϵ achieved in (48) reached a value up to 99%, when the hydrocyclone was injected with an inlet concentration of 1000

mg/l. The separation process inside the hydrocyclone is dependent on many factors, which can change the operating conditions and performance, which makes it severely difficult to compare results from different set-ups across studies. Several factors which could influence the separation are mentioned below:

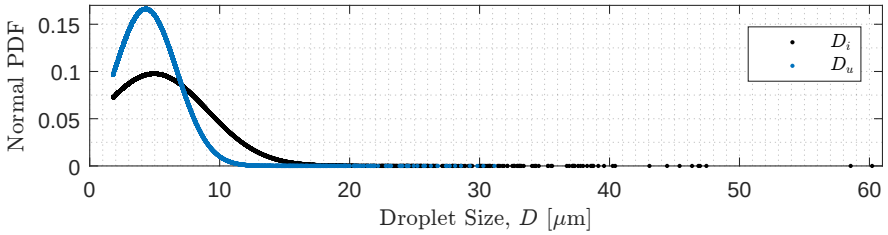

Fig. 2.5: Distribution of the oil droplet sizes D, at the inlet and the underflow of the hydrocyclone.

- **Inlet concentration:** In the experiments performed in paper E, C_i was $\approx$ 400 mg/l whereas in paper (48) a concentration of 1000 mg/l was used in order to reach an ϵ of 99%. In other experiments performed during this Ph.D. the highest ϵ, which was 71.6%, was achieved when the system was injected with an inlet concentration of 650 mg/l and a PDR of 1.55 and a F_i of 0.65 l/s. This further shows that higher inlet concentrations yield higher ϵ under certain operating conditions.

- **Droplet size:** The droplet size distribution in the current work was measured using two VIPA instruments, placed at the inlet and underflow of the hydrocyclone respectively. The result is shown in figure 2.5, which indicates that the majority of the droplets are $< 10\mu$m. Papers (32), (93) and (48) have not measured the particle size. According to papers (102) and (10), the ϵ increases significantly when the droplets sizes increase above 10μm. The droplet sizes are in addition not constant and may be reduced by shearing, which is caused by high intensity turbulence in valves, pipe and pumps, (101). Coalescence can on the other hand increase the oil droplet sizes and therefore measuring the oil droplets precisely and ensuring a consistent oil droplet size can be challanging.

- **Oil Type:** The oil used for the experiments is not the same as the offshore oil which was used in, for example in paper (48). The oil used in our experiments is a type of mineral oil where the volatile components have been removed and different additives are added. The oil used is thus more likely to suffer from droplet breakup which results in a lower droplet size.

Apart from the aforementioned factors, several additional factors could affect the OiW measurement. Calibration is one such factor and is of particular importance if this equipment is to be installed in off-shore installations where oil characteristics are not static. For example, the concentration of aromatics will vary with time thus offsetting the calibration curve shown in figure 2.2 and can thus contribute to a lowered repeatability. In addition, fouling has shown to affect the measurements of the microscopy equipment, as it affects the technologies that rely on optical measurements and with time the equipment's ability to capture images of the oil droplets and detect fluorescent light reduces. With respect to the the TD-4100, the fouling issues can be solved by using the non-contact falling stream flow cell found in the TD-4100XD model E.

Several physical properties of the system have a substantial impact on the performance of the system, such as temperature, design of the upstream system, valve types and the state of the hydrocyclone, (89). The last factor is

Fig. 2.6: Cavitation on the cylindrical section of the hydrocyclone, marked with white and blue colour, the shown example is from a used Vortoil hydrocyclone, which is the same type as used in the scaled pilot plant described in Appendix part III.

time varying, as the hydrocyclone degrades over time due to, for example, cavitation of the internal construction, see figure 2.6. Cavitation is caused by the large forces caused by the large accelerations described in chapter 1 section 2.2. In figure 2.6, the inlet port to the hydrocyclone chamber has been eroded and a semi circular erosion has been shaped in the inlet port marked with a white circle. In addition the internal chamber has been eroded at the point of entry leaving a significant inward deformation in the chamber marked by the blue circle.

3 Summary of the Oil in Water Monitoring

The monitoring of the dynamic behaviour of the hydrocyclone's efficiency (ϵ) was one of the key research objectives. The TD-4100 successfully measured ϵ and monitored its dynamic behaviour. Interestingly it was observed that the de-oiling hydrocyclone's ϵ is less prone towards changes in the pressure drop

ratio (PDR) than the hydrocyclone inlet flow rate (F_i). This presents a challenge to the current offshore installations where F_i is known to fluctuate due fluctuating inflow to the gravity separator and due to the level controller's reference tracking, which has been described and shown in paper F.

Chapter 3

Modelling of the De-Oiling Process

In preparation for the advanced controller described in chapter 4, a model which represents the input and output behaviour of the coupled de-oiling process, as described in chapter 1 section 2 is required. One of the main goals of this model is to represent the interactive dynamics in the de-oiling process, which has been described in chapter 1 section 2.3.

A process model of the hydrocyclone and the gravity separator is introduced in the following section, and hereafter a MIMO model of the de-oiling process is constructed as a combination of the aforementioned models.

1 Modelling of the Hydrocyclone

Modelling of the hydrocyclone systems involving CFD to predict flow behaviour inside the hydrocyclone has been carried out extensively and the following are some of the milestone works: (35), (54), (23), (22), (33), (19), (62), (85), (15), (63), (17) and (52). A control oriented dynamic model of a solid-liquid hydrocyclone in ball grinding circuits is introduced in paper (72). These models are based on solid-liquid hydrocyclones. Thus, although the hydrodynamic equations are similar for solid-liquid hydrocyclones and liquid-liquid (de-oiling) hydrocyclones, the separation behaviour is different due to density and viscosity differences in the phases and due to the differences in the physical construction of solid-liquid and liquid-liquid hydrocyclones (14) and (93). CFD models for de-oiling hydrocyclones have been developed in the literature, some of the works are: (30), (28), (81). With respect to control development the aforementioned CFD models, both with respect to solid-liquid and de-oiling hydrocyclones, are not directly applicable and

instead simplified ODE models are preferred.

A simplified model describing the efficiency of liquid-liquid de-oiling hydrocyclones through trajectory analysis has been done in (102), but the model that is presented only describes the steady-state behaviour and cannot directly be applied to control development.

Hydrocyclone dynamics are currently not well understood and the control of the hydrocyclone is in most cases done by specifying a PDR reference for a PID controller of the overflow valve V_o, as discussed in chapter 1 section 2. Unfortunately, offshore installations often suffer from fluctuating and uncertain operating conditions, where the inlet flow rate (F_i), which is an unmeasured input, has been shown to affect the hydrocyclone's performance (38) and (37).

Since control oriented hydrocyclone models are currently unavailable, as mentioned in papers A and B, such a model was investigated and was the base for the work done in paper B. The hydrodynamics which govern the static and dynamic behaviour of the PDR when it is subjected to changes in the underflow valve V_u and V_o are complicated and challenging to model using ODE models, thus to simplify the model while maintaining the important dynamics, a First-Order-Plus-Dead-Time (FOPDT) model structure was proposed in paper B. In this paper, the dynamics of the PDR with respect to the manipulated variables V_u and V_o was investigated and modelled. The model was aimed for control design which was to be implementable on real offshore installations. Thus the input and output variables of the model were chosen to be the manipulated and controlled variables of the real offshore installation, i.e V_u and V_o as the manipulated variables and the PDR as the controlled variable. A block-diagram is shown in figure 3.1 representing a hydrocyclone model comprising of four individual subsystems $G_v^{V_o}$, $G_v^{V_u}$, $G_h^{V_o}$ and $G_h^{V_u}$. Where $G_v^{V_o}$, $G_v^{V_u}$ have the valves' set position as the input and the valves' actual position as the output and $G_h^{V_o}$ and $G_h^{V_u}$ have the valves' actual position as input and the PDR as the output as shown in figure 3.1.

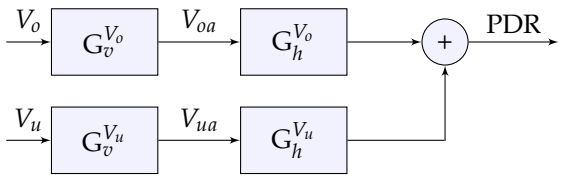

Fig. 3.1: Block Diagram of the hydrocyclone model, figure from paper B

The subsystems shown in the block diagram in figure 3.1 can be represented by equations 3.1 and 3.2, which are used for both the V_o and V_u. Equation 3.3 represents the total hydrocyclone model, where 3.1 and 3.2 have been combined together.

$$G_v = \frac{k_v}{\tau_v s + 1} e^{-T_{dv} s} \tag{3.1}$$

$$G_h = \frac{G_{vh}}{G_v} = \frac{k_v \tau_{vh} s + k_v}{k_{vh} \tau_v s + k_{vh}} e^{-(T_{dvh} - T_{dv})s} \tag{3.2}$$

$$G_{vh} = \frac{k_{vh}}{\tau_{vh} s + 1} e^{-T_{dvh} s} \tag{3.3}$$

Where k_v and k_{vh} are the gains with respect to the valve model G_v and the hydrocyclone model G_h, τ_v and τ_{vh} are the time constants with respect to G_v and G_h and T_{dv} and T_{dvh} are the time delays with respect to the G_v and G_h.

It is known from literature that the hydrocyclone operates within wide PDR ranges during nominal operation, where the PDR can range from 1.5 and 3 (92), and a common industrial controller's PDR set-point is 2. From our investigation it was evident that the hydrocyclone system has non-linear behaviour which is hard to model using one single linear model in the aforementioned range. The non-linearity was shown to exist in the static part of the system where the gain parameter changes through the PDR range, refer to figure 3.2. As a linear model was considered advantageous in the design of advanced control, a set of FOPDT models were identified based on data collected from the scaled pilot plant, see paper B, which enabled the representation of the hydrocyclone in a PDR range of [1.4-3.2]. The measurements from the three pressure transmitters; P_i, P_u and P_o were used to calculate the PDR using equation 1.3 from chapter 1 section 2.2. The openness of the valve was obtained from the valves' tachometers. The pressure data was noisy, and using this raw data to calculate the PDR would further multiply the noise due to the equation used. A low-pass filter with a pass band of 10Hz was applied to the data to filter the noise.

To achieve persistent excitation in the PDR, steps in a pre-determined sequence with 10% increments and decrements were applied to the valves, refer to figure [8] in paper B. A persistent excitation of the PDR was achieved in the entire valve range. The parameters k, τ and T were then identified from the step responses.

The validation of the FOPDT models, in paper B, showed good results when the models were validated using data collected within the same range as the data used for the model's identification. The PDR model G_h displayed a lower precision, which was concluded to be caused by the noise in the PDR signal and the higher order behaviour of the PDR, which had an overshoot and un-dampened oscillations. In paper B and (11), higher order models were utilised to increase the fit to the PDR data. In (11), second order transfer function models were identified with respect to the hydrocyclone's delta pressures, see equations 3.4 and 3.5, where the higher order models

showed improved tracking of the overshoot and oscillations within the operating range but had a reduced performance outside the operating range.

$$\Delta P_o = P_i - P_o \tag{3.4}$$

$$\Delta P_u = P_i - P_u \tag{3.5}$$

Finally the FOPDT models' flexibility was investigated by validating a model from one operating range to data collected outside this range. This was to investigate if the behaviour of the hydrocyclone could be described by a single linear model, which would simplify the grid model structure. The conclusion from the results was that the FOPDT model from one range showed a gain offset when compared to data from another range, but the time constant of the G_h and G_v did not change significantly. The gain offset has been illustrated in figure 3.2a, where the gain parameter with respect to $G_h^{V_o}$ has been plotted for the entire valve range, i.e. a PDR range of [1.4-3.2]. From this plot it is observed that the gain parameter k decreases exponentially as the valves open.

In comparison, the time constant τ of $G_h^{V_o}$, shown in figure 3.2b, remains relatively the same through the entire operating range. The same was observed for $G_h^{V_u}$.

Thus if the system is modelled using a single linear model, its validity will decrease from the static perspective outside its identified range. If the range is kept small then a linear model could be used for modelling the hydrocyclone, in a real case it is assumed that the system has some form of reference tracking controller which would assure this precondition. With respect to $G_v^{V_o}$ and $G_v^{V_u}$ the static and dynamic characteristics are the same throughout the valves operating range, as the valve actuator behaves linearly.

2 Extended Hydrocyclone Model

The hydrocyclone model described above has been extended for use in the de-oiling system's model. To facilitate the higher order dynamics described in this chapter section 1, a second order model is used. The hydrocyclone model structure has two models G_2(s) and G_3(s). Figure 3.3 represents the block diagram of the two hydrocyclone models. Since the hydrocyclone in most cases operates within a narrow operating range due to reference tracking, the model was estimated around a narrow operating range, close to the nominal operation of the PDR.

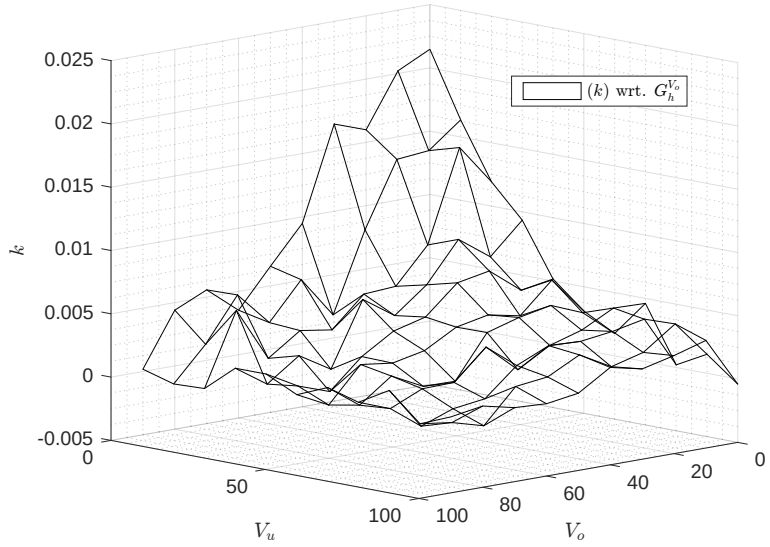

(a) Gain k for the $G_h^{V_o}$ models in the entire PDR range. Figure [14b] in paper B.

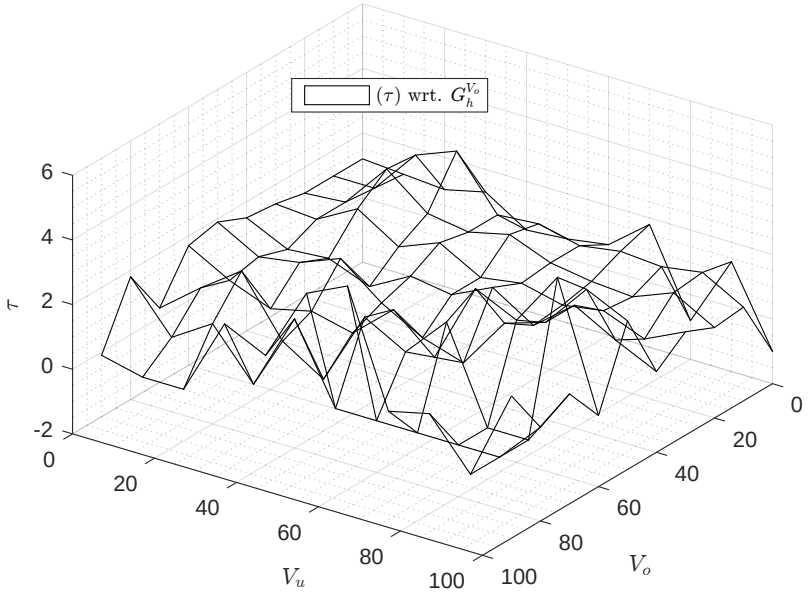

(b) Time constants τ for the $G_h^{V_o}$ models in the entire PDR range.

Fig. 3.2: Gain k and time constant τ with respect to the $G_h^{V_o}$ models in the entire PDR range.

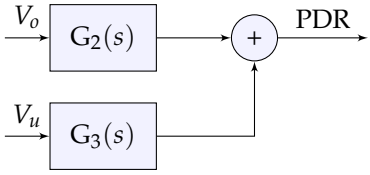

Fig. 3.3: Block Diagram of the hydrocyclone model

3 Modelling of the Gravity Separator

The gravity separator has one manipulated variable and one controlled variable, namely V_u and l respectively. As described in chapter 1 section 2 the water/oil interface level inside the gravity separator, l, is controlled by adjusting V_u, which controls the outflow of liquid from the gravity separator. V_u is located at the underflow of the hydrocyclone. The inlet flow to the gravity separator F_{in} governs the height of the liquid l as well, but it is in most cases not measured, and it is therefore considered a disturbance in the model.

The water volume of the gravity separator is defined by the mass balance in equation 3.6.

$$\frac{dV(t)}{dt} = F_{in}(t) - F_{out}(t) \tag{3.6}$$

Where F_{in} is the inlet volumetric flow rate to the gravity separator and F_{out} is the outlet volumetric flow rate from the gravity separator, which is defined by equation 3.7.

$$F_{out} = C_v f(u) \sqrt{\frac{\Delta P}{\rho g}} \tag{3.7}$$

Where, ΔP is the pressure difference over the valve V_u, ρ is the density of the water, g is the gravitational acceleration and C_v is the valve orifice coefficient, which can be identified by parameter identification. The gravity separator's volume, defined in the mass balance in equation 3.6, is converted into the level inside the gravity separator using the following trigonometric equation:

$$V(l) = \left(r^2 cos^{-1} \left(\frac{r-l}{r} \right) - (r-l)\sqrt{2rl - l^2} L \right) \tag{3.8}$$

Where r is the radius of the separator, and L is the length of the water chamber, i.e from one side of the separator to the weir, as illustrated in figure 3.4. This trigonometric relationship introduces a non-linearity in the model, which is caused by the physical shape of the vessel. The model is linearised around an operating point of 150mm as it is intended for later use in linear control design. The output response of the model and the physical system to a step in the disturbance has been shown in figure 3.5. The goal of this

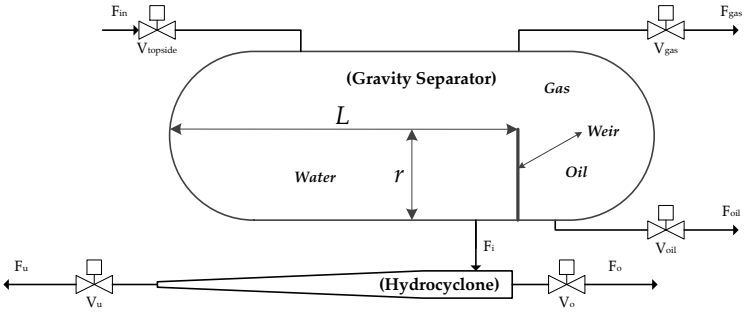

Fig. 3.4: Gravity separator and hydrocyclone units, illustrating the valves and the individual flows in the system. The gravity separator water chamber length L and the radius of the gravity separator r are shown.

was to validate the model's response to a step input in the disturbance. The experiment is set to reach a steady state value of $l = 150$mm, and at time 0s the inlet flow rate F_{in} is set to 0 l/s. The underflow valve V_u is at 44% openness throughout the test allowing some of the liquid to exit through it. With respect to the simulation the initial condition for l was the steady state value from the experiment, at $l = 150$mm.

From the system response in figure 3.5, it can be seen from experimental data that l decreases after the step input and it reaches steady state of $\approx$ 5mm after approximately 185 seconds. The placement of the lower Δ pressure measurement transmitter that is used for the level calculation, is at $\approx$ 5mm and therefore the minimum measured level is limited to $\approx$ 5mm. The simulation data deviates from the experimental data as l decreases, where the experimental data decreases exponentially faster than the simulation data. The simulation data for l reaches 0 mm after 250s. This is caused by the linearisation of the model around the operating point, transforming the separator into a rectangular cuboid instead of a cylinder. Thus the mass of liquid in the vessel is less than the mass of liquid estimated by the linearised model and this difference increases/decreases as the system moves the further away from the operating point. During nominal operation the linearisation has little significance as the system is controlled at a specific reference to ensure safe operation as explained in chapter 1 section 2.1. Figures 2 and 3 in paper F show how the level stays close to the reference point even during severe slugging operation.

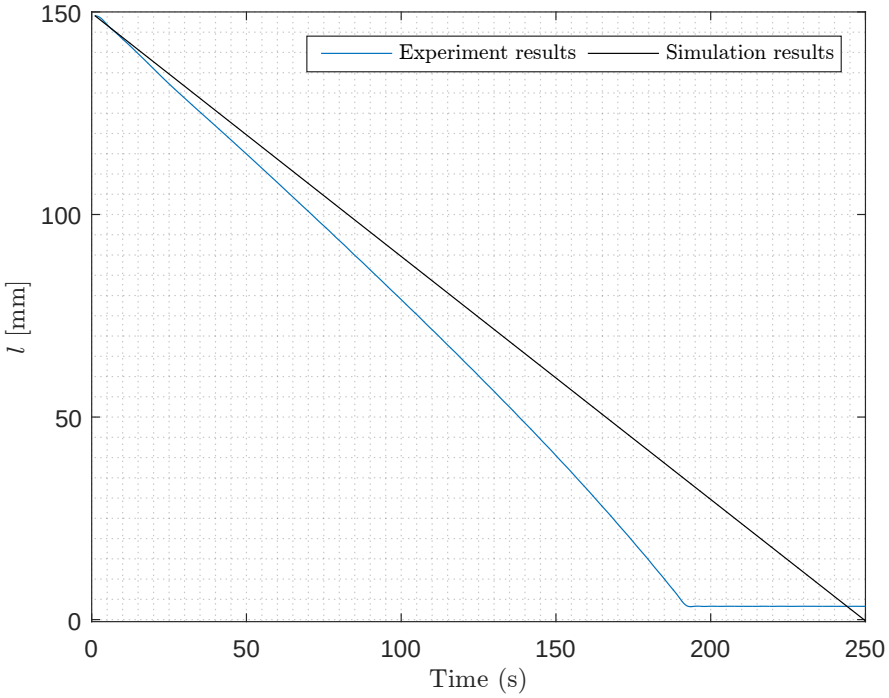

Fig. 3.5: Step response of the the gravity separator model, G_1.

4 De-oiling Process Model

With respect to the block diagram in figure 1.5 in chapter 1 section 2.3, the de-oiling process consists of the gravity separator and the hydrocyclone and has two manipulated variables, the underflow and overflow valves V_u and V_o. The two manipulated variables affect both the gravity separator and the hydrocyclone, with respect to their corresponding controlled variables l and PDR. V_o has a minor influence on the gravity separator and can be neglected in G_1, due to the dominance of V_u whose cross-sectional area is 25 times larger than that of V_o. Figure 3.6 shows a block diagram of the de-oiling process.

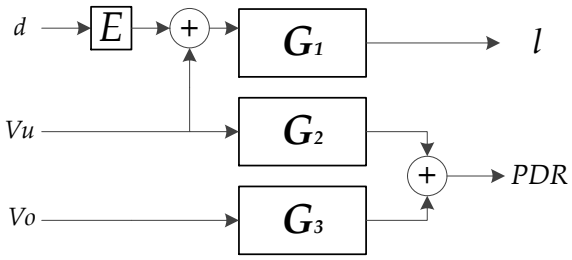

Fig. 3.6: MIMO model of the de-oiling process, consisting of three sub models, G_1 represents the gravity separator and G_2, G_3 represent the hydrocyclone. Figure from paper F

The de-oiling process model consists of two input variables V_u and V_o, and two output variables l and PDR. The de-oiling process model has five states, the first state is l with respect to the gravity separator. The additional four states belong to the two individual second order hydrocyclone models G_2 and G_3. The de-oiling process also has one unmeasured disturbance variable d, the disturbance is added to the input variable through a scaling factor E, where E is adjusted through trial and error. A state space representation of the model is shown in equation 3.9.

$$\begin{bmatrix} \dot{h} \\ \dot{x}_{V_u} \\ \dot{x}_{V_u} \\ \dot{x}_{V_o} \\ \dot{x}_{V_o} \end{bmatrix} = \begin{bmatrix} -1.23 \times 10^{-05} & 0 & 0 & 0 & 0 \\ 0 & -0.97 & -0.76 & 0 & 0 \\ 0 & 1.00 & 0 & 0 & 0 \\ 0 & 0 & 0 & -0.93 & -0.65 \\ 0 & 0 & 0 & 1 & 0 \end{bmatrix} \begin{bmatrix} h \\ x_{V_o} \\ x_{V_o} \\ x_{V_u} \\ x_{V_u} \end{bmatrix} + \begin{bmatrix} -0.0014 & 0 \\ -1 & 0 \\ 0 & 0 \\ 0 & 1 \\ 0 & 0 \end{bmatrix} \begin{bmatrix} V_u \\ V_o \end{bmatrix}$$

$$\begin{bmatrix} h \\ PDR \end{bmatrix} = \begin{bmatrix} 1 & 0 & 0 & 0 & 0 \\ 0 & 0 & 2.72 & 0 & 1.69 \end{bmatrix} \begin{bmatrix} h \\ x_{V_u} \\ x_{V_u} \\ x_{V_o} \\ x_{V_o} \end{bmatrix} \tag{3.9}$$

5 Summary of the De-oiling Process Model

Since the hydrocyclone and the gravity separator are physically coupled, a MIMO model was structured including a gravity separator model two hydrocyclone models. The hydrocyclone models were derived from parameter identification based on experimental data acquired on the scaled pilot plant. The final de-oiling process model is capable of representing the de-oiling systems manipulated variables and the output controlled variables which makes it highly applicable for evaluation and control development with respect to real offshore platforms.

Chapter 4

Robust Control of the De-Oiling Facility

This chapter describes the design of a suboptimal H_∞ robust control solution and the evaluation of its performance in comparison to a conventional PID control solution with respect to the de-oiling separation system.

1 PID Control Solution

The PID control solution was developed to be used as a benchmark for evaluating the H_∞ control solution.

The goal of the PID control solution was to mimic the existing offshore PID control solution, and was thus designed according to the general offshore control structure, described in chapter 1 section 2. The PID control solution consists of an interface level (l) feedback loop and a pressure drop ratio (PDR) feedback loop. The PID control solution as shown in the block diagram in figure 4.1, was implemented onto the scaled pilot plant. The behaviour of the PID control solution was compared to the offshore control solution, wherein the scaled pilot plant was subjected to severe fluctuating inlet flow rate F_{in} to recreate a phenomena analogous to offshore slugging flow. A comparison of the offshore facility and the scaled pilot plant during severe operations has been presented in figures [2] and [3] in paper F. When subjected to fluctuating F_{in}, the corresponding fluctuations in the l and the PDR of the proposed PID control solution resembles that of the offshore control solution. Thus the PID control solution could be used as a benchmark against which the proposed H_∞ control solution could be evaluated.

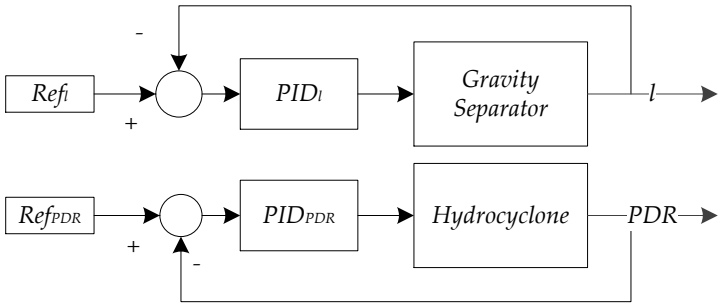

Fig. 4.1: Block diagram of the PID control solution for the de-oiling process.

2 H_∞ Control Solution

The process model of the de-oiling system, which was used to develop the H_∞ control solution, was derived in chapter 3 section 4 and its block diagram is shown in figure 3.6. The de-oiling process model has coupled dynamics with respect to the input variables V_u and V_o, which are not explicitly handled by the conventional PID control solution as mentioned in paper A. The de-oiling system has also been shown to be sensitive towards the inlet flow rate F_{in} in (80), (38) and (37). In many cases F_{in} is considered a disturbance, as it is not directly measured and when its values are available it is estimated based on density and pressure measurements (97), (27), (26) and (90). Thus the disturbance d is added to the part of the process model that describes the gravity separator due to its influence on l. In some cases the coupling dynamics are handled using an ad-hoc designed cascaded control solution as discussed in (37) where the system efficiency ϵ was improved by reducing the impact of the fluctuating F_{in} on the process.

This work, however, aims at using a methodological approach to develop a control solution that fulfils the following requirements:

- Improve the system's disturbance rejection, i.e. reduce the impact of a fluctuating F_{in} on the output variables and on the inlet flow rate to the hydrocyclone F_i, which was shown to have a significant influence on ϵ in (37).
- Take the coupling of the dynamics of the input variables V_u and V_o into

consideration, as it severely affects the transmission of the fluctuations occurring in F_{in} to F_i.

To comply with the second requirement, a MIMO model based control solution is preferred as it can handle the coupling of the dynamics of V_u and V_o. Based on the first requirement, a suboptimal H_∞ control solution was chosen due to its disturbance rejection properties. In addition, the suboptimal H_∞ control solution is an advantage as the de-oiling system does not require optimal reference tracking. This is beneficial with respect to the hydrocyclone's efficiency ϵ as it is sensitive towards fluctuation in F_i, as was shown in chapter 2 and paper E. And reduced reference tracking of the l could possibly reduce the transmission of fluctuations from F_{in} to F_i.

2.1 H_∞ Control Development

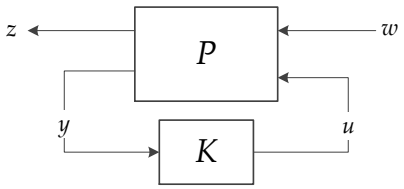

Fig. 4.2: General closed-loop inter-connection

Figure 4.2 represents a sketch of the general closed-loop interconnected structure where P is the plant and K is the controller. Applying this structure to the de-oiling process the interconnected system consists of the parameters defined in equations (4.1, 4.2, 4.3 and 4.4):

$$w = \begin{bmatrix} \Delta ref \\ \Delta d \end{bmatrix} = \begin{bmatrix} \begin{bmatrix} \Delta ref_l \\ \Delta ref_{\text{PDR}} \end{bmatrix} \\ \Delta d \end{bmatrix} \tag{4.1}$$

$$u = \begin{bmatrix} V_u \\ V_o \end{bmatrix} \tag{4.2}$$

$$z = \begin{bmatrix} l \\ \text{PDR} \end{bmatrix} \tag{4.3}$$

$$y = \begin{bmatrix} \Delta e_l \\ \Delta e_{\text{PDR}} \end{bmatrix} \tag{4.4}$$

The external inputs to the system defined by w are the reference Δref and the disturbance Δd, where the reference accounts for the interface level reference Δref_l and the PDR reference Δref_{PDR}. Here the Δ represents the linear

models deviation from the real value. The un-modelled disturbance and the reference are included into the design of the robust controller, since the aim is that it should include disturbance rejection and reference tracking properties. The output signals are defined as z, which consists of the two output variables l and PDR. The vector of control signals defined as u consists of input variables, the underflow valve V_u and the overflow valve V_o. The vector of the available measurements defined as y consists of the error signals Δe_l and Δe_{PDR}. The closed loop system P is set into a linear fractional transformation (LFT) framework:

$$\begin{aligned} \dot{x}(t) &= Ax(t) + B_1 w(t) + B_2 u(t) \\ z(t) &= C_1 x(t) + D_{11} w(t) + D_{12} u(t) \\ y(t) &= C_2 x(t) + D_{21} w(t) + D_{22} u(t) \end{aligned} \tag{4.5}$$

Where the A, B, C and D matrices are the state matrices of the linear MIMO de-oiling process model described in chapter 3. This leads to the following matrix representation of the system's interconnected matrix P:

$$\begin{bmatrix} \dot{x} \\ \hline \begin{bmatrix} z_1 \\ z_2 \end{bmatrix} \\ y \end{bmatrix} = \left[\begin{array}{c|cc} A & [0\ B] & B \\ \hline C & [0\ 0] & 0 \\ -C & [1\ 0] & 0 \end{array}\right] \begin{bmatrix} x \\ \hline \begin{bmatrix} ref \\ d \end{bmatrix} \\ u \end{bmatrix} \tag{4.6}$$

The interconnected closed loop system has the block diagram representation shown in figure 4.3.

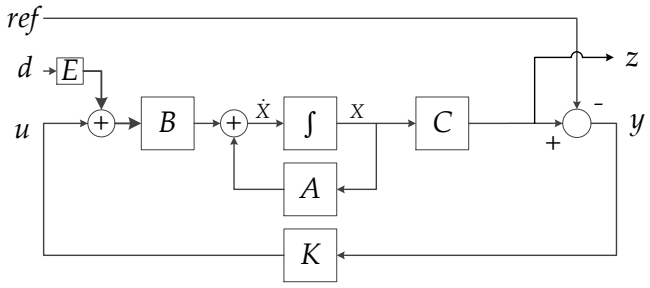

Fig. 4.3: Interconnected closed loop system, with the disturbance and reference that were introduced. Figure from paper F.

2.2 H_∞ Control Design Method

The suboptimal H_∞ control solution aims to minimize the infinity norm of the closed-loop transfer function $F_l(P, K)$ from w to z by designing a stable

dynamic controller K, subject to keeping the closed-loop system's internal stability. For a given $\gamma > 0$, a dynamic controller K is designed such that equation 4.7 is satisfied, subject to the internal stability constraint.

$$||F_l(P,K)||_\infty < \gamma \tag{4.7}$$

Before the controller K is obtained, several assumptions must be satisfied with respect to the generalised system P, refer to equation 4.5. The four assumptions are listed as follows:

1. (A, B_2) must be stabilizable and (C_2, A) must be detectable.
2. $D_{12} = \begin{bmatrix} 0 \\ I \end{bmatrix}$ and $D_{21} = \begin{bmatrix} 0 & I \end{bmatrix}$.
3. $\begin{bmatrix} A - j\omega I & B_2 \\ C_1 & D_{12} \end{bmatrix}$ has full column rank for all ω.
4. $\begin{bmatrix} A - j\omega I & B_1 \\ C_2 & D_{21} \end{bmatrix}$ has full row rank for all ω.

Where all four assumptions were satisfied with respect to P. The control problem can be solved using an iterative numerical approach namely the D-K iteration, which is done by iteratively solving for D and K, for more information refer to (84), (108), (107), (29) and (7).

3 Controller evaluation

The H_∞ control solution was implemented onto the scaled pilot plant and compared to the PID control solution. The two control solutions were subjected to several scenarios:

1. Reference step input, with respect to: l and PDR.
2. Fluctuating disturbance.
3. System start-up.
4. System shut-down.

The aim was to test the control solutions with respect to disturbance rejection and reference tracking. The results of all the experiments performed are presented in paper F, and one feature is evident in all the results, that is the PID control solution has a consistent reference tracking with respect to l, in comparison to the H_∞ control solution. This has a negative impact on the PDR, the F_i and the V_o as discussed in paper F. The result is that the

PDR heavily fluctuates during fluctuating F_{in} and the fluctuations in F_{in} are transmitted to the F_i. This leads to the saturation of V_o in many cases.

In figures 4.4 and 4.5 one of the scenarios has been illustrated with respect to the PID and H_∞ control solution, where the de-oiling facility is subjected to a severe condition when a fluctuating F_{in} is injected into the gravity separator. The F_{in} was carefully engineered to saturate the input variables.

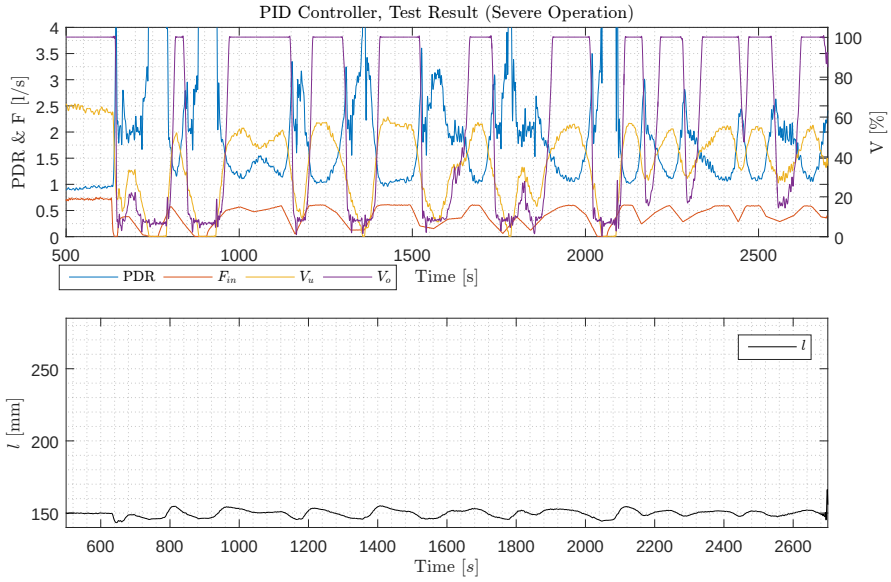

Fig. 4.4: PID control solution during severe operation, which involves the introduction of a fluctuating F_{in} to the gravity separator, Reference values: PDR = 2, l = 150mm.

The PID control solution was found to struggle with the fluctuating l, and in order to track the reference, the controller actuated V_u aggressively which directly impacted the PDR. The PDR loop of the PID control solution, equally compensated for the fluctuating PDR by aggressively actuating the V_o. This resulted in heavily oscillating l and PDR values, which is similar to the performance observed from offshore systems, refer to figure (2) in paper F for a comparison. In addition, it resulted in a repeated saturation of V_u and V_o, which could impact ϵ as described in chapter 1 section 2. Where saturation of V_o accounted for $\approx$ 45% of the total experiment time.

With respect to the H_∞ control solution, the valves were not saturated and in addition their fluctuation was reduced and their openness maintained within 30-60%, while sacrificing the reference tracking of the PDR and l.

This resulted in a more fluctuating l which is shown in the right plot in figure 4.6 where the H_∞ control solution has a larger steady state gain

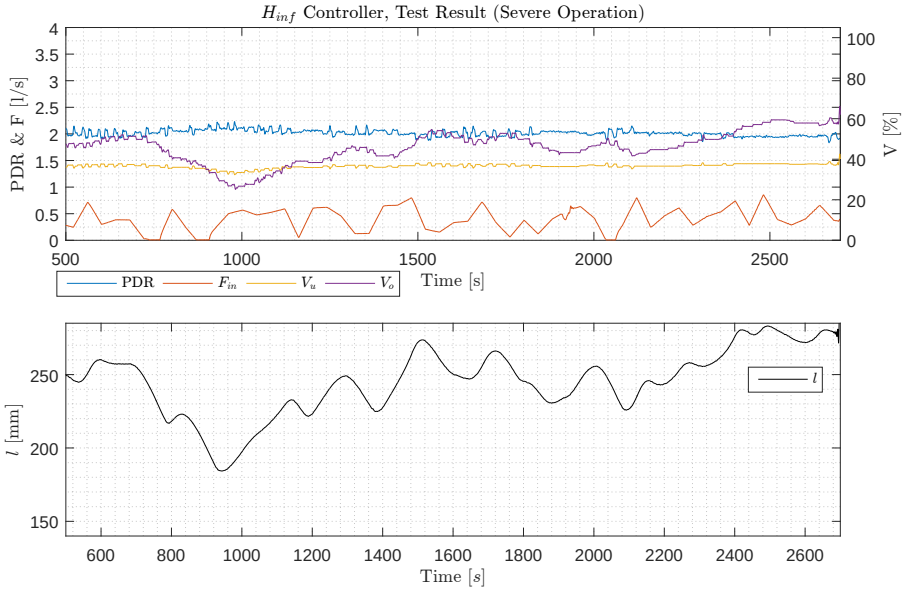

Fig. 4.5: H_∞ control solution during severe operation, which involves a fluctuating F_{in} to the gravity separator, Reference values: PDR = 2, l = 150mm.

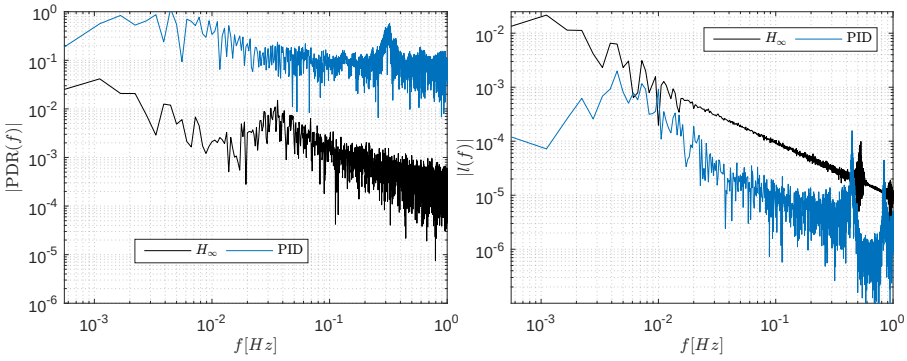

Fig. 4.6: Single sided amplitude spectrum of the PDR and the l with respect to the H_∞ and PID controller, unfiltered data has been used to compute the FFT.

than the PID control solution. The opposite is true for the PDR, where the steady state gain of the H_∞ control solution is lower than that of the PID control solution and it stays lower through the frequency band. Note that the fluctuating amplitudes of the PDR and l for the larger frequencies are predominantly caused by noise, i.e. above 0.01Hz.

4 Summary of the Robust Control of the De-Oiling Facility

With respect to the design requirements, stated in section 2 in this chapter, the first requirement which was disturbance rejection was significantly improved with the H_∞ control solution. The disturbance rejection is further demonstrated in figure 4.7, where the transmission of the fluctuating disturbance's impact from F_{in} to F_i is illustrated for both the H_∞ control solution and the PID control solution.

With respect to the PID control solution, the disturbance in F_{in} is directly transferred to F_i which can be seen from the frequency plot in the bottom sub-plot of figure 4.7. But, with the H_∞ control solution, the fluctuations from F_{in} are filtered out, and from the bottom sub-plot in figure 4.7 it is observed that the DC gain is reduced by three times and the frequency amplitude is strongly dampened until 0.04Hz, after which, F_i and F_{in} have a similar frequency profiles. The fluctuating frequency profile occurring beyond 0.04Hz is mostly due to measurement noise. The reason for the filtering effect is the relaxed actuation of V_u, which allows the l to fluctuate within the boundaries and thus attenuates the oscillation of F_{in}, and in this case the gravity separator acts as a low-pass filter.

In addition, the relaxed operation of the valves by the H_∞ control solution led to a longer operation during shut down and a faster start up time, which in real life scenarios can have positive economic benefits as described in paper F.

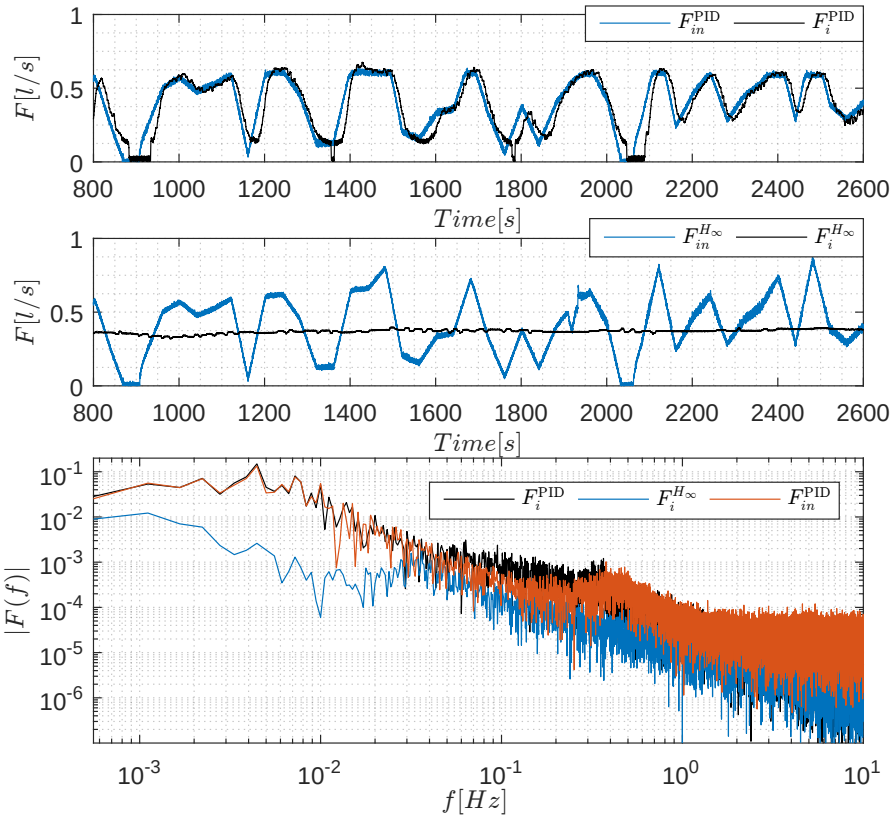

Fig. 4.7: Comparison of F_{in} and F_i, with respect to the H_∞ and the PID controller, the plots represent unfiltered data.

Chapter 5

Conclusion

This study was initiated to optimise the performance of offshore de-oiling systems. A scaled pilot plant was built to enable the emulation of offshore scenarios such that the solutions proposed by this study could be applicable to the Offshore Oil and Gas industry. A series of initial experimental investigations led to the identification of some of the issues affecting the performance of the de-oiling system.

The main achievements of this work are:

- Method of real-time Hydrocyclone efficiency (ϵ) monitoring, which can be used to evaluate the de-oiling process' performance.
- A model of the de-oiling process, combing the gravity separator and the hydrocyclone, which was used for control design.
- A sub-optimal H_∞ control solution, which handled the disturbances affecting the de-oiling system.

A lack of suitable real-time ϵ measurements led to an investigation of three monitoring technologies. A reliable real-time and on-line method of measuring ϵ was achieved using a florescence based monitor (TD-4100). The TD-4100 successfully tracked the dynamic behaviour of ϵ under changing input conditions. Such measurements are a crucial tool in evaluating the de-oiling system's operating performance and in the development of efficiency based feedback control of the de-oiling system; which is of both monetary and environmental benefit to the Oil and Gas industry. In addition through the experiments it was observed that the ϵ was more sensitive towards dynamic changes in the inlet flow rate to the hydrocyclone F_i than to dynamic changes in the pressure drop ratio (PDR). Which is consistent with the literature stating that ϵ is sensitive towards fluctuating flow rates.

Two additional instruments were tested, where the first, Electrical Resistivity Tomography (ERT), showed good potential in displaying a cross-sectional 2D image of the flow in the pipes, containing a conductive and non-conductive material but the low concentrations of OiW which are common on the hydrocyclone outlet were difficult to measure and this method was thus determined unsuited for the purpose of real-time measurements of OiW and thus ϵ. The second, a microscopy based technology (VIPA), performed well as a statistical droplet size analyser of the droplet sizes in the inlet and outlet of the hydrocyclone. Having a reliable measurement of the droplet sizes is crucial in understanding the operating contritions under which the de-oiling system is performing, as the droplet size is proportional to ϵ. This instrument performed poorly in the real-time perspective and it was only used for statistical analysis of droplet sizes. Further research in the application of TD-4100 for the purpose of OiW monitoring could be focused on repeatability of the measurements, the influence of oil type, droplet sizes and the inlet concentrations on the measurement. Calibration of the equipment has to be thoroughly explored as the technology is sensitive towards changes in the oil's chemical composition. A reduction in the length of side-stream pipes could reduce the delay in the measurements improving the response of the real-time measurements.

Another aspect of this work was improving the current control paradigms of the de-oiling process. Therefore the aim was to derive a control oriented MIMO model of the de-oiling system, which would include the coupling of the process dynamics into the model. As process models of the hydrocyclone were unavailable, a novel process model of a hydrocyclone was derived, using data collected on the scaled pilot plant to identify the parameters of the model. A MIMO model was constructed using the hydrocyclone model and a gravity separator model. This MIMO model provided a starting point for model based control solutions by modelling the dynamics of the physical coupling of the gravity separator and the hydrocyclone, which are believed to negatively affect the de-oiling systems performance if not addressed.

The investigation of a new control solution, which performed better under unknown and unmeasured fluctuating flow conditions was performed. The physical coupling was shown to be an important factor, as the input variables of the de-oiling system had coupled dynamics which reduced the performance of the current control solution, especially under severe input conditions. The proposed H_∞ control solution demonstrated significant disturbance attenuation and robustness in maintaining the system stable. The fluctuating flow rate's effect on the de-oiling system, measured as the transmission of the fluctuations through the gravity separator to the hydrocyclone, were reduced by three times during a specific case of severe operating conditions using the H_∞ control solution in comparison to the benchmark PID control solution. This indicates that with the H_∞ control solution the inflow

to the hydrocyclone can be maintained stable even during severe conditions, which is believed to improve the hydrocyclones separating performance under such conditions. The H_∞ control solution in addition allowed relaxed actuation of the manipulated variables, which in the case of offshore installations will result in reduced wear on the system, potentially prolonging the service life and thus lowering the maintenance costs. This performance of the H_∞ control solution demonstrates that the reference tracking performance of the current PID control solution, is in some cases, is not necessary to keep the system stable and in some cases affects the de-oiling system negatively. Further research is required, to establish the improvement of ϵ when using the H_∞ control solution instead of the benchmark PID control solution.

The work done in this thesis has introduced a new method of measuring the de-oiling efficiency in offshore systems, which has huge potential in the use as a feedback parameter and for evaluation and development of novel control methodologies. There is still more to be explored and perfected with the method and this work has provided a starting point. The work done with respect to the process MIMO model has aided in design of a new control solution for the de-oiling facility, initiating the design of model based control of de-oiling facilities. The H_∞ control solution has shown good initial results, and the introduction of robust control into the de-oiling process could improve the control of the current systems. The experiences with the de-oiling process have shown that it is a process which has scope for improvement and this work has provided some solutions to improve the current systems.

References

[1] "Danish production of oil, gas and water (danish energy agency)," https://ens.dk/en/our-services/oil-and-gas-related-data/monthly-and-yearly-production, Acssessed (09-11-2016).

[2] "Total petroleum and other liquids production (eia u.s. energy information administration)," http://www.eia.gov/beta/international, Acssessed (09-11-2016).

[3] H. K. Abdel-Aal, M. A. Aggour, and M. A. Fahim, *Petroleum and Gas Field Processing*, 2nd ed., ser. Chemical Industries. CRC Press, 2015.

[4] K. Arnold and M. Stewart, *Surface Production Operations: Design of Oil-Handling Systems and Facilities*, 2nd ed. Butterworth-Heinemann, 1999, vol. 1.

[5] B. Bailey, M. Crabtree, J. Tyrie, J. Elphick, F. Kuchuk, C. Romano, and L. Roodhart, "Water control," *Oilfield Review*, vol. 12, no. 1, pp. 30–51, 2000.

[6] T. Bakke, J. Klungsøyr, and S. Sanni, "Environmental impacts of produced water and drilling waste discharges from the norwegian offshore petroleum industry," *Marine environmental research*, vol. 92, pp. 154–169, 2013.

[7] G. Balas, R. Chiang, A. Packard, and M. Safonov, "Robust control toolbox," *User's Guide*, vol. 3, 2005.

[8] J. Bamberg, *British Petroleum and Global Oil 1950-1975: The Challenge of Nationalism*, ser. British Petroleum series. Cambridge University Press, 2000.

[9] J. Behin and M. Aghajari, "Influence of water level on oil–water separation by residence time distribution curves investigations," *Separation and purification technology*, vol. 64, no. 1, pp. 48–55, 2008.

[10] A. Belaidi and M. Thew, "The effect of oil and gas content on the controllability and separation in a de-oiling hydrocyclone," *Chemical Engineering Research and Design*, vol. 81, no. 3, pp. 305 – 314, 2003.

[11] M. V. Bram, A. A. Hassan, D. S. Hansen, P. Durdevic, S. Pedersen, and Z. Yang, "Experimental modeling of a deoiling hydrocyclone system," in *20th International Conference on Methods and Models in Automation and Robotics*. IEEE, 2015, pp. 1080–1085.

[12] F. Brette, B. Machado, C. Cros, J. P. Incardona, N. L. Scholz, and B. A. Block, "Crude oil impairs cardiac excitation-contraction coupling in fish," *Science*, vol. 343, no. 6172, pp. 772–776, 2014.

[13] Y. Çengel and J. Cimbala, *Fluid Mechanics: Fundamentals and Applications*, ser. McGraw-Hill series in mechanical engineering. McGraw-HillHigher Education, 2006.

[14] D. Colman and M. Thew, "The concept of hydrocyclones for separating light dispersants and a comparison of field data with laboratory work," *2nd International Conference on Hydrocyclones, Bath England*, pp. 217–232, 1984.

[15] J. Cullivan, R. Williams, T. Dyakowski, and C. Cross, "New understanding of a hydrocyclone flow field and separation mechanism from computational fluid dynamics," *Minerals Engineering*, vol. 17, no. 5, pp. 651–660, 2004.

[16] A. Dantas, A. Maitelli, F. Araujo, L. Linhares, and J. E. M. G. Pinto, "Evaluation and optimization of three-phase separator vessel controlled by pi controls applying particle swarm optimization," in *CONTROLO'2012, Funchal, Madeira Island*, 2012.

[17] J. A. Delgadillo and R. K. Rajamani, "A comparative study of three turbulence-closure models for the hydrocyclone problem," *International Journal of Mineral Processing*, vol. 77, no. 4, pp. 217–230, dec 2005.

[18] F. Di Meglio, G. O. Kaasa, N. Petit, and V. Alstad, "Reproducing slugging oscillations of a real oil well," in *Decision and Control (CDC), 2010 49th IEEE Conference on*. IEEE, 2010, pp. 4473–4479.

[19] J. G. Dueck, O. V. Matvienko, and T. Neesse, "Modeling of Hydrodynamics and Separation in a Hydrocyclone," *Theoretical Foundations of Chemical Engineering*, vol. 34, no. 5, pp. 428–438, 2000.

[20] H. Duhon, "Produced water treatment: Yesterday, today, and tomorrow," *Oil and Gas Facilities*, vol. 1, no. 1, pp. 29–30, 2012.

[21] G. Durell, T. Røe Utvik, S. Johnsen, T. Frost, and J. Neff, "Oil well produced water discharges to the North Sea. Part I: Comparison of deployed mussels (Mytilus edulis), semi-permeable membrane devices, and the DREAM model predictions to estimate the dispersion of polycyclic aromatic hydrocarbons," *Marine Environmental Research*, vol. 62, no. 3, pp. 194–223, 2006.

[22] T. Dyakowski, A. Nowakowski, W. Kraipech, and R. Williams, "A three dimensional simulation of hydrocyclone behaviour," in *Second International Conference on CFD in the Minerals and Process Industries. CSIRO, Melbourne, Australia*, 1999, pp. 205–210.

[23] T. Dyakowski and R. Williams, "Modelling turbulent flow within a small-diameter hydrocyclone," *Chemical Engineering Science*, vol. 48, no. 6, pp. 1143–1152, 1993.

[24] A. Fakhru'l-Razi, A. Pendashteh, L. C. Abdullah, D. R. A. Biak, S. S. Madaeni, and Z. Z. Abidin, "Review of technologies for oil and gas produced water treatment," *Journal of hazardous materials*, vol. 170, no. 2, pp. 530–551, 2009.

[25] M. Farghaly, V. Golyk, G. Ibrahim, M. Ahmed, and T. Neesse, "Controlled wash water injection to the hydrocyclone underflow," *Minerals Engineering*, vol. 23, no. 4, pp. 321–325, 2010.

[26] J. M. Godhavn, M. P. Fard, and P. H. Fuchs, "New slug control strategies, tuning rules and experimental results," *Journal of process control*, vol. 15, no. 5, pp. 547–557, 2005.

[27] J. M. Godhavn, S. Strand, and G. Skofteland, "Increased oil production by advanced control of receiving facilities," *IFAC Proceedings Volumes*, vol. 38, no. 1, pp. 567–572, 2005.

[28] S. Grady, G. Wesson, M. Abdullah, and E. Kalu, "Prediction of 10-mm hydrocyclone separation efficiency using computational fluid dynamics," *Filtration & separation*, vol. 40, no. 9, pp. 41–46, 2003.

[29] D. Gu, P. Petkov, and M. M. Konstantinov, *Robust control design with MATLAB®*, 2nd ed. Springer Science & Business Media, 2005.

[30] J. Hargreaves and R. Silvester, "Computational fluid dynamics applied to the analysis of deoiling hydrocyclone performance," *Chemical engineering research & design*, vol. 68, no. 4, pp. 365–383, 1990.

[31] L. Hasselberg, S. Meier, and A. Svardal, "Effects of alkylphenols on redox status in first spawning atlantic cod (gadus morhua)," *Aquatic Toxicology*, vol. 69, no. 1, pp. 95–105, 2004.

[32] J. J. Hayes, W. C. Carroll, D. W. J. Fothergill, and G. J. J. Prendergast, "Hydrocyclones for Treating Oily Water: Development and Field Testing in Bass Strait," *Offshore Technology Conference*, pp. 549–556, 1985.

[33] P. He, M. Salcudean, and I. Gartshore, "A numerical simulation of hydrocyclones," *Chemical Engineering Research and Design*, vol. 77, no. 5, pp. 429–441, 1999.

[34] B. T. Hjertaker, G. A. Johansen, and P. Jackson, "Level measurement and control strategies for subsea separators," *Journal of Electronic Imaging*, vol. 10, no. 3, pp. 679–689, 2001.

[35] K. T. Hsieh and R. K. Rajamani, "Mathematical model of the hydrocyclone based on physics of fluid flow," *AIChE Journal*, vol. 37, no. 5, pp. 735–746, may 1991.

[36] T. Husveg, "Operational Control of Deoiling Hydrocyclones and Cyclones for Petroleum Flow Control," PhD Thesis, University of Stavanger, 2007.

[37] T. Husveg, O. Johansen, and T. Bilstad, "Operational control of hydrocyclones during variable produced water flow rates—frøy case study," *SPE Production & Operations*, vol. 22, no. 03, pp. 294–300, 2007.

[38] T. Husveg, O. Rambeau, T. Drengstig, and T. Bilstad, "Performance of a deoiling hydrocyclone during variable flow rates," *Minerals Engineering*, vol. 20, no. 4, pp. 368–379, Apr. 2007.

[39] K. Hylland, "Polycyclic aromatic hydrocarbon (pah) ecotoxicology in marine ecosystems," *Journal of Toxicology and Environmental Health, Part A*, vol. 69, no. 1-2, pp. 109–123, 2006.

[40] I. Ismail, J. Gamio, S. Bukhari, and W. Yang, "Tomography for multi-phase flow measurement in the oil industry," *Flow Measurement and Instrumentation*, vol. 16, no. 2-3, pp. 145–155, apr 2005.

[41] E. Jahanshahi and S. Skogestad, "Simplified dynamical models for control of severe slugging in multiphase risers," *IFAC Proceedings Volumes*, vol. 44, no. 1, pp. 1634–1639, 2011.

[42] E. Jahanshahi, S. Skogestad, and A. H. Helgesen, "Controllability analysis of severe slugging in well-pipeline-riser systems," *IFAC Proceedings Volumes*, vol. 45, no. 8, pp. 101–108, 2012.

[43] B. Jansen, M. Dalsmo, L. Nøkleberg, K. Havre, V. Kristiansen, and P. Lemetayer, "Automatic Control of Unstable Gas Lifted Wells," *SPE Annual Technical Conference and Exhibition*, pp. 1–9, 1999.

[44] A. J. Jaworski and G. Meng, "On-line measurement of separation dynamics in primary gas/oil/water separators: challenges and technical solutions—a review," *Journal of Petroleum Science and Engineering*, vol. 68, no. 1, pp. 47–59, 2009.

[45] G. A. Johansen, T. Frøystein, B. T. Hjertaker, and Ø. Olsen, "A dual sensor flow imaging tomographic system," *Measurement Science and Technology*, vol. 7, no. 3, pp. 297–307, Mar 1996.

[46] JORIN, "Offshore water treatment plant optimisation and chemical trials using the jorin vipa," pp. 1–20, Acssessed (01-12-2016). [Online]. Available: http://www.jorin.co.uk/

[47] L. W. Lake and P. B. Venuto, "A niche for enhanced oil recovery in the 1990s," *Oil & Gas Journal*, vol. 88, no. 17, pp. 62–67, 1990.

[48] N. Meldrum, "Hydrocyclones: A Solution to Produced-Water Treatment," *SPE Production Engineering*, vol. 3, pp. 669 – 676, November, 1988.

[49] J. Merrill and L. Robinson, "Chapter 7 - shale shakers," in *Drilling Fluids Processing Handbook*, B. ASME, Ed. Burlington: Gulf Professional Publishing, 2005, pp. 111 – 182.

[50] Miljøstyrelsen, "Status for den danske offshorehandlingsplan til udgangen af 2009," *Ministry of Environment and Food of Denmark*, pp. 1–36, Acssessed (01-11-2016). [Online]. Available: http://mst.dk/media/mst/68095/StatusrapportOHP20101008.pdf

[51] Miljøstyrelsen, "Afsluttende rapport for de danske offshorehandlingsplaner 2005 - 2010," *Ministry of Environment and Food of Denmark*, pp. 1–42, Acssessed (01-11-2016). [Online]. Available: http://mst.dk/service/nyheder/nyhedsarkiv/2013/dec/afsluttende-rapport-for-de-danske-offshorehandlingsplaner/

[52] L. Minkov and J. Dueck, "Cfd-modeling of a flow in a hydrocyclone with an additional water injector," *Computer Research and modeling*, vol. 3, no. 1, pp. 63–76, 2011.

[53] S. Mokhatab, W. A. Poe, and J. Y. Mak, *Handbook of Natural Gas Transmission and Processing: Principles and Practices*. Elsevier Science, 2015.

[54] T. C. Monredon, K. T. Hsieh, and R. K. Rajamani, "Fluid flow model of the hydrocyclone: an investigation of device dimensions," *International Journal of Mineral Processing*, vol. 35, no. 1-2, pp. 65–83, jun 1992.

[55] B. R. Munson, D. F. Young, T. H. Okiishi, and W. W. Huebsch, *Fundamentals of fluid mechanics*, 6th ed. John Wiley and Sons Ltd, 2010.

[56] T. Neesse and F. Donhauser, "Advances in the theory and practice of hydrocyclone technique," *AT Aufbereitungs Technik*, vol. 41, no. 9, pp. 403–408, 2000.

[57] T. Neesse, V. Golyk, P. Kaniut, and V. Reinsch, "Hydrocyclone control in grinding circuits," *Minerals engineering*, vol. 17, no. 11, pp. 1237–1240, 2004.

[58] T. Neesse, M. Schneider, J. Dueck, V. Golyk, S. Buntenbach, and H. Tiefel, "Hydrocyclone operation at the transition point rope/spray discharge," *Minerals Engineering*, vol. 17, no. 5, pp. 733–737, 2004.

[59] T. Neesse, M. Schneider, V. Golyk, and H. Tiefel, "Measuring the operating state of the hydrocyclone," *Minerals Engineering*, vol. 17, no. 5, pp. 697–703, 2004.

[60] J. Neff, K. Lee, and E. M. DeBlois, *Produced Water: Overview of Composition, Fates, and Effects*. New York, NY: Springer New York, 2011, pp. 3–54.

[61] T. S. Nel, *Good Practice Guide: An Introduction to Produced Water Management*, March 24, 2011.

[62] A. F. Nowakowski, W. Kraipech, R. A. Williams, and T. Dyakowski, "Hydrodynamics of a hydrocyclone based on a three-dimensional multi-continuum model," *Chemical engineering journal*, vol. 80, no. 1-3, pp. 275–282, dec 2000.

[63] A. Nowakowski, J. Cullivan, R. Williams, and T. Dyakowski, "Application of cfd to modelling of the flow in hydrocyclones. is this a realizable option or still a research challenge?" *Minerals Engineering*, vol. 17, no. 5, pp. 661–669, 2004.

[64] Oil & Gas UK, "Environment Report 2015," pp. 1–64, Acssessed (01-11-2016). [Online]. Available: http://oilandgasuk.co.uk/wp-content/uploads/2015/11/Environment-Report-2015-FINAL-for-PDF-reduced.pdf

[65] S. Ookawara, T. Ishikawa, and K. Ogawa, "Applicability of a miniaturized micro-separator/classifier to oil-water separation," *Chemical engineering & technology*, vol. 30, no. 3, pp. 316–321, 2007.

[66] S. Pedersen, P. Durdevic, and Z. Yang, "Challenges in slug modeling and control for offshore oil and gas productions: A review study," *International Journal of Multiphase Flow*, vol. 88, pp. 270 – 284, 2017.

[67] S. Pedersen, P. Durdevic, K. Stampe, S. L. Pedersen, and Z. Yang, "Experimental study of stable surfaces for anti-slug control in multi-phase flow," *International Journal of Automation and Computing*, vol. 13, no. 1, pp. 81–88, 2016.

[68] S. Pedersen, P. Durdevic, and Z. Yang, "Review of Slug Detection, Modeling and Control Techniques for Offshore Oil and Gas Production Processes," *IFAC-PapersOnLine*, vol. 48, no. 6, pp. 89–96, 2015.

[69] S. Pedersen, C. Mai, L. Hansen, P. Durdevic, and Z. Yang, "Online Slug Detection in Multi-phase Transportation Pipelines Using Electrical Tomography," *IFAC-PapersOnLine*, vol. 48, no. 6, pp. 159–164, 2015.

[70] S. Pedersen, K. Stampe, S. L. Pedersen, P. Durdevic, and Z. Yang, "Experimental Study of Stable Surfaces for Anti-Slug Control in Multi-phase Flow," in *Proceedings of the 20th International Conference on Automation and Computing, ICAC 2014*, 2014, pp. 43–48.

[71] K. A. Pericleous, "Mathematical simulation of hydrocyclones," *Applied Mathematical Modelling*, vol. 11, no. 4, pp. 242–255, 1987.

[72] R. K. Rajamani and J. A. Herbst, "Optimal control of a ball mill grinding circuit. grinding circuit modeling and dynamic simulation," *Chemical Engineering Science*, vol. 46, no. 3, pp. 861–870, 1991.

[73] K. Rietema and S. I. R. Maatschappij, "Performance and design of hydrocyclones—iii: Separating power of the hydrocyclone," *Chemical Engineering Science*, vol. 15, no. 3-4, pp. 310–319, 1961.

[74] A. G. Ryder, P. Iwanski, and L. Montanari, "Light emissions from oil," *Upstream*, vol. 2, pp. 9–14, 2004.

[75] I. Sandrea and R. Sandrea, "Global oil reserves: Recovery factors leave vast target for eor technologies," *Oil and Gas Journal*, vol. 105, no. 41, p. 44, 2007.

[76] A. Sausen, M. de Campos, and P. Sausen, *The Slug Flow Problem in Oil Industry and Pi Level Control*. INTECH Open Access Publisher, 2012.

[77] A. F. Sayda and J. H. Taylor, "Modeling and control of three-phase gravilty separators in oil production facilities," in *2007 American Control Conference*. IEEE, 2007, pp. 4847–4853.

[78] Z. Schmidt, D. R. Doty, and K. Dutta-Roy, "Severe slugging in offshore pipeline riser-pipe systems," *Society of Petroleum Engineers Journal*, vol. 25, no. 01, pp. 27–38, 1985.

[79] M. Schneider and T. Neesse, "Overflow-control system for a hydrocyclone battery," *International Journal of Mineral Processing*, vol. 74, pp. 339–343, 2004.

[80] M. Schubert, F. Skilbeck, and H. Walker, "Liquid hydrocyclone separation systems," in *Hydrocyclones*. Springer, 1992, pp. 275–293.

[81] V. Siangsanun, C. Guigui, J. Morchain, P. Marteil, C. Levecq, C. Puprasert, and G. Hebrard, "Velocity measurement in the hydrocyclone by oil droplet, doppler ultrasound velocimetry, and cfd modelling," *The Canadian Journal of Chemical Engineering*, vol. 89, no. 4, pp. 725–733, 2011.

[82] A. Silset, G. R. Flåten, H. Helness, E. Melin, G. Øye, and J. Sjöblom, "A multivariate analysis on the influence of indigenous crude oil components on the quality of produced water. comparison between bench and rig scale experiments," *Journal of Dispersion Science and Technology*, vol. 31, no. 3, pp. 392–408, 2010.

[83] A. B. Sinker, M. Humphris, and N. Wayth, "Enhanced deoiling hydrocyclone performance without resorting to chemicals," in *Offshore Europe Oil and Gas Exhibition and Conference, Aberdeen, United Kingdom*. Society of Petroleum Engineers, 7-10 September, 1999.

[84] S. Skogestad and I. Postlethwaite, *Multivariable feedback control: analysis and design*. Wiley New York, 2007, vol. 2.

[85] M. Slack, S. Del Porte, and M. Engelman, "Designing automated computational fluid dynamics modelling tools for hydrocyclone design," *Minerals Engineering*, vol. 17, no. 5, pp. 705–711, 2004.

[86] E. D. Sloan, C. A. Koh, and A. Sum, *Natural gas hydrates in flow assurance*. Gulf Professional Publishing, 2010.

[87] I. Smyth, M. Thew, and D. Colman, "The effect of split ratio on heavy dispersive liquid-liquid separation in hydrocyclones," *2nd International Conference on Hydrocyclones, Bath England*, pp. 177–190, 1984.

[88] L. Stasiuk and L. Snowdon, "Fluorescence micro-spectrometry of synthetic and natural hydrocarbon fluid inclusions: crude oil chemistry, density and application to petroleum migration," *Applied Geochemistry*, vol. 12, no. 3, pp. 229–241, 1997.

[89] M. T. Stephenson, *A Survey of Produced Water Studies*. Boston, MA: Springer US, 1992, pp. 1–11.

[90] E. Storkaas, "Stabilizing Control and Controllability: Control Solutions to Avoid Slug Flow in Pipeline-Riser Systems," Ph.D. dissertation, Fakultet for naturvitenskap og teknologi, NTNU, 2005.

[91] L. Svarovsky, *Solid-liquid Separation*, 4th ed. Butterworth-heinemann, 2000.

[92] M. T. Thew, "Cyclones for oil/water separation," in *Encyclopaedia of Separation Science*, 4th ed. Academic Press, 2000, pp. 1480–1490.

[93] M. Thew, "Hydrocyclone redesign for liquid-liquid separation," *Chemical Engineer (London)*, no. 427, pp. 17–23, 1986.

[94] M. Thew and I. Smyth, "Development and performance of oil-water hydrocyclone separators: a review," 1998.

[95] M. Thew, C. Wright, and D. Colman, "R.t.d. characteristics of hydrocyclones for the separation of light dispersions," *2nd International Conference on Hydrocyclones, Bath England*, pp. 163–176, 1984.

[96] K. Thomas, K. Langford, K. Petersen, A. Smith, and K. Tollefsen, "Effect-directed identification of naphthenic acids as important in vitro xeno-estrogens and anti-androgens in north sea offshore produced water discharges," *Environmental science & technology*, vol. 43, no. 21, pp. 8066–8071, 2009.

[97] R. Thorn, G. A. Johansen, and E. A. Hammer, "Three-Phase Flow Measurement in the Offshore Oil Industry Is There a Place for Process Tomography ?" *1st World Congress on Industrial Process Tomography*, pp. 228–235, 1999.

[98] E. Tzimas, A. Georgakaki, C. G. Cortes, and S. Peteves, "Enhanced oil recovery using carbon dioxide in the european energy system," *Report EUR*, vol. 21895, no. 6, 2005.

[99] J. A. Veil, M. G. Puder, D. Elcock, and R. J. Redweik Jr, "A white paper describing produced water from production of crude oil, natural gas, and coal bed methane," *Argonne National Laboratory, Technical Report*, vol. 63, 2004.

[100] C. Völcker, J. B. Jørgensen, and P. G. Thomsen, "Production optimization of oil reservoirs," Ph.D. dissertation, Technical University of Denmark, Center for Energy Resources Engineering, 2011.

[101] J. M. Walsh, "The savvy separator series: Part 5. the effect of shear on produced water treatment." *Society of Petroleum Engineers*, 2016.

[102] D. Wolbert, F. Ma, B, Y. Aurelle, and J. Seureau, "Efficiency estimation of liquid-liquid hydrocyclones using trajectory analysis," *AIChE Journal*, vol. 41, no. 6, pp. 1395–1402, 1995.

[103] M. Yang, *Measurement of Oil in Produced Water*. New York, NY: Springer New York, 2011, pp. 57–88.

[104] Z. Yang, S. Pedersen, P. Durdevic, C. Mai, L. Hansen, K. L. Jepsen, A. Aillos, and A. Andreasen, "Plant-wide Control Strategy for Improving Produced Water Treatment," *Proceedings of 2016 International Field Exploration and Development Conference (IFEDC)*, 2016.

[105] Z. Yang, J. P. Stigkjær, and B. Løhndorf, "Plant-wide control for better de-oiling of produced water in offshore oil & gas production," *IFAC Proceedings Volumes*, vol. 46, no. 20, pp. 45–50, 2013.

[106] G. Young and W. Wakley, "Oil-water separation using hydrocyclones: An experimental search for optimum dimensions," *Journal of Petroleum Science and Engineering*, vol. 11, no. 93, pp. 37–50, 1994.

[107] K. Zhou and J. C. Doyle, *Essentials of robust control*. Prentice hall, New Jersey, 1998.

[108] K. Zhou, J. C. Doyle, and K. Glover, *Robust and optimal control*. Prentice hall, New Jersey, 1996.

Part II

Papers

Paper A

Challenges in Modeling and Control of Offshore De-oiling Hydrocyclone Systems

Petar Durdevic, Simon Pedersen and Zhenyu Yang

The paper has been presented at:
Advanced Control and Diagnosis – 13th ACD 2016, 17 - 18 November 2016, Lille, France
Published in:
Journal of Physics: Conference Series, Volume 783, conference 1; doi: 783 (2017) 012048

The layout has been revised.

Challenges in Modelling and Control of Offshore De-oiling Hydrocyclone Systems

Petar Durdevic, Simon Pedersen and Zhenyu Yang
Aalborg University, Esbjerg Campus, Niels Bohrs Vej 8, 6700 Esbjerg, Denmark
E-mail: pdl@et.aau.dk, spe@et.aau.dk, yang@et.aau.dk

Abstract. Offshore de-oiling installations are facing an increasing challenge with regards to removing oil residuals from produced water prior to discharge into the ocean. The de-oiling of produced water is initially achieved in the primary separation processes using gravity-based multi-phase separators, which can effectively handle large amounts of oil-well fluids but may struggle with the efficient separation of small dispersed oil particles. Thereby hydrocyclone systems are commonly employed in the downstream Produced Water Treatment (PWT) process for further reducing the oil concentration in the produced water before it can be discharged into the ocean. The popularity of hydrocyclone technology in the offshore oil and gas industry is mainly due to its rugged design and low maintenance requirements. However, to operate and control this type of system in an efficient way is far less simple, and alternatively this task imposes a number of key control challenges. Specifically, there is much research to be performed in the direction of dynamic modelling and control of de-oiling hydrocyclone systems. The current solutions rely heavily on empirical trial-and-error approaches. This paper gives a brief review of current hydrocyclone control solutions and the remaining challenges and includes some of our recent work in this topic and ends with a motivation for future work.

1. Introduction

Many matured offshore oilfields have a high water content and the pumped well-fluids in some cases contain more than 90 % water, and this water is referred to as *produced water*. It has been surveyed that globally around 250 million barrels of produced water along with 80 million barrels of oil is produced each day [1]. This high water-cut situation requires effective Produced Water Treatment (PWT) to achieve pure oil product on the platforms, but also to fulfil governmental effluent discharge regulations. For instance, the current limitation for hydrocarbon discharge in North Sea is set at 30 mg/l (30ppm) [2]. It has been shown that the discharged hydrocarbons could have a negative effect on the surrounding marine life, for example a small concentration of Polycyclic Aromatic Hydrocarbons (PAH) as low as 100 parts per billion (PPB) can affect fish development [3]. Produced water can also contain different harmful materials, such as metals (barium and zinc), benzene, toulene, ethylbenzene xylene (BTEX), naphthalene, phenanthrene, dibenzothiophene (NPD), polyaromatic hydrocarbons (PAHs) and phenols etc. [4], and hence direct discharge of the produced water is strictly prohibited in order to protect the marine life and environment.

In offshore installations, on-site cleaning of produced water, which is referred to as PWT, is needed as it is expensive to send such large quantities of water to the onshore separation facilities [5]. However, due to the space and weight restrictions on offshore installations, the

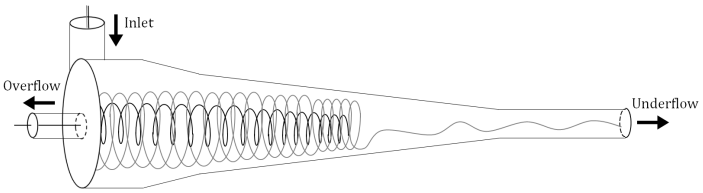

Figure 1: Hydrocyclone Separation principle - the grey/black line indicates the water/oil flow

installation and operation of offshore PWT must be very cost-effective while providing sufficient capability and quality. Moreover, due to the harsh weather and marine conditions, especially in the North Sea, the PWT requires robust installations and instrumentation. Even though almost all PWT of the current offshore installations perform to an acceptable level, the consistent increase in water-cut will sooner or later bring extra difficulties and challenges to the current PWT technologies and systems.

To achieve the required effluent discharge concentrations for oil in the produced water, the separation of water and hydrocarbon products is generally achieved in two stages. The initial separation processes uses gravity-based multi-phase separators, which can effectively handle large amounts of well-fluids, but cannot efficiently separate small dispersed oil droplets. The next stage in separation is by the hydrocyclones that reduce the dispersed oil content to the required levels before the effluent is discharged into the ocean.

It is common knowledge that the hydrocyclone's de-oiling performance is very sensitive to fluctuating inflow rates [6], [7]. The efficient operation and control of this type of system imposes a number of key control challenges. The current modelling and analysis heavily rely on CFD-based approaches, and the control development heavily relies on empirical trial-and-error approaches. We found that there is lack of research in cost-effective modelling and control of de-oiling hydrocyclone dynamic systems. In 2013 Aalborg University in collaboration with one of the Danish oil operators and an oil service company, launched a research project - PDPWAC - with one of the research objectives being the optimization of the hydrocyclone-based PWT using plant-wide control strategy. This paper gives a brief review of modelling and control of offshore de-oiling hydrocyclone systems, presents some of our work in this direction and points out some remaining challenges.

The rest of this paper is organized as follows: Section 2 introduces the basic configuration and operating principle of typical de-oiling hydrocyclone systems; section 3 gives a brief overview of hydrocyclone modelling methods and the challenges that lie within; section 4 presents some key challenges in the control of hydrocyclone systems, along with some latest solutions from our work; finally section 5 concludes this work.

2. Hydrocyclone Principle and Control

Hydrocyclone technology emerged in the oil industry in the 1980's and has been increasingly used since then. Hydrocyclone systems represent more than 90% of current de-oiling facilities in the offshore oil and gas installations [8], and this popularity is mainly due to its simplicity and ruggedness [9].

2.1. Hydrocyclone Configuration & Principle

A typical de-oiling hydrocyclone consists of one or more tangential inlets, where the produced water flowing out of the separator stack enters the hydrocyclone facilities. The mixed water and

oil are accelerated in a circular movement inside the cylindrical chamber as shown in Figure 1. As the mixture rotates, the centripetal force separates these two phases with the heavier phase (water) moving towards the walls while the lighter phase (dispersed oil) moves to the cylinder's centre, where eventually an oil core is generated. Besides the cylindrical chamber segment, a hydrocyclone also consists of two conical sections and two outlets, namely *overflow* and *underflow* outlets. Ideally, the oil trapped in the oil core will gradually exit through the overflow outlet, while the water will go through the underflow outlet [7]. In practical applications, especially for the offshore situations, a number of hydrocyclone liners are need to be stacked in parallel inside one holding vessel, so that the handling capability of produced water can be significantly increased without requiring a lot of installation space [9].

2.2. Hydrocyclone control

An offshore installation relevant to PWT is sketched in Figure 2, where the separator and the hydrocyclone are directly connected. Normally, the underflow control valve located at the hydrocyclone's underflow outlet is used for the purpose of separator water level control ("LC" in Figure 2). The hydrocyclone separation performance is controlled via the *PDR control* ("PDR" in Figure 2) loop by manipulating the overflow control valve located at the hydrocyclone's overflow outlet, where PDR is the Pressure Drop Ratio over the hydrocyclone's outlets and inlet, i.e.,

$$PDR = \frac{P_i - P_o}{P_i - P_u} \tag{1}$$

Where P_i is the measured inlet pressure, and P_u/P_o is the the underflow/overflow pressure measurement. It has been experimentally discovered that the PDR and the flow-split inside the hydrocyclone are closely linearly-dependent [10]. The flow-split directly determines the amounts of flow going through the underflow and the overflow outlets, respectively. To maintain a satisfactory separation efficiency, the flow-split is crucial for hydrocyclone's operation, as it will determine how much oil and water will be able to escape through the under- and over-flow respectively.

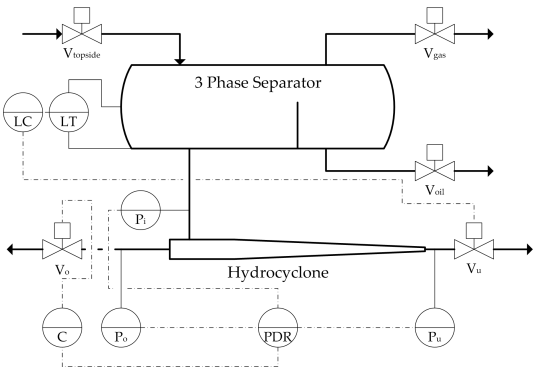

Figure 2: Two control loops in a typical control structure.

It can be observed that the dynamics of the hydrocyclone's PDR and the separator's level are physically coupled and thereby may affect each other's performance. Furthermore, the separator level control is often disturbed by the varying inflow rate to the separator system. A typical

influence to the separator is slugging inflow which could be caused by the riser configuration or hydrodynamics [11], [12], [13] and [14]. A measured severe slug that occurred at one installation in North Sea is illustrated in Figure 3, where the severe slug is indicted by large oscillating pressure measurements at the riser top. All these issues lay out many challenges to the efficient and reliable control of the hydrocyclone .

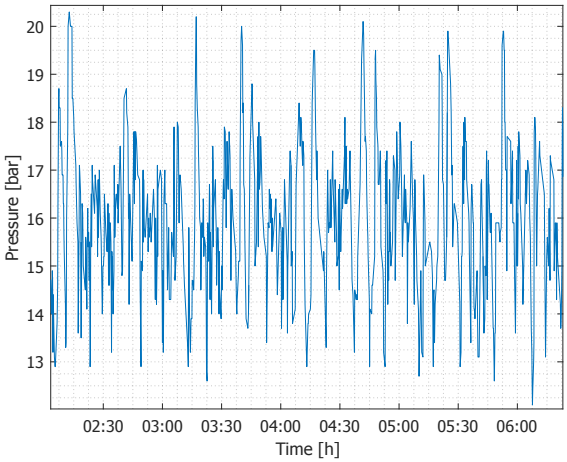

Figure 3: One example of riser-induced slugging flow indicated by topside pressure fluctuations

3. Modeling De-oiling Hydrocyclone Operation

It has been observed that there has been little work done focusing on the control-oriented modelling of de-oiling hydrocyclone systems, instead, there are plenty of different models and analysis based on Computational Fluid Dynamics (CFD) technology [15, 16, 17]. Although CFD-based models have a sophisticated capability and power in illustrating detailed information, they are not oriented or suited for the purpose of control design due to their complexity. For dynamic control purposes simple dynamic models, which can express the key dynamic characteristics between the system's inputs and outputs, are preferred instead.

The first-principle-based modelling is investigated in [18] for a solid-liquid hydrocyclone setup, and this work is further extended in [19]. [20] described a solid-liquid hydrocyclone with a simple dynamic model by using transport balance by considering the slip velocity and turbulent particle diffusivity, based on the $k-\eta$ model developed in [21] and [22]. However, the extension of these models to handling liquid-liquid de-oiling hydrocyclone is not clear. Similar situation exists regarding the work done in [20], which only focused on the solid-liquid hydrocyclone and also assumed that the inlet flow is fed through the entire top section of the hydrocyclone. As many of these relatively simple models (when compared to CFD-based models) are regarding solid-liquid separating cyclones, the correlation between solid-liquid cyclone separation and liquid-liquid hydrocyclone separation needs further investigations before we can answer whether some models developed for one type of cyclone system could be applied or extended to another type of cyclone system.

In our previous work a black-box modelling method was used for a de-oiling hydrocyclone setup in [23] by regarding the PDR as the controlled variable (output). The opening degrees of two controllable valves, i.e., the underflow valve V_u and overflow valve V_o, were regarded as the manipulated variables (controllable inputs). Based on experimental data, a set of linear models were identified by using PE system identification method. However, due to the heavy nonlinearity of cyclone's separation dynamics, it was noticed that some nonlinear model(s) should be developed if a relatively large operating range and different operating conditions need to be considered. An extension of this work to employ the Hammerstein-Weiner nonlinear model is currently underway as part of our work, and some of the preliminary results have showed a huge potential for this type of model to explain the nonlinearity in the de-oiling hydrocyclone system.

4. Challenges in de-oiling hydrocyclone control

There is little literature to be found in the systematic design of de-oiling hydrocyclone control solutions, including the standardized PID-based PDR control described in section 2 where there is no systematic approach described to tune these controllers except extensive empirical tunings, though some control designs can be found for solid-liquid cyclone separation.

4.1. Solid-liquid hydrocyclone control

The volume-split regulation has been developed in [24] by controlling the overflow valve for solid-liquid cyclone systems, which is quite similar to the PDR control for de-oiling hydrocyclones. The measured signals are the inlet pressure, the overflow pressure and an underflow discharge pattern recognition sensor, the manipulated variables are the speed of the feeding pump and the opening degree of the overflow valve. The control systems balance the underflow output between the rope discharge and spray discharge, so that the clogging problem can be avoided at the bottom of the hydrocyclone [25], [24], [26]. However, any direct application of these solid-liquid control solutions for liquid-liquid hydrocyclone separation is still very open and challenging.

The control of the inflow rate is not possible in offshore de-oiling hydrocyclone situations, as the inflow rate is determined by the separator level control loop, as shown in figure 5. Furthermore, the usage of monitoring spray rope discharge pattern for control purposes is not possible for de-oiling hydrocyclones. Moreover, the de-oiling hydrocyclones are not subjected to clogging problem, instead, water has a low viscosity compared to the infinite viscosity of solid materials. A thorough investigation of the likeness between these two types of separations needs to be done before the control techniques used for solid-liquid cyclones can be applied for liquid-liquid de-oiling hydrocyclones.

4.2. Coordinated separator and cyclone controls

The (water) level controller is designed to keep the water level inside the separator at a certain level based on a pre-determined set-point. From a practical perspective, the water level set-point is not crucial as long as the water level can be maintained within a safety range. Maintaining the level within a specified range is important to ensure a correct residence time which is directly related to the separator's efficiency. According to [27] the normal residence time for oil production separators is about $2-4$ minutes. Residence time is an optimization or trade-off problem, as a longer residence time ensures a better separation, and a lower residence time ensures faster process flow. The problem with longer residence times is that if the mass flow rate is to be kept high the equipment will correspondingly grow in size. In our investigations we have discovered a coupling effect of V_u and V_o functionalities, [28]. However, the opening cross-section area of V_u is about 25 times larger than that of V_o, thereby V_u acts as the dominant influence. Figure 4 illustrates a scenario where PID controllers are applied on both the level and PDR control loops, and a severe oscillating inflow rate F_{in} was generated to emulate a severe

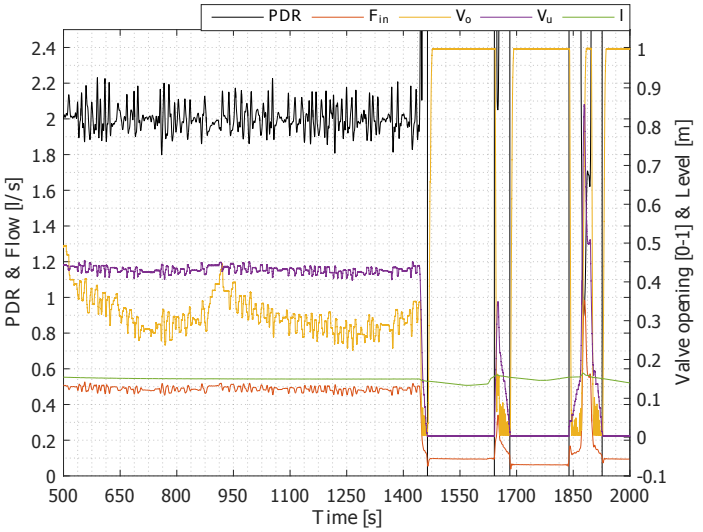

Figure 4: Test illustrating the coupling phenomena in the separation system.

condition. This test illustrates the impact of a sudden reduction in F_{in} (which happens at 1420s) on the controlled level and PDR performances. The halt of F_{in} caused the level in the separator to quickly decrease, which directly resulted in shutting of V_u due to the level controller. This action consequently increased the pressure over V_u, and then the PDR controller was forced to open V_o further. This scenario results in an unnecessary change of system efficiency ϵ, where $\epsilon = 1 - \frac{C_u}{C_i}$ and C_i & C_u are the inlet and outlet oil concentrations respectively. In addition, the dominance of V_u is evident from $500 - 1420$s, where small changes in V_u are equal to relatively larger fluctuations in V_o.

A block diagram of the combined level control and hydrocyclone PDR control is illustrated in Figure 5, the coupling effect is illustrated by the dotted lines. The current control consists in most cases of individually tuned and implemented PID controller on the level and the PDR, respectively. But a solution could lie in extending this with a controller structure which takes both the objectives into consideration. This control design problem can be formulated as a typical MIMO control problem, as long as we have the dynamic models describing the separator level dynamics as well as PDR dynamics.

In this case a MIMO feedback solution could be proposed to introduce a systematic design paradigm to the system which will help avoid the struggle of the two individual systems, and instead link them together into a cooperative control scheme.

4.3. Cyclone performance's sensitivity

Even with a good control solution, the hydrocyclone performance can still be very sensitive to fluctuations of inflow rates, which could be caused by the upstream separation processes (e.g., three-phase separators). The flow rate is equally important to the hydrocyclone's separation performance. If the flow through the hydrocyclone is insufficient, the swirl motion inside the hydrocyclone will not be formed or the velocity will be insufficient [30]. If this occurs, there

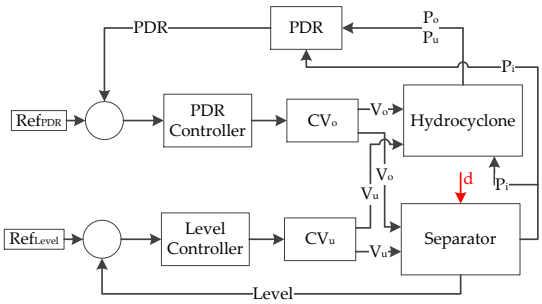

Figure 5: Control formulation of combined separator and cyclone controls [29]

will not be enough centripetal force to split the heavier liquid from the lighter one and push it towards the wall of the liner.

The plot in figure 6 shows a test performed on our pilot plant set-up, where F_{in} was increased from 0.2l/s to 0.68l/s, with 9 steps. During these increases ϵ was measured by measuring the Oil-in-Water (OiW) concentration in the inlet and the underflow of the hydrocyclone using the TD4100 equipment described in [31]. As F_{in} increases the ϵ increases, due to the fact that the centripetal force is being increased.

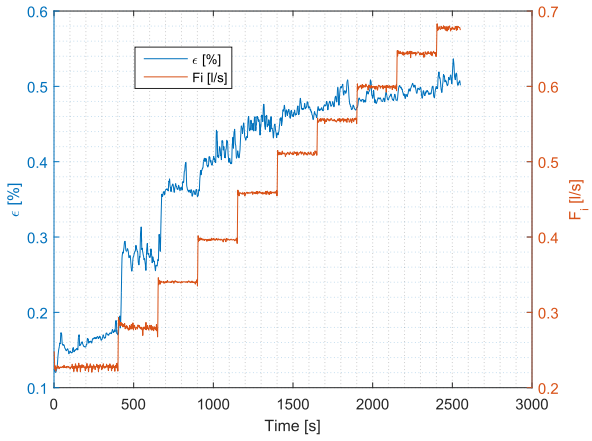

Figure 6: Dependency of ϵ on F_{in} at a controlled PDR

4.4. Efficiency real-time measurement

One of the important factors with regard to hydrocyclone operation is its efficiency measurement and prediction, which relates to the OiW concentration measurement. For the purpose of real-time applications, the OiW technology is not yet matured and the existing solutions are quite methodology dependent. Extensive investigations and development are needed in this area. A mathematical model of the liquid-liquid hydrocyclone's efficiency was introduced in [32] by modelling the dispersed droplet trajectories. This model can be very efficient in predicting the d_{100} value for a Coleman Thew type of hydrocyclone, however, it did not take into account the coalescence and breakup of droplets, and this can limit the prediction accuracy due to the fact that some high inflow rates often create a high shear stress which can break up droplets. d_{100} classifies the smallest droplet size which can be separated with an 100% efficiency, equally d_{50} would correspond to a separation efficiency of 50% [32]. One possibility is to measure droplet sizes at different stages in the separation system to investigate how the separation is affected by different droplet sizes, and if any improvement can be done during different operating conditions.

[31] investigated different OiW measurement technologies in terms of their precision and real-time measurement capabilities. The oil droplet size measurement was done with high precision using a microscopy based measurement instrument. However, due to the specific measurement principle, consistent online OiW concentration measurements have not yet been achieved, which casts a doubt about the instrument's capability for reliable real-time OiW measurement. Still, this does enable for steady state analysis of system performance at different particle sizes, which was performed in [33], but it does not assist in the possible design of control based models. Alternative measurement equipment using the same measuring principle is presented in [34] and their results seem quite promising.

In addition [31] evaluated another OiW instrument, which measures the concentration of OiW based on fluorescence principle. This method yielded far better OiW concentration results and has also be able to provide data in real-time. One result is illustrated in Figure 7. In this experiment, mixtures with different OiW concentrations were injected into the view-cell of this instrument with 10s intervals. The right plot illustrates a zoomed-in view of a step from 5 to 10 PPM. However, due to the extreme low concentrations, some measurements drift slightly. Regarding the OiW concentration measurement, this measuring instrument yields us some promising results, but further research is still needed to evaluate the reliability and repeatability of this method if it is to be used for dynamic model development and system dynamic performance evaluation.

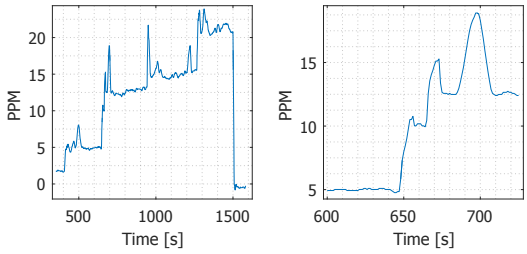

Figure 7: OiW measurement performed using a fluorescence based instrument Turner Design TD4100, [31]

5. Conclusions

The systematic solutions for de-oiling hydrocyclone control are still quite open with respect to its inherent complexity and heavy coupling with its upstream and downstream facilities. However, the real-time performance of the de-oiling hydrocyclone is crucial in determining the discharged water quality, and thereby the reduction of the environmental footprint caused by the offshore oil and gas production.

The current control solutions for hydrocyclones are PID-type solutions which lack systematic tuning strategies. Some advanced control solutions can be found in handling solid-liquid cyclone systems. However, the extension of these solutions to liquid-liquid de-oiling hydrocyclones is not straightforward. One of the key issues which blocks the application of advanced control methods in de-oiling hydrocyclone systems, lies in the lack of a deep understanding of the hydrocyclone's separation dynamics from the control point of view. This is reflected in reality, as there are no control-oriented modelling methods, nor models available for de-oiling hydrocyclone systems at this moment. Here CFD-based models and methods can play a very powerful role in emulating and analysing hydrocyclone separation processes, but they cannot yet be applied for control purposes. Instead a less detailed model strategy based on simple ODE models is preferred that describes the system from the control perspective, which is the PDR, with an extension of efficiency measurements.

For offshore de-oiling, the hydrocyclone performance is heavily coupled with the upstream separator's dynamics due to a lack of buffer vessels between them. Thereby, a coordination of the separator's (water) level control and hydrocyclone's PDR control is recommended. A MIMO control strategy can be applied to handle this control design problem, as long as some mathematical models of both parts are available. If the hydrocyclone's efficiency can be measured in a real-time and reliable manner, the hydrocyclone's PDR control strategy can be extended to be a direct-efficiency-based feedback solution. However, at this moment, the OiW real-time measurement technology, which fundamentally detects the hydrocyclone's efficiency, is still quite open and not yet matured.

Acknowledgments

The authors would like to thank the support from the Danish Innovation Foundation (via PDPWAC Project (J.nr. 95-2012-3)). Thanks also go to colleagues J.P. Stigkær, A. Aillos, K. G. Nielsen and T. I. Bruun from Mærsk Oil A/S, colleagues P. Sørensen, A. Andreasen and Jakob Biltoft from Ramboll Oil & Gas A/S, for many valuable discussions and supports. Thanks also go to AAU colleagues: C. Mai, K. Jepsen, L. Hansen, M. Bram and D. Hansen for their contributions to this project.

References

[1] Fakhru'l-Razi A, Pendashteh A, Abdullah L C, Biak D R A, Madaeni S S and Abidin Z Z 2009 *Journal of hazardous materials* **170** 530–551
[2] The-Danish-Environmental-Protection-Agency 2016 Status for den danske offshorehandlingsplan til udgangen af 2009 `http://www.mst.dk/` accessed: 2016-09-22
[3] Brette F, Machado B, Cros C, Incardona J P, Scholz N L and Block B A 2014 *Science* **343** 772–776
[4] Ekins P, Vanner R and Firebrace J 2007 *Journal of Cleaner Production* **15** 1302–1315 ISSN 09596526
[5] Bailey B, Crabtree M, Tyrie J, Elphick J, Kuchuk F, Romano C, Roodhart L *et al.* 2000 *Oilfield Review* **12** 30–51
[6] Thew M 1986 *The Chemical Engineer* 17–23
[7] Meldrum N 1988 *SPE Production Engineering* **3** 669–676
[8] Georgie W J 2002 *Offshore Technology Conference* 1–13
[9] Thew M 2000 *Encyclopaedia of Separation Science* 1480 – 1490
[10] Husveg T, Rambeau O, Drengstig T and Bilstad T 2007 *Minerals Engineering* **20** 368–379 ISSN 0892-6875
[11] Pedersen S, Durdevic P and Yang Z 2014 *Experimental Study of Stable Surfaces for Anti-Slug Control in Multi-phase Flow* (IEEE Press) pp 43–48 ISBN 978-1-909522-02-2

[12] Biltoft J, Hansen L, Pedersen S and Yang Z 2013 *IFAC Proceedings Volumes* **46** 47–52
[13] Jepsen K, Hansen L, Mai C and Yang Z 2013 Emulation and control of slugging flows in a gas-lifted offshore oil production well through a lab-sized facility *Control Applications (CCA), 2013 IEEE International Conference on* (IEEE) pp 906–911
[14] Havre K, Stornes K O and Stray H 2000 *ABB review* **4** 55–63
[15] Delgadillo J a and Rajamani R K 2005 *International Journal of Mineral Processing* **77** 217–230 ISSN 03017516
[16] Sayda A F and Taylor J H 2007 Modeling and control of three-phase gravilty separators in oil production facilities *2007 American Control Conference* (IEEE) pp 4847–4853
[17] Slack M, Del Porte S and Engelman M 2004 *Minerals Engineering* **17** 705–711 ISSN 08926875
[18] Hsieh K T and Rajamani R K 1991 *AIChE Journal* **37** 735–746 ISSN 0001-1541
[19] Monredon T, Hsieh K and Rajamani R 1992 *International Journal of Mineral Processing* **35** 65–83 ISSN 03017516
[20] Neesse T and Dueck J 2007 *Minerals engineering* **20** 380–386
[21] Hinze J 1975 *Turbulence:* McGraw-Hill classic textbook reissue series (McGraw-Hill) ISBN 9780070290372
[22] Goldberg U, Peroomian O and Chakravarthy S 1998 *Journal of Fluids Engineering* **120** 457–462
[23] Durdevic P, Pedersen S, Bram M, Hansen D, Hassan A and Yang Z 2015 *IFAC-PapersOnLine* **48** 291–296
[24] Neesse T, Tiefel H and Kaniut P 2007 *Minerals Engineering* **20** 355–360 ISSN 08926875
[25] Schneider M and Neesse T 2004 *International Journal of Mineral Processing* **74** S339–S343 ISSN 03017516
[26] Farghaly M, Golyk V, Ibrahim G, Ahmed M and Neesse T 2010 *Minerals Engineering* **23** 321–325
[27] Laleh A P, Svrcek W Y and Monnery W D 2012 *The Canadian Journal of Chemical Engineering* **90** 1547–1561 ISSN 00084034
[28] Durdevic P, Pedersen S and Yang Z November, 2016 *Under Review: Journal of Computers & Chemical Engineering (Elsevier)*
[29] Yang Z, Pedersen S and Durdevic P 2014 Cleaning the produced water in offshore oil production by using plant-wide optimal control strategy *2014 Oceans-St. John's* (IEEE) pp 1–10
[30] Kharoua N, Khezzar L and Nemouchi Z 2010 *Petroleum Science and Technology* **28** 738–755 ISSN 1091-6466
[31] Durdevic P, Simon P and Zhenyu Y 2016 *Proc of Oceans' 16 Mts/ieee Shanghai*
[32] Wolbert D, Ma B F, Aurelle Y and Seureau J 1995 *AIChE Journal* **41** 1395–1402 ISSN 0001-1541
[33] Young G, Wakley W, Taggart D, Andrews S and Worrell J 1994 *Journal of Petroleum Science and Engineering* **11** 37 – 50 ISSN 0920-4105
[34] Husveg R, Husveg T, van Teefelen N, Ottestad M and Hansen M R 2016 *Produced Water Workshop NEL*

Paper B

Control Oriented Modeling of a De-oiling Hydrocyclone

Petar Durdevic, Simon Pedersen, Mads Bram, Dennis Hansen, Abdiladif Hassan, Zhenyu Yang

The paper is in proceedings of:
17th IFAC Symposium on System Identification SYSID 2015 Beijing, China, 19-21 October 2015, IFAC-PapersOnLine, vol. 48, no. 28, pp. 291–296, 2015; doi: 10.1016/j.ifacol.2015.12.141

The layout has been revised.

Available online at www.sciencedirect.com

ScienceDirect

IFAC Papers Online CONFERENCE PAPER ARCHIVE

IFAC-PapersOnLine 48-28 (2015) 291–296

Control Oriented Modeling of a De-oiling Hydrocyclone

Petar Durdevic * **Simon Pedersen** * **Mads Bram** *
Dennis Hansen * **Abdiladif Hassan** * **Zhenyu Yang** *

* *Aalborg University, Esbjerg, 6700 Denmark (e-mail: pdl@et.aau.dk).*

Abstract: Deoiling hydrocyclones are an important part of the downstream water treatment in offshore oil & gas production, they ensure a low discharge of oil and thus a higher yield of produced oil. This work investigates the possibility of developing a simple control-oriented model of a de-oiling hydrocyclone based on experimental data that can support systematic analysis and control design of hydrocyclone systems. The most widely used control solution of a hydrocyclone is a Pressure Drop Ratio (PDR) control strategy, which is often empirically designed and experimentally tuned in a case-by-case manner. There is a lack of a systematic and deep-insight analysis of the capability, stability and limitations of these control solutions, as there are few control-oriented models available for de-oiling hydrocyclone systems. This paper proposes a method of retrieving a set of simple 1st-order transfer function models from a set of designed experiments based on a lab-scaled hydrocyclone system. Some preliminary results are also illustrated and discussed. The conclusion of this preliminary study is that the models obtained can emulate the dynamics of the system in a reasonable manner subject to the trade-off between simplicity and accuracy. In addition, higher order state space models are introduced and their relative advantage of depicting the complicated dynamics of the hydrocyclone's pressures is investigated.

Keywords: De-oiling hydrocyclones, FOPDT estimation, Multi-Model Frame, multi-phase flow

1. INTRODUCTION

In the off-shore oil and gas industry, hydrocyclones are a part of the de-oiling procedure which is crucial in separating the oil from water before the produced water is discarded into the ocean. Off-shore production of oil in most cases yields a high amount of water where 90% water concentration is not uncommon (Husveg et al. (2007)), and the amount of produced water is constantly increasing as the fields mature (Fakhru'l-Razi et al. (2009)). Hydrocyclones are chosen due to their simple and rugged design which makes their maintenance low and hence the operational costs low. In addition they have the ability to separate oil down to concentrations of 20 parts per million (PPM) Yang et al. (2013). Although widely used, the knowledge about hydrocyclones is mostly acquired from the mechanical perspective, for the design and efficiency optimization of the unit, as seen in: Narasimha et al. (2005); Maddahian et al. (2011). From the dynamic control oriented perspective little work has been discovered in favor of the hydrocyclone. The commonly used hydrocyclone control solution in the off-shore oil & gas production follows a type of Pressure Difference Ratio (PDR) control strategy, where both the upstream separator's water level control and hydrocyclone's PDR control are coupled. The assignments and tuning of these control parameters are still empirical, due to the complicated system dynamics and coupling. Getting a reasonably performing control system for a particular setup can be very time-consuming and ad hoc. A systematic approach method for handling this challenge could be very promising from both scientific and industrial perspectives. A model which can simulate PDR is useful as it is a very important factor in the offshore operation of the hydrocyclone. This preliminary work investigates the feasibility of constructing a simple dynamic model of the hydrocyclone by system identification approach, where the experimental data is retrieved based on an in-house built hydrocyclone platform. The model developed and investigated in this article concerns the relationship between the control valve opening degrees and the PDR. As the underflow V_u and overflow V_o valves are the only controllable valves, they have been selected as the input to the model.

⋆ Supported by the Danish National Advanced Technology Foundation through PDPWAC Project (J.nr. 95-2012-3).

2. PRINCIPLES OF THE HYDROCYCLONES

A typical de-oiling hydrocyclone consists of four major parts as illustrated in figure 1 a cylindrical chamber where the influent flows in, two conical pipe sections and a long cylindrical underflow pipe, which is 15 times longer than the first chamber's diameter as described in Wolbert et al. (1995) and Colman and Thew (1988). The cleaned water effluent exits through the underflow outlet located at the end of the long cylindrical pipe and the separated oil effluent exits through the overflow outlet located at the top-center of the cylindrical chamber. The inlet is placed tangential to the surface of the cylindrical chamber, this sends the fluid spiraling inside the hydrocyclone, and the resulting centripetal force acts as a gravity multiplier which forces the phases of different densities to separate

2405-8963 © 2015, IFAC (International Federation of Automatic Control) Hosting by Elsevier Ltd. All rights reserved.
Peer review under responsibility of International Federation of Automatic Control.
10.1016/j.ifacol.2015.12.141

from each other. The conical shape forces the lighter liquid towards the overflow and the rest of the liquid flows down to the underflow outlet.

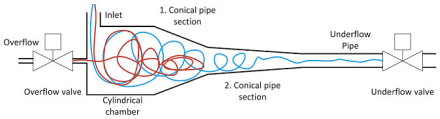

Fig. 1. Illustration of a hydrocyclone, where the blue line is the water flow and the red line is the oil flow.

3. TESTING FACILITY

The test setup consists of an in-house designed transparent hydrocyclone liner, which is constructed from Poly-methyl methacrylate (PMMA) and polished such that it is see-through. To design the hydrocyclone liner, the diameter of the cylindrical chamber was designed to be 50mm which is slightly wider than typical industrial de-oiling liners. Based on this diameter, the rest of the dimensions of the hydrocyclone liner were calculated according to the design criteria as described in Wolbert et al. (1995). The advantage of using a design that emulates an industrial liner is the scalability of the setup, as offshore installations stack multiple liners in parallel. The transparent hydrocyclone is depicted in figure 3, the hydrocyclone was constructed with two inlets to enable better vortex creation. The input fed to the hydrocyclone is pumped using a vane pump which is variable-speed controllable. Three pressure transmitters are installed, one on the inlet and two located upstream of the underflow and the overflow valve respectively, the placement of the equipment resembles that of an off-shore installation. Refer to figure 2 for an overview of the setup diagram showing the three pressure transmitters: P_i,P_u and P_o; and the two controllable valves V_o and V_u.

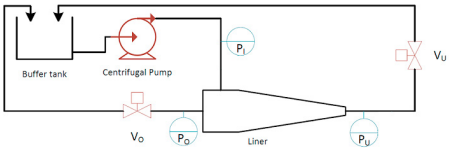

Fig. 2. Diagram of the test setup.

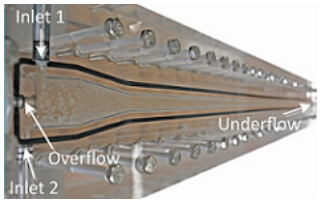

Fig. 3. See-through acrylic hydrocyclone liner used for the tests.

4. SYSTEM IDENTIFICATION

4.1 System Pre-Analysis

The hydrocyclone setup is designed to withstand pressures up to 6 bars, and for fluid mass flow rates up to $3.5m^3/h$, the pressure and flow range is a trade-off between safety measures and vortex creation. Figure 4 illustrates an oil-core phenomenon when the feeding consists of water and oil, for this test a mineral motor oil was used (IQ-X 'Kroon Oil' 5W-40 Super) with density: 0.877 g/cm^3 @ $20°C$ and viscosity 102 mm^2/s @ $40°C$. This phenomenon is only possible if a vortex is created inside the hydrocyclone and the centrifugal forces are adequate to separate the two fluids. The test results illustrated in figure 5 shows the

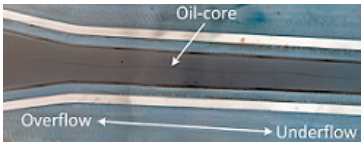

Fig. 4. Creation of the oil core inside of the transparent hydrocyclone, the colors have been inverted to help illustrate the thin core.

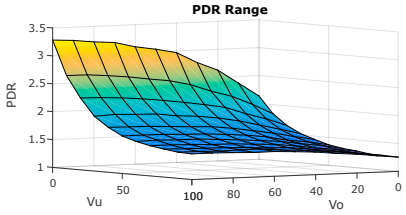

Fig. 5. Valve opening influence on the PDR at steady state, at 100% pump capacity.

PDR at different valve openings, and the experimental results are as expected. For low underflow valve values the PDR is very high, which is caused by the geometry of the hydrocyclone, where the overflow diameter is 5 times smaller than the underflow diameter and 3.5 times smaller than the inflow. Thus the overflow suffers from a high pressure when all the flow is forced through it, leading to a high PDR value. The PDR, $PDR = \frac{(P_i - P_o)}{(P_i - P_u)}$, for this test is kept around 1.4 and 3.2, and is a wide range when compared to the range described in Thew (2000), which specifies a PDR between 2 and 3 to be optimal for a typical industrial cyclone setup.

4.2 System Identification

In the first stage of investigation, it is assumed that the model of the hydrocyclone has linear system characteristics as shown in the figure 6, where G_v describes the valve model and the valve's position is the model's output. The hydrocyclone transfer function G_h has the valve

position as the input and the PDR as the output. Transfer function G_{vh} is used to present the system model from valve control input to PDR and is henceforth referred to as the PDR model. It is assumed that all system transfer function models are a type of First-Order-Plus-Dead-Time (FOPDT) systems at this stage.

In figure 6 the valve and the PDR models are connected into a unified structure, as the dynamics of the two systems are dependent on each other through the two valves, which are also the inputs. The outputs used in this work are the two valve positions V_{ua}, V_{oa} and the PDR and the inputs are the two valve set points, V_u and V_o.

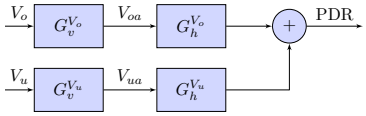

Fig. 6. System Block Diagram

$$G_v = \frac{k_v}{\tau_v s + 1} e^{-T_{dv} s} \tag{1}$$

$$G_{vh} = \frac{k_{vh}}{\tau_{vh} s + 1} e^{-T_{dvh} s} \tag{2}$$

$$G_h = \frac{G_{vh}}{G_v} = \frac{k_v \tau_{vh} s + k_v}{k_{vh} \tau_v s + k_{vh}} e^{-(T_{dvh} - T_{dv}) s} \tag{3}$$

Where k_v and k_{vh} are the gains, τ_v and τ_{vh} are the time constants and T_{dv} and T_{dvh} are the time delays.

4.3 Experiment Design and Data Acquisition

The aim of the experiment is to investigate the system's dynamics in a wide array of operating conditions, i.e. for the entire effective valve opening range. This will give a sufficient representation of the system and will allow for analysis of the whole system inside and outside the normal operational areas. A constant frequency was applied to the vane pump in order to reduce the amount of controllable variables. The data retrieved from the sensors is filtered using a low-pass filter with a cut-off frequency of $10Hz$, which is the bandwidth used for the experiments. The tests that were made strive towards evaluating the operation of both valves and their influence on the system, operating in two directions, opening and closing. The first valve was opened from 0% to 100% and down to 0% again in increments of 10%, while the second valve was kept at one specific opening. The settings of the first valve are repeated for different valve openings of the second valve, again between 0% and 100% in increments of 10%. The cycle is repeated using the settings of the first valve for the second valve and vice versa, the input signals to the valves are illustrated in figure 8. This in the end gives 4 combinations, illustrated in figure 7, where each arrow represents a specific valve opening in a specific direction. For each direction, one model can be obtained. This not only investigates the system transients during the changes of each valve, but also allows for comparison of valve opening and valve closing action. In order to check the diversity of the linear model of the hydrocyclone in a wide range of operations, a set of FOPDT were individually estimated for different (grid) operating conditions.

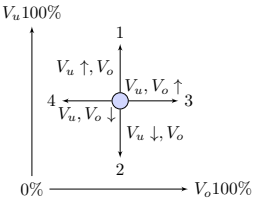

Fig. 7. Valves opening directions, where each of the four directions is used for system identification

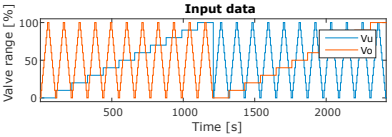

Fig. 8. Input used to produce the data for model estimation, the blue and the red curve represent the underflow and the overflow valves set-point respectively.

4.4 Model Validation

The preliminary results have been plotted in figures 9 and 11. Two sets of test data are presented in all the plots, the first is the (mod) data which is the data used to create the model, and the (val) data which is data sourced from a different test used for validation. The simulation and test were done with the following initial conditions: $V_o = 10\%$, $V_u = 10\%$, $P_v = 100\%$, where P_v is the pump control signal. In the test V_o was increased from 10% to 20% this was done at time $1s$, the result of the simulation is plotted in figure 9, note that the increase in the test occurs from 8% to 18% this is caused by an offset in the valve and this same error occurs in every test data presented. This can be corrected by calibrating the valves, but for the purpose of this work the gain offset does not influence our intention as it exists in all the tests made.

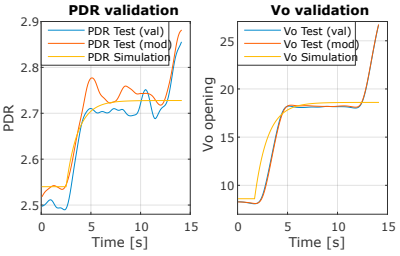

Fig. 9. Validation of the system and valve model, based on a step input to V_o, where the step is an increase from 10% to 20%.

PDR model The simulated model tendencies, presented in figure 9 follow the validation test data (val). The low order of the model is a clear disadvantage, as it cannot recreate the oscillations occurring in the test. The dead time and the time constant for the simulated model is close to the test data, indicating that the model is valid in this range. At steady state there is an offset from the simulated and the validated data, although the simulated PDR crosses a spike in the validation data at time $10.5s$. It appears that the test data suffers from oscillations in steady state, this can be seen in the validation data (val) where after the system reaches steady state, there occurs a spike at time $10.5s$ as mentioned. The model test data continues to oscillate in the entire steady state range. By analyzing figure 10, which is a steady state response of the overflow valve V_o and the PDR, it is clear that the PDR does indeed oscillate after reaching steady state. The oscillations in figure 10 reach an amplitude deviation of 0.054, whereas the steady state amplitude deviation in figure 9 has an approximate maximum of 0.05. This can be caused by measurement noise in the pressure transmitters or by the complex dynamic of the hydrocyclone and the flows inside it. The data in 10 is unfiltered in order to show the amount of noise in the pressure measurement. The settling time of the PDR is around $10s$, although the steady state does fluctuate after this point similarly as seen in figure 9. One reason for the fluctuations of the PDR comes from the PDR calculation itself as it involves a derivative action, which notoriously increases the noise sensitivity.

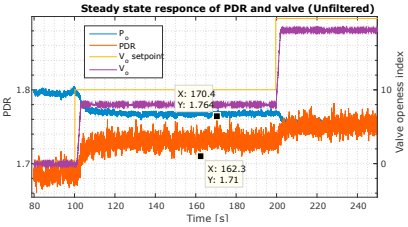

Fig. 10. Steady state response of the overflow valve and the PDR and the overflow pressure. The underflow valve V_u is set to a constant 50% openness while the overflow valve V_o is adjusted from $0\% - 10\% - 20\%$. After each opening of V_o the system is set to rest for $100s$ to ensure that the system reaches steady state.

Valve model The tendency of the simulated model, presented in figure 9, is comparable to the test data. The fitness of the valve model is better when compared to the PDR model. The better fit is mainly due to the mechanical dynamic of the valve and its driving system, and is thus more suitably described by the FOPDT model. From the test results it appears that the valve has a slight overshoot before settling to the steady state value. This of course could be due to the tachometers precision and the noise sensitivity. The linearity of the valve results in a more easy representation by the first order model designed in this work. The valve test data has a close to linear behavior and it settles instantaneously, which indicates that the valve probably has no internal feedback control and/or that the step motor's slow speed is a dominant factor. The calibration offset is clearly seen in this test where the valves' actual position is 2% lower than the set-points. Another experiment was performed with the following initial conditions: $V_o = 20\%$, $V_u = 20\%$, $P_v = 100\%$, which is illustrated in figure 11. In the test V_u is increased from 20% to 30% at time $1s$.

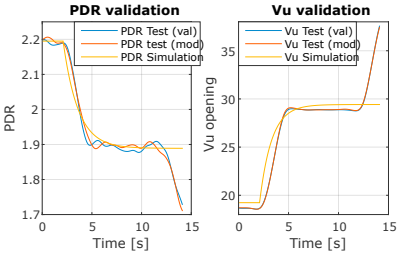

Fig. 11. Validation of the PDR and valve model, based on a step input to V_u.

PDR model The simulation shown in figure 11 follows the test data closely, but the low order model cannot follow the oscillations in the test data at steady state. The steady state offset is minimal compared to the first test in figure 9.

Valve model The response of this simulation compared to the test data is almost identical to the first test in figure 9. The similarity of these two tests is, as described earlier, due to the linearity of the valve.

4.5 Validating the Flexibility of the Model

This test aims at validating the flexibility of the model in different regimes, where the model is simulated in one valve regime and validated with a test from another valve regime. The first test presented in figure 12 represents the test data for an underflow valve V_u increase from $30-40\%$ and the simulated model data for an underflow valve V_u increase from $40 - 50\%$. The second test presented in figure 13 represents the test data for an overflow valve V_o increase from $20 - 30\%$ and the simulated model data for an underflow valve V_o increase from $40 - 50\%$. The PDR model simulation has similar tendencies as the test data although there is an offset. The dynamics of the PDR do not follow the test data as good as the valve model in the same test. By ignoring the static offset, to get a better impression of the fitting, some curves are shifted as shown in purple color in figure 12. The same goes for the second test in figure 13, where the PDR model cannot follow the complex dynamics, and where the valve dynamics are much more precisely replicated by the FOPDT model. This observation indicates that the PDR FOPDT model developed for one segment of the valve opening is not suited directly for another segment.

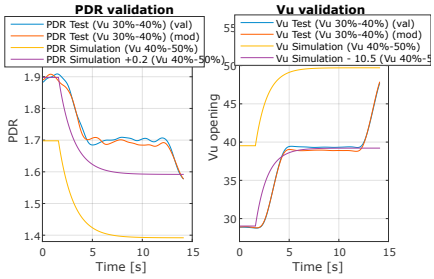

Fig. 12. Flexibility test of the model, the underflow valve opening of $30-40\%$ is validated using test data from a $40-50\%$ opening.

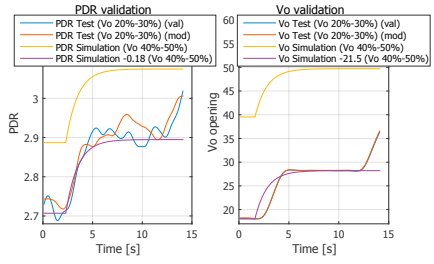

Fig. 13. Flexibility test of the model, the overflow valve opening of $20-30\%$ is validated using test data from a $40-50\%$ opening

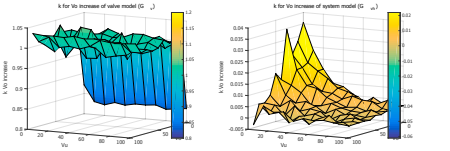

(a) Plot of the gain k parameter for the valve model for an increasing overflow valve V_o.

(b) Plot of the gain k parameter for the PDR model (PDR) for an increasing overflow valve V_o.

Fig. 14. The tests are made for 10 different valve openings, from 0% to 100% with 10% intervals.

Discussion of Valve and PDR Dynamics The difference in the system complexity can best be seen in the gain plots 14a and 14b. The valve model gain curve in figure 14a, changes slightly throughout the valve openness regime, in fact the biggest change can be traced to the initial valve opening, i.e. from 0% to 10%. The reason for the sudden jump is that the valves behave highly non-linear when starting from end positions, as there is some non-linearity between the tachometer and the valve position itself which could be caused by backlash in the system. There exists a loose gap between the servo motor and valve's piston coupling which results in a dead-band, refer to figure 15 for a picture of this gap. The gap is indicated by two horizontal red lines. The backlash has been measured by manually by winding the servo motor and observing when it starts pulling the valve piston, and the backlash has been measured to $\approx 8-10\%$ of the active valve range. The small variations in the valve's gain could be caused

Fig. 15. Gap occurring in the coupling of the servomotor and the valve piston.

by noise in the system. On the other side, the PDR's dynamics are vastly complicated and caused by different flow regimes inside the hydrocyclone and through the valves. This is illustrated in figure 14b, where the gain is changing throughout the whole valve openness regime.

5. HIGHER ORDER MODELS

Higher order models (HOM) were identified for the valves and the PDR to investigate if these models describe the test data better than the FOPDT, and if they are flexible enough to be used in different operating ranges. ($2nd$,$3rd$,$4th$) and ($2nd$,$3rd$,$5th$,$6th$) order state space models were created for the valves and the PDR respectively, and compared to validation data. Figures 16a and 17a present the results for an overflow valve opening region of $10\%-20\%$. As seen in the earlier section 4.5, the data is compared to an alternative region, in this case a overflow valve opening of $30\%-40\%$ and the result is presented in figures 16b and 17b for the valve and PDR respectively.

5.1 High Order Model Results

Regarding the valve HOM, the second order model already is capable of recreating the overshoot that is witnessed in the valve dynamics, as seen in figure 16a. The $2nd$ order model does have a slightly higher overshoot, but the $3rd$ order model copes with the overshoot. All three models do tend to rise earlier then the test data and this can be caused by the slight oscillations in the valve steady state, making them difficult to model. A comparison of all the valve HOM that were used to the test data, as seen in figure 16b from the overflow valve opening region $30\%-40\%$ indicates that the models from one region cannot be directly used in other regions. To fix this, the model could be updated with a appropriate gain according to the region in which the system is operating to adjust for the offset in the steady state. In case of the PDR HOM, only the $6th$ order model can follow the test data and the lower orders do not recreate the dynamics of the test data. The $6th$ order model, does not reach steady state in the available simulation time but nether does the test data as discussed earlier. Figure 17b illustrates a model which does not fit the test, where all the HOM from one overflow valve regime ($10\%-20\%$ valve opening) are compared to test data from another overflow valve regime ($30\%-40\%$

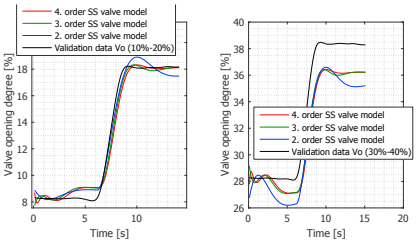

(a) State space black box models simulation, describing the relationship between the valve input signal and the overflow valve opening V_o.

(b) State space black box models simulation, describing the relationship between the valve input signal and the overflow valve opening V_o

Fig. 16. Plot of the generated models of the valve

valve opening). In this case the $5th$ order model has the best fit, but none of the HOM reach steady state within the simulation time.

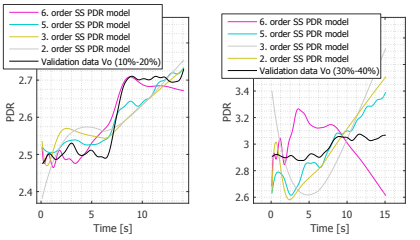

(a) State space black box models simulation, describing the relationship between the overflow valve opening V_o.

(b) State space black box models simulation describing the relationship between the overflow valve opening V_o.

Fig. 17. Plot of the generated models of the valve

6. CONCLUSION

The modeling of the hydrocyclone was done for the entire valve opening range for both valves, and a set of FOPDT models were identified for different operating conditions. The preliminary investigation concluded the following: (1) Simple LTI model, like FOPDT can reflect the control valve's dynamic reasonably, while it doesn't work for the PDR dynamic in a wide range. For small operating ranges, for example ±10% deviation, the FOPDT model can track the general PDR dynamic without the capability to emulate small oscillations along the general intention. State space HOM were generated from the same data that was used to generate the FOPDT models and the tracking performance and the overshoot of the valve models was improved already by using $2nd$ order models. More importantly the PDR model using $6th$ order state space model can recreate the dynamics much better than the FOPDT model. Although the performance of the models is improved by using higher order models for the valve and the PDR model, the models have a poor fit outside their operating region especially with regards to the PDR model. (2) If the linear model is still preferred, a group of LTI models could be adopted for modeling the PDR dynamic, where each LTI model is only valid for some specific operating range. Correspondingly, based on this type of multi-model framework, the control could be some kind of gain-scheduling solution or hybrid control solution Yang and Izadi-Zamanabadi (2009). The multi-model frame may lead to a much more complicated model structure and computation load than the models introduced so far, but compared to CFD-based models, the multi-model or hybrid system model is still very promising, especially with respect to the supporting capability for control design and systematic analysis Yang and Blanke (2007). The multi-model representation and reliable identification of this model, as well as the corresponding control design of PDR dynamics are part of our future work. Furthermore the models can be applied to offshore installations and evaluated and similar models can be identified and compared to the existing models using offshore data in small regions, as offshore platforms cannot be taken far out of their operating conditions during normal operation.

REFERENCES

Colman, D. and Thew, M. (1988). Cyclone separator. US Patent 4,793,924.

Fakhru'l-Razi, A., Pendashteh, A., Abdullah, L.C., Biak, D.R.A., Madaeni, S.S., and Abidin, Z.Z. (2009). Review of technologies for oil and gas produced water treatment. *Journal of Hazardous Materials*, 170(2–3), 530 – 551.

Husveg, T., Rambeau, O., Drengstig, T., and Bilstad, T. (2007). Performance of a deoiling hydrocyclone during variable flow rates. *Minerals Engineering*, 20(4), 368–379.

Maddahian, R., Farhanieh, B., and Saemi, S. (2011). Numerical Simulation of Deoilin Hydrocyclones. *World Academy of Science, Engineering and Technology 59*, 2044–2049.

Narasimha, M., Sripriya, R., and Banerjee, P. (2005). CFD modelling of hydrocyclone—prediction of cut size. *International Journal of Mineral Processing*, 75(1-2), 53–68.

Thew, M. (2000). Cyclones for oil/water separation. *Encyclopaedia of Separation Science*.

Wolbert, D., Ma, B.F., Aurelle, Y., and Seureau, J. (1995). Efficiency estimation of liquid-liquid Hydrocyclones using trajectory analysis. *AIChE Journal*, 41(6), 1395–1402.

Yang, Z. and Izadi-Zamanabadi, R. (2009). Design of Reconfigurable Nonlinear Control Using On-Line Piecewise Affine System Approximation. *The 7th IFAC International Symposium on Fault Detection, Supervision and Safety of Technical Processes*, 680–685.

Yang, Z. and Blanke, M. (2007). A unified approach to controllability analysis for hybrid control systems. *Nonlinear Analysis: Hybrid Systems*, 1(2), 212–222.

Yang, Z., Stigkær, J.P., and Løhndorf, B. (2013). Plant-wide control for better de-oiling of produced water in offshore oil & gas production. *3rd IFAC International Conference on Intelligent Control and Automation Science (2013)*, 3, 45–50.

Paper C

Cost-Effective ERT Technique for Oil-in-Water Measurement for Offshore Hydrocyclone Installations

Petar Durdevic and Leif Hansen and Christian Mai and Simon Pedersen and Zhenyu Yang

The paper is in proceedings of:
2nd IFAC Workshop on Automatic Control in Offshore Oil and Gas Production OOGP 2015 - Florianopolis, Brazil, 27-29 May 2015, IFAC-PapersOnLine, Volume 48, Issue 6, pp.147-153, 2015; doi: 10.1016/j.ifacol.2015.08.023

The layout has been revised.

Available online at www.sciencedirect.com

ScienceDirect

IFAC Papers Online
CONFERENCE PAPER ARCHIVE

IFAC-PapersOnLine 48-6 (2015) 147–153

Cost-Effective ERT Technique for Oil-in-Water Measurement for Offshore Hydrocyclone Installations

Petar Durdevic * **Leif Hansen** * **Christian Mai** *
Simon Pedersen * **Zhenyu Yang** *

* *Institute of Energy Technology, Aalborg University, Esbjerg Campus, Niels Bohrs Vej 8, 6700 Esbjerg, Denmark, e-mail: pdl@et.aau.dk, +45 31 75 13 20*

Abstract: The goal of this paper is to introduce and design a cost-effective Oil-in-Water (OiW) measuring instrument, which will be investigated for its value in increasing the efficiency of a deoiling hydrocyclone. The technique investigated is based on Electrical Resistivity Tomography (ERT), which basic principle is to measure the resistivity of substances from multiple electrodes and from these measurements create a 2-D image of the oil and gas component in the water. This technique requires the measured components to have different electrical resistances, such as seawater which has a lower electrical resistance than hydrocarbon oil and gas. This work involves construction of a pilot plant, for testing the feasibility of ERT for OiW measurements, and further exploring if this measured signal can be applied as a reliable feedback signal in optimization of the hydrocyclone's efficiency. Different algorithms for creating 2-D images and the feasibility of estimating OiW concentrations are studied and evaluated. From both steady state and continuous laminate flow perspectives, with respect to the objective which is to use this measurement for feedback control purposes.

Keywords: Electrical Resistivity Tomography, Water Treatment, Process Control, Oil in Water, Offshore.

NOMENCLATURE

Symbol	Description	Unit
Q_o	Hydrocyclone overflow flow	m^3/h
Q_i	Hydrocyclone inlet flow	m^3/h
P_i	Hydrocyclone inlet pressure	kPa
P_o	Hydrocyclone overflow pressure	kPa
P_u	Hydrocyclone underflow pressure	kPa
C_u	Concentration of oil in the underflow	mg/L
C_i	Concentration of oil in the inlet	mg/L
ϵ	Hydrocyclone efficiency	%
$i_{\alpha\beta}$	Measured current	A
$v_{\alpha\beta}$	Measured voltage drop	V
$G_{\alpha\beta}$	Measured line conductance	S
$g_{\alpha\beta}$	Line conductance pr distance	$S \cdot m$
v^{β}_{high}	Passive electrode high side voltage	V
v^{β}_{low}	Passive electrode low side voltage	V
v^{α}_{high}	Active electrode high side voltage	V
v^{α}_{low}	Active electrode low side voltage	V
r_m	Measurement resistance value	Ω
f_{frame}	2-D Frame rate of measurement	Hz
f_s	Sampling rate	Hz
n_c	Channel count	–
$a_{\alpha\beta}$	Coefficient of electrode-electrode line	–
$b_{\alpha\beta}$	Coefficient of electrode-electrode line	–
$c_{\alpha\beta}$	Coefficient of electrode-electrode line	–
$l_{\alpha\beta}$	Distance between electrodes	m
α, β	Active and passive probe designation	–
$\mathbf{S}$	Set of all measurements	–
$w_{\alpha\beta}$	Measurement weight	–
$\mathbf{x}$	Point in 2-D plane cross-section of pipe	m
x_1	First coordinate of electrode-electrode line	m
x_2	Second coordinate of electrode-electrode line	m
d_{min}	Minimum distance electrode-electrode line	m

⋆ Supported by the Danish National Advanced Technology Foundation through PDPWAC Project (J.nr. 95-2012-3).

1. INTRODUCTION

Hydrocyclones are commonly used to separate oil from water downstream the three phase separator in the upstream offshore oil & gas production, this means that the oil concentration which they have to handle is low as some separation has already taken place in the three phase separator. During normal North Sea operation the oil concentration exiting the three phase separator is below 5000 parts per million (PPM) or 0.5%, see Kharoua et al. (2010), while the oil concentration in a normally operating hydrocyclone's water outlet, should be around 50 PPM to 20 PPM. The goal of using hydrocyclones for produced water treatment in offshore oil & gas industry is to keep the concentration of hydrocarbon content (mainly oil part) in the treated water below 30 PPM as this is the current North Sea regulation (Miljoestyrelsen (2010)). A typical hydrocyclone consists of a cylindrical chamber to which a tangential inlet inputs a mixture of oil and water. Due to the curvature of the cylindrical shape, this fluid mixture will start to flow in a rotating path. The centrifugal forces then act on the fluid, and consequently the fluid with the higher density is pushed furthest out to the cylinder wall. The cylindrical part is connected to a long conical pipe, where at the end the water exits, this is called the *underflow* (Wolbert et al. (1995)). The conical part presses some of the lighter fluids upwards to the opposite end of

2405-8963 © 2015, IFAC (International Federation of Automatic Control) Hosting by Elsevier Ltd. All rights reserved.
Peer review under responsibility of International Federation of Automatic Control.
10.1016/j.ifacol.2015.08.023

the cylindrical chamber, where a pipe of a small diameter is used to let out the oil, and this is called the *overflow* (Wolbert et al. (1995)).A schematic illustration of a typical hydrocyclone is shown in figure 1, where the paths of oil (red) and water (blue) are depicted respectively. During

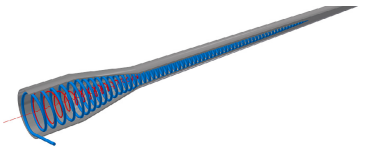

Fig. 1. A cut-trough image of the hydrocyclone, showing the hypothetical water (blue) and oil (red) paths.

normal offshore operation, the pressures at the inlet and the two outlets are measured and used to calculate the pressure drops over the inlet and the two outlets, these two pressure drops are then employed to calculate a so-called Pressure Drop Ratio (PDR) as described by equation 1, which is used to control the hydrocyclone. The PDR is correlated to the flow split Q_o/Q_i, which is the volumetric flow rate of the overflow over the volumetric flow-rate of the inflow (Husveg et al. (2007)).

$$PDR = \frac{(P_i - P_o)}{(P_i - P_u)} \tag{1}$$

It has been discovered by Husveg et al. (2007) that the flow split and the PDR can be related through a linear approximation. By adjusting the PDR and thus the flow split the controller will allow a certain amount of oil to pass through the overflow and thus ensure an efficient operation of the hydrocyclone. The PDR is linearly approximated to be proportional to the flow split, and the flow split can be further related to the efficiency which is illustrated in figure 2 (Husveg et al. (2007)). The hydrocyclone efficiency is usually defined as a percentage of the concentration of oil in the underflow C_u over the concentration of oil in the inlet C_i, resulting in the following equation $\epsilon = 1 - C_u/C_i$, see Young and Wakley (1994). This type of PDR-

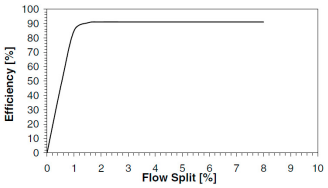

Fig. 2. Hydrocyclone efficiency related to the flow split, the result is based on an empirical analysis of a typical offshore liner (Husveg et al. (2007)).

based feedback control loop, which is the most commonly used in the offshore E&P, does not measure the OiW concentration and thus has no direct control regarding the quality of the treated water exiting the hydrocyclone. The development of the PDR control is thus done based on plenty empirical knowledge of the system, and the reference value given to the closed-loop system varies for different systems and is typicality kept at around 2-3 (Husveg et al. (2007)). One of the effective techniques commonly applied for measuring multiphase flow in the offshore industry is to separate different phases and then measure each phase individually using different single phase flow measurement (Ismail et al. (2005)), (Thorn et al. (1999)). However this kind of approach is not a directly applicable solution for feedback control of hydrocyclones, with respect to the fact that different measurements could variate and lead to some unpredictable time-delay, i.e. from the time the mixture enters the separation process until it is separated and measured. This type of measurement is more sensibly used, for example, for logic-level supervisory control or offshore evaluation. This work aims at using Electrical Resistivity Tomography (ERT) for measuring the OiW concentration at the hydrocyclone's inlet and outlets. Compared to other relevant techniques, such as γ-ray tomography, the proposed ERT technique has no use of radiation, as well as to its non-invasive and structurally robust and cost effective characteristics. Other alternative solutions could be, such as the Advanced Sensors $EX-100$ (Advanced Sensors (2014)), which uses Laser Induced UV Fluorescence to measure the amount of hydrocarbons in water. This instrument can measure in various ranges, from $0-10$ PPB, to 20.000 PPM, which can be extremely sensitive and precise. With regard to real-time purpose this instrument can have a sampling-rate of $1sec$, which could be applicable for feedback control purpose. However this type of sensoring instrument can be very expensive in a range of 30,000-40,000 USD. From our experience this equipment is difficult to calibrate in ranges of around $5-50$ PPM, mainly due to the coalescence of oil in water. Normally the test samples need to be thoroughly mixed beforehand. Other available commercial instruments, like the Agar Corporation MPFM 50 Multiphase flow meter which could be found at Agar Corporation (2014), and the Jorin VIPA which could be found at Jorin (2014). Nevertheless, all of these mentioned products are quite expensive. Thereby instead of concentrating on the usage of these sophisticated and expensive equipments, we chose to concentrate on some cost-effective electric tomography for OiW measurement, for instance, the constructed tomography sensor used in this paper costs less than 20 USD. The potential economic benefits of using cost-effective ERT for OiW concentration measurement is quite obvious. In addition, by analyzing the time-dependent tomography results, dynamic changes in the flow-rate and flow-regime can also be detected, which allows for a wide range of applications, such as slug-detection, separator and pipeline monitoring (Dong et al. (2001)). The technique is also scalable for both the pipe size and number of electrodes to suit the fidelity/resolution requirements of each individual application. In general, more electrodes would give better resolution but with slightly increased cost and computation requirements.

2. TOMOGRAPHY TECHNIQUES

Tomography is a non-invasive technique for visualizing some information over a cross-sectional segment of a pipe, which could be filled with two components with different electrical characteristics. Measurements are usually taken from several points around the pipe and the test results are then used to create a image of the segment. Tomography data can be retrieved based on different measurement techniques, such as: electrical, radioactive, optical, microwave,

ultrasonic and magnetic resonance, where the last is well known from MRI scanning used for medical imaging (Ismail et al. (2005)). Our work will concentrate on electrical tomography as this could be the cheapest and most simple technique to implement, and it is also structurally robust which is the primary objective for the offshore instruments. The application of ERT on solid-liquid hydrocyclones applied in the clay industry has been reported in Williams et al. (1999). A test setup is introduced with electrodes in several segments of the hydrocyclone such that different performances at different segments inside the hydrocyclone can be possibly observed. This work discovered that it is possible to determine if an air-core is formed inside the hydrocyclone as well as which type of underflow discharge is occurring. However the approaches and methods proposed in Williams et al. (1999) cannot be directly applied for de-oiling/liquid-liquid hydrocyclones, due to the dramatically different structural and operational characteristics of liquid-liquid hydrocyclones from solid-liquid hydrocyclones. For instance, within one of actual cases we experienced, the offshore liners often receive the flow from the separator with a maximal amount of 5% which is equal to 0.5 % mass fraction of oil in water (Kharoua et al. (2010)), while according to Williams et al. (1999), their clay hydrocyclone units receive up to 15 % mass fraction of solids. Also the pilot plant in Williams et al. (1999) involves installation of electrodes on the hydrocyclone wall. In the offshore industry this is not possible, with respect to the very high safety specifications in the constructions of equipment. We will therefore concentrate on installing the electrodes upstream the inlet and downstream the underflow of the hydrocyclone. Dong et al. (2003) investigated ERT for measuring two phase flow in pipes in terms of water and air, their results showed the potential capability of ERT instrument of measuring different types of flow regimes. They successfully distinguished between Bubble, Slug, Multi-Bubble and Annular flow. Two and three dimensional images were successfully constructed in a real-time manner. We believe that once techniques can be successfully used for gas with water, they can also be potentially used for oil with water with respect to the fact that both air and oil have very low conductivities. Hydrocarbon oil has a conductivity less than $10pS/m$ (Michael Lindner (2014)) and a gas mixture such as air has a conductivity as low as $2.95fS/m$ with high aerosol concentration (Pawar et al. (2009)). These two conductivities both have much lower values than water does, for instance the water with a salinity of $20g/kg$ and $20°C$ has a conductivity of $2.901S/m$ according to NPL (2014). Therefore these techniques could be extrapolated and used to examine OiW concentrations in evaluating deoiling system's performance. Ismail et al. (2005) pointed out some potential drawback of using electric tomography methods, i.e. their inability to send electrons in direct paths, which is different from γ-ray where the rays can be sent in a direct path from the source. Thereby using ERT, there is some risk that the electrical current from one electrode to the other through the medium may travel around obstacles of high resistivity, by following the path of least resistance. Apart from the direct path which the γ-ray tomography can handle, γ-ray tomography is also able to make fast measurements, Thorn et al. (1999) mentioned that their system developed at the University of Bergen can handle several hundred frames per second if a sufficient computing power is available. Johansen et al. (1996) mentioned the safety issue of using γ-ray tomography, though with their setup the radiation is less than $0.1\mu Svh^{-1}$ at 1 meters distance, with is far below the recommended maximum dose of $7.5\mu Svh^{-1}$. To achieve this low radiation, the setup described in Johansen et al. (1996) requires carefully construction using thick steel plates to shield the radiation. Although the γ-ray method has some advantages over the electric tomography, as shown in figure 3, it won't be the main focus in this work, mainly due to the complexity of design and the high price of it.

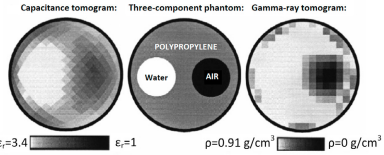

Fig. 3. Compassion between ECT and γ-ray tomography, the test benchmark is illustrated as the middle image. The γ-ray tomography can be improved to show the water phase (Johansen et al. (1996)).

3. TEST SETUP

The ERT method is, from the manufacturing perspective, cheap and easy to construct, however it requires direct electrical connection to the pipe contents thereby this method requires the use of somewhat specific materials. The resolution of the method depends on the permissible number of electrodes. The test setup is constructed to enable the liquid to be stationary and to be flowing subject to a pumping system. This setup consists of several parts: the ERT pipe which is constructed out of polymethyl methacrylate (PMMA, acrylic glass) with a nominal diameter of $50mm$ and $30cm$ length; a centrifugal pump; connecting pipes with an inner diameter of $12mm$ and a buffer tank. A schematic diagram of the test setup is illustrated in figure 4. Water and oil can be added to the system by filling up the buffer tank. The electrodes have been placed

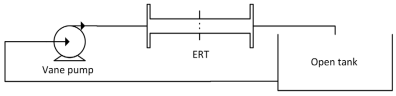

Fig. 4. Diagram of the test system, containing a controllable pump, and the ERT unit which is connected to a I/O card. (National instruments PCI-6229)

around the pipe in 360 degrees to cover the entire circle. 12 electrodes are placed 30° apart, as illustrated in figure 5. The electrodes are threaded stainless steel rods of equal length, which can be adjusted by screwing and whereto the measurement connections are made using cable clamps. Further mounting improvement could be achieved by using machined non-reactive metal electrodes (for example platinum, titanium or "Hastelloy", depending on the process conditions), similar to the design and materials used in magnetic flow meters, see Emerson (2014). Each electrode is connected to a digital voltage source through a precision

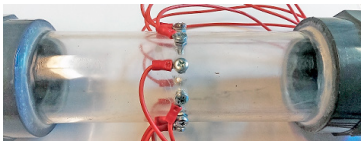

Fig. 5. Illustration of the ERT sensor configuration

$\pm 1\%$ measurement resistor, where each end of the resistor is connected to an ADC channel on the NI PCI-6229 data acquisition card, as illustrated in figure 6. Conductance

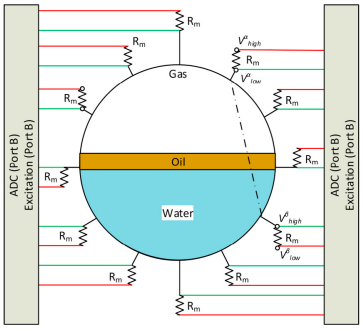

Fig. 6. Probe layout and electrical connection with measurement resistors for ERT setup. Red wires represent excitation/measurement connections and green wires represent passive measurement connections

measurement is performed by exciting one electrode at 5 volts while all the other electrodes are set to 0 volts, then measuring the voltage on all channels including the excitation channel. The conductance for one electrode pair, $G_{\alpha\beta}$, can then be calculated as in equations 2 to 4. α represents the active electrode while β represents the passive electrode, such that v^{α}_{high} and v^{α}_{low} is the high add low voltages respectably for the measurement resistor at the active electrode, and v^{β}_{high} and v^{β}_{low} is for the measurement resistor at the passive electrode, see figure 6.
Similarly $i_{\alpha\beta}$ is the current through the passive electrode β wile α is the active electrode, and $v_{\alpha\beta}$ is the voltage drop from α to β.

$$i_{\alpha\beta} = \frac{v^{\beta}_{high} - v^{\beta}_{low}}{R_m} \tag{2}$$

$$v_{\alpha\beta} = v^{\alpha}_{low} - v^{\beta}_{high} \tag{3}$$

$$G_{\alpha\beta} = \frac{i_{\alpha\beta}}{v_{\alpha\beta}} \tag{4}$$

After one measurement frame is completed, the same procedure will be repeated for all other electrodes. By the end $12 \cdot 11 = 132$ (channel) samples are collected. These measurements can be performed at a maximal sampling rate of $f_s = 1000[Hz]$, which is subdivided over the channel count $n_c = 16$ (due to coding specifics, 4 extra channels are scanned but not connected to electrodes), so that each full measurement cycle (frame) can be performed at a rate as: $f_{frame} = \frac{f_s}{n_c} = 62.5[Hz]$. This sampling rate can be increased by using equipment with a faster analog converter, if this is required by the application.

4. TOMOGRAM GENERATION ALGORITHMS

In the following, two algorithms, which are based on a 2-D plane representing the cross-section of the pipe in which all the electrodes are situated, are considered. The origin corresponds to the center of the pipe, the x_1-axis represents the width of the pipe, the x_2-axis represents the height of the pipe. The radius of the pipe is normalized to 1. The position of each electrode is represented by a point in this plane. For each pair of the active and the passive electrode (α, β), a standard line equation in the form of equation 5 is defined for the line trough these points.

$$a_{\alpha\beta}\, x_1 + b_{\alpha\beta}\, x_2 + c_{\alpha\beta} = 0 \tag{5}$$

Each of the measured conductances is multiplied with the distance between the electrodes, $l_{\alpha\beta}$, in order to get a conductance per normalized length unit (radius), $g_{\alpha\beta}$.

$$g_{\alpha\beta} = G_{\alpha\beta}\, l_{\alpha\beta} \tag{6}$$

For each point in the plane, $\mathbf{x}$, an interpolated conductance per length unit, $g(\mathbf{x})$, is calculated as a weighted average of $g_{\alpha\beta}$, which is inspired by Shepard's method, see Shepard (1968).

$$g(\mathbf{x}) = \begin{cases} \dfrac{\sum\limits_{(\alpha,\beta)\in\mathbf{S}} w_{\alpha\beta}(\mathbf{x}) g_{\alpha\beta}}{\sum\limits_{(\alpha,\beta)\in\mathbf{S}} w_{\alpha\beta}(\mathbf{x})} \end{cases} \tag{7}$$

$$\mathbf{S} = \{(\alpha,\beta) | \beta \neq \alpha\} \tag{8}$$

In this $\mathbf{S}$ is the set of all measurements represented by its pair of electrodes, and the weight, $w_{\alpha\beta}(\mathbf{x})$ is defined as:

$$w_{\alpha\beta}(\mathbf{x}) = \frac{1}{D_i\,(\mathbf{x},\alpha,\beta)^u} \tag{9}$$

Where the constant u controls how much the influence of each measurement decreases with distance. According to Shepard (1968) $u = 2$ is suggested, while Lukaszyk (2004) noted that $u > 2$ usually is assumed and $u > 1$ is needed for a smooth interpolation function. $D_i(\mathbf{x},\alpha,\beta)$ is one of two different distance quantities denoted either $D_{dis}(\mathbf{x},\alpha,\beta)$ or $D_{\mathbf{L}uk}(\mathbf{x},\alpha,\beta)$, these quantities are what makes the two algorithms different in our concern. Both quantities are related to the minimum distance, $d(\mathbf{x},\alpha,\beta)$, from a point, $\mathbf{x}$ to the line defined for a pair of electrodes (α,β) (see figure 7):

$$d(\mathbf{x},\alpha,\beta) = \frac{|a_{\alpha\beta}\, x_1 + b_{\alpha\beta}\, x_2 + c_{\alpha\beta}|}{\sqrt{a^2_{\alpha\beta} + b^2_{\alpha\beta}}} \tag{10}$$

$D_{dis}(\mathbf{x},\alpha,\beta)$ is the maximum between $d(\mathbf{x},\alpha,\beta)$ and a

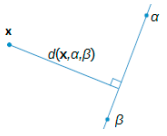

Fig. 7. Relation between $\mathbf{x}$, α, β and $d(\mathbf{x},\alpha,\beta)$

lower bound for the distance d_{min}, which is used in order not to over emphasize the value of a single $g_{\alpha,\beta}$ for points on the line defined for the corresponding pair of electrodes (α,β):

$$D_{dis}(\mathbf{x},\alpha,\beta) = \max\left(d(\mathbf{x},\alpha,\beta), d_{min}\right) \tag{11}$$

The algorithm that applies this quantity is noted as: Minimum distance algorithm in this paper. $D_{\mathrm{L}uk}(\mathbf{x}, \alpha, \beta)$ is an adaptation of Łukaszyk-Karmowski probability metric for a distance between two random vectors according to Łukaszyk (2004). A new set of axes is defied with the projection of $\mathbf{x}$ on the line for $g_{\alpha\beta}$ as origin, the y_1-axis is on the line and has positive direction from α to β, the y_2-axis is particular on the y_1-axis and has positive direction from the line to $\mathbf{x}$. The point $\mathbf{x}$ is described by Dirac delta distributions, i.e. an exact value:

$$f_{\mathbf{x},1}(y_1) = \delta(y_1) \tag{12}$$

$$f_{\mathbf{x},2}(y_2) = \delta(y_2 - d(\mathbf{x}, \alpha, \beta)) \tag{13}$$

While the line is described by an uniform distribution on the line and a Dirac delta distribution particular on it:

$$f_{l,1}(y_1) = \begin{cases} \frac{1}{z_\alpha + z_\beta} y_1 & \text{if} - z_\alpha \leq y_1 \leq z_\beta \\ 0 & \text{otherwise} \end{cases} \tag{14}$$

$$f_{l,2}(y_2) = \delta(y_2) \tag{15}$$

Where z_α and z_β are the distance from the point's projection on the line to the active and passive electrode respectively. The definition of $D_{\mathrm{L}uk}(\mathbf{x}, \alpha, \beta)$ in equation 16 is valid for independent marginal distributions.

$$D_{\mathrm{L}uk}(\mathbf{x}, \alpha, \beta) \equiv \left(\sum_{i=1}^{2} \left(\int_{-\infty}^{\infty} \int_{-\infty}^{\infty} f_{\mathbf{x},i}(y_a) f_{l,i}(y_b) \, \mathrm{d}y_a \mathrm{d}y_b \right)^p \right)^{\frac{1}{p}} \tag{16}$$

Where p defines which p-norm is used to get the norm of the vector, as this vector represents a physical distance the 2-norm is most commonly used, resulting in equation 17.

$$D_{\mathrm{L}uk}(\mathbf{x}, \alpha, \beta) = \left(\left(\frac{z_\alpha^2 + z_\beta^2}{2 \cdot (z_\alpha + z_\beta)} \right)^p + d(\mathbf{x}, \alpha, \beta)^p \right)^{\frac{1}{p}} \tag{17}$$

The algorithm that applies this quantity is noted as: Łukaszyk-Karmowski algorithm in this paper.

5. TEST PROCEDURE AND CALIBRATION

Two test scenarios are considered: (i) static testing, where the ERT-pipe is filled with liquid consisting of a predetermined water & oil contents with a mixture ratio of 15/85%, which we name as low water case, and 85/15% which we name as high water case. The static tests are used as the baseline for exploring the capabilities of the setup; (ii) dynamic flowing test, where the pipe is subjected to a liquid flow, in order to investigate the dynamic performance of the measurement solution. Ideally an oil & water mixture would have been used, however due to limitations in the pumping system the dynamic flow rate test contains water and a small gas phase (air) within this early investigation phase, where the air is existing solely due to turbulence in the pipes; no dedicated gas flow was added to this test. In order to calibrate the electrode connections, the pipe is filled with water, and the electrodes are manually adjusted by screwing until the measured conductivity per length in all paths are the same.

6. TEST RESULTS AND DISCUSSION

The obtained results for stationary low water levels are illustrated in figures 8 and 9, and the high water level results are illustrated in figures 10 and 11. By comparing both concerned algorithms, it is evident that the Łukaszyk-Karmowski algorithm can lead to more smooth results (in the terms of the gradient), whereas in the minimum distance approach, the results are affected by the electrode positions, as compared from figures 8a and 9a. However the smoothing of the Łukaszyk-Karmowski algorithm results in a transient between conductive and non-conductive material having a lesser gradient than in the minimum distance cases, as illustrated from the comparison of figures 8b and 9b. This increases the difficulty of determining the phase separation from the 2-D results if a gradient based approach is utilized. Another option is to estimate the water fraction using a simple threshold on the conductance values over the set of points χ, as shown in equation 18.

$$w_{water} = \frac{\sum_{\mathbf{x} \in \chi} (g(\mathbf{x}) > g_{thres})}{n_x} \tag{18}$$

Where the threshold g_{thres} is selected from the largest transition of the minimum distance algorithm in the low water case, where the transition is easily determined. In these experiments the threshold becomes $1.236 * 10^{-}5$. Applying the equation to the results yields the water fractions listed in table 1. It is observed that the tests

Experiment	Low water	High water
Minimum distance	8.5 %	87.6 %
Łukaszyk-Karmowski	12.1 %	87.7 %

Table 1.

with high concentration of water have worse results than the tests with a high concentration of oil/gas, here referring to figures 8a, 8b, 9a, 9b, 10a, 10b, 11a and 11b. We observed that the conductivity transition (high-low), which is illustrated the following 1-D figures 8b, 9b, 10b and 11b, is occurring more prominently for the low water concentration tests than the high water concentration tests. To illustrate this refer to the gradient of the slope in figures 8b and 9b, where the slope has a high gradient and where it is lower in figure 11b, which represents the high water concentration calculated using the minimum distance algorithm. It has a similar gradient as figures 8b and 9b, although the oil water transition is more curved when observing the 2-D figure 10a. A possible reason for this behavior is that only a small amount of oil/gas around the electrodes results in almost 0 conductivity measurement, thus the oil/gas is more likely to effect a high water concentration than the opposite. This effect is worsened with a lower amount of electrodes, as this leaves relatively big gaps between electrodes and thus the transition where oil occurs on the electrodes will be larger, and the results will have a less precise illustration of the phases during high water phase concentrations. For the test with mixed gas/water flow, illustrated in figure 12 and 13 the individual gas bubbles cannot be distinguished from the liquid due to the low resolution using either method, which is critical if the gas bubble sizes are to be directly determined, however the overall content of the pipe is well represented as being mostly conductive material. The mean conductance, which is calculated and presented in figures 8a, 8b, 9a, 9b, 10a, 10b, 11a, 11b, 12 and 13, can be used for determination of the pipe contents. However this is heavily effected by several factors, including salinity and oil composition, therefore some form of calibration or secondary measurement will be needed to allow this value to be used for control and monitoring purposes. An investigation of the mean conductance of the low water level in figure 8a ($0.35348 \cdot 10^{-5}$), the mean conductance

of the high water level in figure 10a ($2.1784 \cdot 10^{-5}$) and the mean conductance of the running water and gas mixture from figure 12 ($2.3279 \cdot 10^{-5}$) indicate that there is a logical relation between the mean conductance and the amount of water in the pipe. This means that it is indeed feasible to use this technique for measuring the concentration of water/oil or water/gas in the pipes.

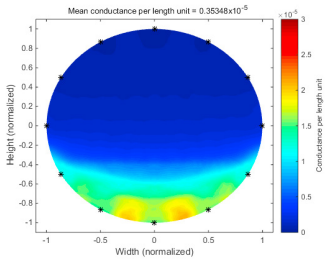

(a) Minimum distance algorithm, 2D

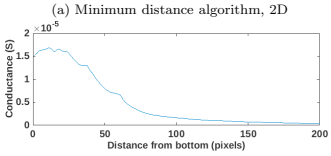

(b) Minimum distance algorithm, average levels

Fig. 8. Low water level using minimum distance algorithm

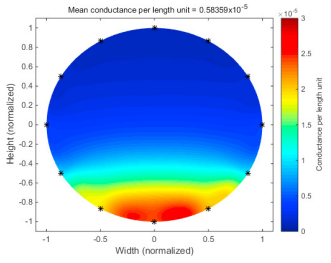

(a) Łukaszyk-Karmowski algorithm, 2D

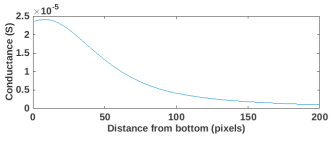

(b) Łukaszyk-Karmowski algorithm, average over width

Fig. 9. Low water level using Łukaszyk-Karmowski algorithm

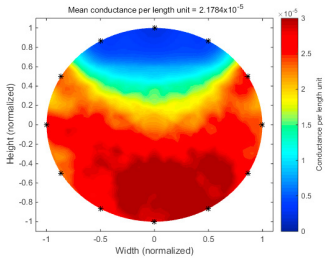

(a) Minimum distance algorithm, 2D plot

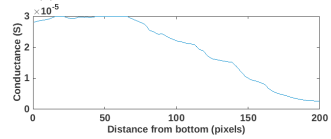

(b) Minimum distance algorithm, average levels

Fig. 10. High water level using minimum distance algorithm

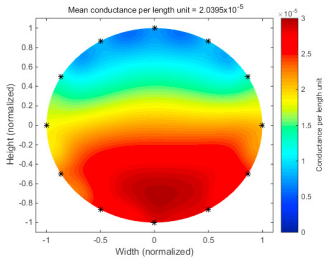

(a) Łukaszyk-Karmowski algorithm, 2D

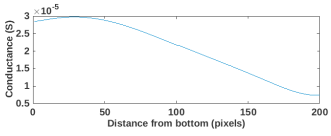

(b) Łukaszyk-Karmowski algorithm, average levels

Fig. 11. High water level using Łukaszyk-Karmowski algorithm

7. CONCLUSION

In this preliminary study, a cost-effective and non-invasive method based on ERT technique for OiW measuring and analysis has been investigated. The ultimate objective of this undergoing investigation aims for a potential cost-effective real-time measurement technique for OiW concentration at the hydrocyclones inlet and underflow. To test the feasibility of the proposed method and approach,

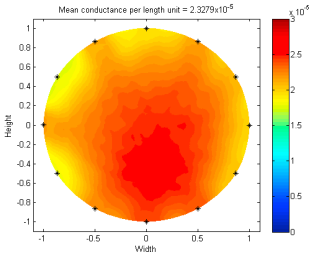

Fig. 12. Running water and gas mixture using minimum distance algorithm, 2-D

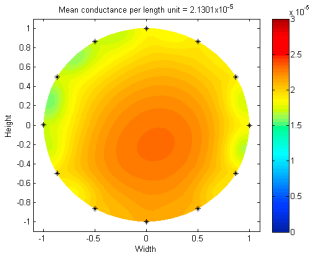

Fig. 13. Running water and gas mixture using Łukaszyk-Karmowski algorithm, 2-D

a pilot plant consisting of a 50mm pipe with attached electrodes and a pumping circulatory system, is constructed. The oil and water interface in the pipe for static cases can be clearly observed in the generated 2-D tomograms. For dynamic flow measurements, where the medium was water with a small amount of non-purposed gas mixture, the overall content of the pipe can still be determined. Trough analysis of the average conductivity in the mixture, we are able to detect a link between OiW concentration and the average of measured conductivities.

Future work will involve testing of the concentration of oil/gas in water of known concentrations to investigate if concentrations can be registered precisely, thus simplifying the use of 2-D imaging for feedback control. Another extend of our work will be to increase the amount of electrodes to allow for higher resolution and thus investigate if this will enable us to visualize small particles in 2-D images. Also electric capacitive tomography (ECT) will be investigated, to compare the merits of this technology with ERT.

ACKNOWLEDGEMENTS

The authors would like to thank the support from the Danish National Advanced Technology Foundation. Our thanks also goes to colleagues J.P. Stigkjær, A. Aillos, K. G. Nielsen, M. Haubjerg and P. Molinari from Maersk Oil A/S, colleagues P. Sørensen, A. Andreasen, B. Løhndorf, S. A. Meybodi and J. M. Holm from Ramboll Oil & Gas A/S, and H. Enevoldsen from AAU, for many valuable discussions and technical support.

REFERENCES

Advanced Sensors (2014). Advanced Sensors - Oil in Water Analyzers. URL `http://www.advancedsensors.co.uk/`.

Agar Corporation (2014). Agar Corporation - MPFM 50. URL `http://www.agarcorp.com/Animation/MPFM/50/MPFM50.html`.

Dong, F., Jiang, Z., Qiao, X., and Xu, L. (2003). Application of electrical resistance tomography to two-phase pipe flow parameters measurement. *Flow Measurement and Instrumentation*, 14(4-5), 183–192.

Dong, F., Liu, X., Deng, X., Xu, L., and Xu, L.a. (2001). Identification of two-phase flow regimes in horizontal, inclined and vertical pipes. *Measurement Science and Technology*, 12(8), 1069–1075.

Emerson (2014). Magnetic flowmeter material selection guide. URL `http://www2.emersonprocess.com/siteadmincenter/PM%20Rosemount%20Documents/00816-0100-3033.pdf`.

Husveg, T., Rambeau, O., Drengstig, T., and Bilstad, T. (2007). Performance of a deoiling hydrocyclone during variable flow rates. *Minerals Engineering*, 20(4), 368–379.

Ismail, I., Gamio, J., Bukhari, S., and Yang, W. (2005). Tomography for multi-phase flow measurement in the oil industry. *Flow Measurement and Instrumentation*, 16(2-3), 145–155.

Johansen, G., Frøystein, T., Hjertaker, B.T., and Olsen, O. (1996). A dual sensor flow imaging tomographic system. *Measurement Science and Technology*, 7(3), 297–307.

Jorin (2014). Jorin - Vipa product range. URL `http://www.jorin.co.uk/products/`.

Kharoua, N., Khezzar, L., and Nemouchi, Z. (2010). Hydrocyclones for De-oiling Applications—A Review. *Petroleum Science and Technology*, 28(7), 738–755.

Michael Lindner (2014). Oil condition monitoring using electrical conductivity, oelcheck gmbh. URL `http://www.machinerylubrication.com/Read/29407/oil-condition-monitoring`.

Miljoestyrelsen (2010). Status for den danske offshorehandlingsplan til udgangen af 2009. *Miljoestyrelsen*.

NPL (2014). Physical properties of sea water. URL `http://www.kayelaby.npl.co.uk/general_physics/2_7/2_7_9.html`.

Pawar, S., Murugavel, P., and Lal, D. (2009). Effect of relative humidity and sea level pressure on electrical conductivity of air over indian ocean. *Journal of Geophysical Research: Atmospheres (1984–2012)*, 114(D2).

Shepard, D. (1968). A two-dimensional interpolation function for irregularly-spaced data. In *Proceedings of the 1968 23rd ACM National Conference*, ACM '68, 517–524. ACM, New York, NY, USA.

Thorn, R., Johansen, G., and Hammer, E. (1999). Three-Phase Flow Measurement in the Offshore Oil Industry: Is There a Place for Process Tomography? *Industrial Process Tomography*, 228–235.

Łukaszyk, S. (2004). A new concept of probability metric and its applications in approximation of scattered data sets. *Computational Mechanics*, 33(4), 299–304.

Williams, R.A., Jia, X., West, R.M., Wang, M., Cullivan, J., Bond, J., Faulks, I., Dyakowski, T., Wang, S., Climpson, N., Kostuch, J., and Payton, D. (1999). Industrial monitoring of hydrocyclone operation using electrical resistance tomography. *Minerals Engineering*, 12(10), 1245–1252.

Wolbert, D., Ma, B.F., Aurelle, Y., and Seureau, J. (1995). Efficiency estimation of liquid-liquid Hydrocyclones using trajectory analysis. *AIChE Journal*, 41(6), 1395–1402.

Young, G. and Wakley, W. (1994). Oil-water separation using hydrocyclones: An experimental search for optimum dimensions. *Journal of Petroleum Science and Engineering*, 11(93), 37–50.

Paper D

Evaluation of OiW Measurement Technologies for Deoiling Hydrocyclone Efficiency Estimation and Control

Petar Durdevic, Simon Pedersen, Zhenyu Yang

The paper is in proceedings of:
OCEANS'16 MTS/IEEE Shanghai 2016; doi:
10.1109/OCEANSAP.2016.7485361

The layout has been revised.

Evaluation of OiW Measurement Technologies for Deoiling Hydrocyclone Efficiency Estimation and Control

Petar Durdevic
Department of Energy Technology
Aalborg University
Esbjerg 6700, Denmark
Email: pdl@et.aau.dk

Simon Pedersen
Department of Energy Technology
Aalborg University
Esbjerg 6700, Denmark
Email: spe@et.aau.dk

Zhenyu Yang
Department of Energy Technology
Aalborg University
Esbjerg 6700, Denmark
Email: yang@et.aau.dk

***Abstract*—Offshore oil and gas industry has been active in the North Sea for more than half a century, contributing to the economy and facilitating a low oil import rate in the producing countries. The peak production was reached in the early 2000s, and since then the oil production has been decreasing while the water cut has been increasing rapidly. The water dominates some of the wells and a water cut of 90% is not uncommon, where all of the water has to be separated from the oil before it is discharged into the ocean. As the oil cut in the Danish part of the North Sea decreases the pumped volume is increased to reach the desired oil production capacity, consequently the discharged amount of oil increases.This leads to oceanic pollution, which has been linked to various negative effects in the marine life. The current legislation requires a maximum oil discharge of 30 parts per million (PPM). The oil in water (OiW) concentration is difficult to measure and currently is done manually and offline. This poses a challenge in continuously monitoring the actual amount of oil that is being discharged into the ocean. Our goal is to optimize the separation efficiency in a deoiling hydrocyclone, by developing a novel control technology which is based on online and dynamic OiW measurements. This article evaluates some currently available online measuring technologies to measure OiW, and the possibility to use these techniques for hydrocyclone efficiency evaluation, model development and as a feedback parameter. We additionally look at particle size measurements, as they play a big role in the separation process' efficiency.**

***Index Terms*—Control, Offshore, Oil & Gas, OiW, Instrumentation**

I. Introduction

Offshore separation of oil, gas and water, has become an increasing part of the petroleum industry, with increasing water cuts and depleted oil reservoirs resulting, in some cases, in a water cut of more than 90% [1], [2]. To fulfill the current OiW requirements of 30PPM, set by the government [3], the offshore installations have to work under an increasingly higher strain. Current separation processes consist of a series of gravity separators, which separate three phases, oil, water and gas. The water effluent from the separator still contains, in some cases, around 500PPM of oil. The water is therefore further purified using downstream hydrocyclone facilities, which are able to reduce the amount of OiW by approximately 90% [4]. In our experience the offshore operators report an OiW concentration of the effluent of 20PPM. The efficiency is governed by multiple varying factors; inlet particle size, concentration, temperature, but most important of all is efficient hydrocyclone control. At present hydrocyclone control is based on a Pressure Drop Ratio (PDR), which is approximated to be linearly proportional to the hydrocyclone's efficiency under steady state [5], [6]. Efficient online OiW monitoring could facilitate a solid basis for further investigation of this relationship. Furthermore continuous OiW monitoring would enable a feedback based control of the deoiling operation and help determine and improve its efficiency. As a part of our team's research in this area, we have designed and constructed a pilot plant at Aalborg University Esbjerg, which is a scaled model of an offshore deoiling installation, the separation part is illustrated in figure 1. The pilot plant has a scaled version of a three phase separator ($S_{\text{3-Phase}}$) which is connected to a hydrocyclone separator array ($H_{1..n}$), downstream of the separator's water outlet. The hydrocyclone separator array holds two individual offshore hydrocyclone liners, which are connected in parallel and with the possibility of extending to more individual liners, both in parallel and in series. Upstream of the three phase separator, a $\approx$6m vertical pipeline leads to a $\approx$25m horizontal pipeline, see figure 2, this long pipeline emulates the pipelines on the seabed and the riser leading to the platform. In our experiments we have been able to successfully recreate slugging behavior using these pipelines, for more information refer to [7]. The entire setup is fed using two different pumps for oil, water and a compressor for gas (air), and the setup has the ability to inject a feed of more than 4m^3/h at 10.5bars with an oil cut ranging from 20PPM to $30,000$PPM, with possibility for more. Hydrocyclone liners are difficult to scale due to their complex internal hydrodynamics, and thus original offshore units are used. Every part of the setup is therefore scaled around the industrial hydrocyclone liner. The pilot plant is constructed with the same instrumentation as an offshore setup, but for this article we specifically concentrate on our OiW measurement installation. We use two measuring techniques, a fluorescence based (Turner Design, TD-4100XD [8]) with the ability to measure OiW concentration and an

978-1-4673-9724-7/16/$31.00 ©2016 IEEE

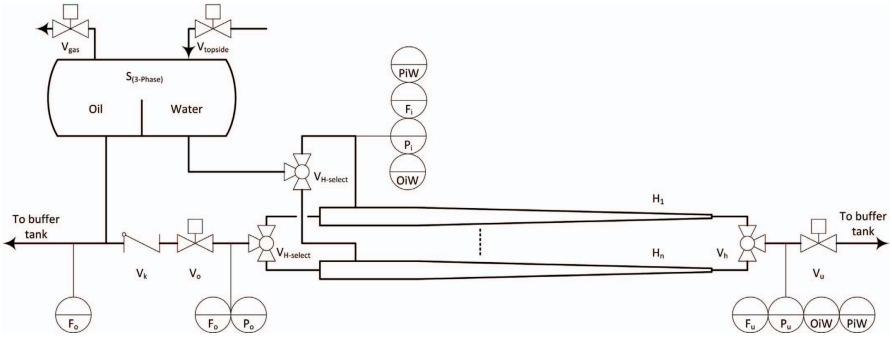

Fig. 1: Diagram of the separation pilot plant, including a three phase separator and parallel hydrocyclone liners.

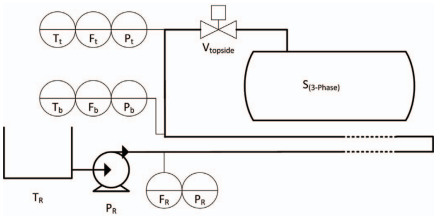

Fig. 2: A simplified diagram of the horizontal and vertical pipeline system.

optical based (Jorin, VIPA Model B HF [9]) with the ability to measure OiW concentration, particle size and distribution, both equipment are illustrated in figure 3. The two instruments will henceforth be referred to as Turner and VIPA respectively.

Fig. 3: OiW measurement equipment, (top) VIPA [9] and (bottom) Turner [8].

II. Measurement Equipment & Technique Analysis

Both techniques involve a side-stream technology where the sample is redirected from a side-stream in the flow pipe and into the view-cell. This makes the equipment applicable on all installations, regardless of their size or flow rate. The Turner instrument, which is based on fluorescence principle, sends in a calibrated wavelength into the view-cell, and then the reflected light is captured using a photosensitive sensor. The oil absorbs the energy and emits a lower wavelength, the emitted energy is then captured by the sensor. Oil's composition, here mainly the aromatics, have the ability to fluoresce, on the other side water does not and thus only the oil phase will emit energy. The data acquired by the photosensitive sensor is translated into relative florescence units (RFU), which, when calibrated, are proportional to a specific value of PPM of oil in the mixture. The view cell, light source and the photosensitive sensor are depicted in figure 4. The VIPA instrument is based

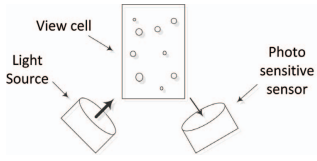

Fig. 4: Fluorescence view-cell.

on a microscopy technique, where the view cell is lit up by a visible light source while a camera records the stream through a microscope lens, see figure 5. When the liquid mixture enters the view-cell, it passes through a focal zone of the camera

lens, and a picture is captured of the mixture every 33.3ms or 30fps. These pictures, an example of twelve images captured by the VIPA are depicted in figure 6, are then analyzed by specifically designed software for particle shape, size and count. Different algorithms calculate the type of particle, its size and shape and based on this, the overall concentration and size of particles in the liquid in which they are dispersed are estimated. The benefit of using the microscopy is the ability

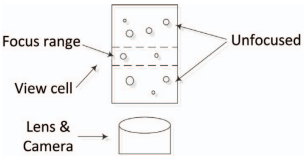

Fig. 5: Video microscopy view-cell.

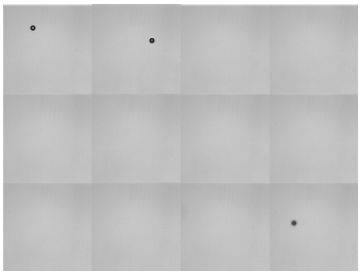

Fig. 6: A set of 12 VIPA images as they were captured, from left to right.

to visualize the particle size and shape, which enables the distinction between solids, oil and water and to determine the concentration of each. The particle sizes are very important for the separation, for more information refer to [5], and monitoring of these can assure a more precise control and evaluation of the process. The VIPA microscope views a small sample space of the entire flow as seen in figure 7. The figure illustrates the side stream technique, where a relatively small stream is redirected from the main flow stream into the view cell. To make matters worse, the microscope has narrow focal point, as illustrated in figure 5, and thus particles far from this point will be out of focus and thus not clear to the camera and thus excluded from the capture. The small sample space results in a less valid statistical representation of the entire flow, as the particles are randomly dispersed in the flow stream. Therefore dynamic OiW concentration and the particle size are not directly measurable with this technology, only a statistical tendency can be achieved by filtering the acquired data.

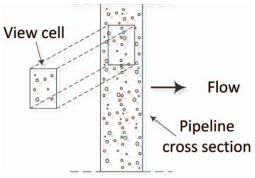

Fig. 7: Sampling techniques used in the instruments, where a sample is redirected into the side-stream and then trough the view-cell.

III. Calibration of Equipment for OiW Concentration and Particle Size Measurement

Both instruments were calibrated for the specific oil used in the tests. We chose a commercially available oil with similar color and viscosity as crude oil from the North Sea (GARDEN OIL SAE 30 [10]). The Turner and VIPA were calibrated regarding OiW concentration, in addition, the VIPA, since it measures particle sizes, was also calibrated with solid particles of known sizes.

A. Turner Calibration

The calibration of the Turner was done by following the producer's specifications, and involved the preparation of different oil concentrations dispersed in Isopropyl alcohol. For the calibration of the Turner the following concentrations were used: $[20, 25, 50, 75, 100, 150, 200]$PPM. Each of the concentrations were injected into the measurement chamber using two 50ml syringes, where one injection took $\approx$10 seconds while injecting the mixture with a steady and consistent flow. The

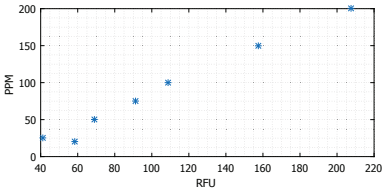

Fig. 8: Calibration results of the Turner instrument.

results of the calibration are illustrated in figure 8, the y axis represents the OiW concentration and the x axis the observed Relative fluorescence units (RFU).

B. VIPA Calibration

The calibration method used for the Turner could not be used for the VIPA as Isopropyl alcohol dissolves the oil droplets and they cannot be detected by the VIPA. The VIPA was instead calibrated with oil dispersed in distilled water, but oil emulsification and sticking of the oil to the equipment

sidewalls made precise calibration difficult. To solve this issue the liquid mixture was pumped first through the Turner and then through the VIPA. This would mix the oil in to the water through a pump and circulate the mixture constantly to keep the oil dispersed in the water. By doing so we could also use the calibrated Turner as a tool for validation. The result of

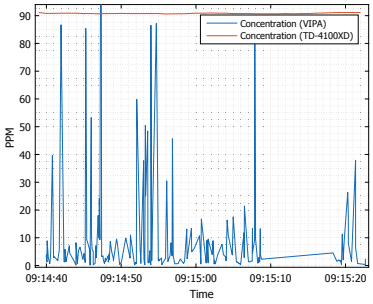

Fig. 9: Measurement results from the VIPA and Turner connected in series, where the feed mixture (90 PPM in OiW) is circulated by a cavitation pump.

the series test is presented in figure 9, where a mixture of 90 PPM was injected into the loop and measured through both instruments. The Turner was successfully calibrated at this point based on the method mentioned earlier, and it reported a mean value of 90.8181PPM with a standard deviation of 0.1364. The VIPA data had a mean value of 9.7269PPM and a standard deviation of 20.3587. Assuming that the we have a normal distribution the normal Probability Density Function (PDF) of the PPM measurements for the two instruments are as plotted in figure 10. The Turner measurements lie in a narrow area $[90.6 - 91.11]$PPM, the reason for recurrence of samples is believed to be caused by disorganization of the signal by the instrument. The VIPA result is very scattered, and judging on the frequency of occurrence it is not a statistically credible method of measuring PPM, although the instrument does measure a concentration of close to 90PPM $[82.83 - 87.17]$PPM five times.

C. VIPA Calibration and Validation using Calibrated Particle Sizes

The calibration of the VIPA equipment was approached from a more deterministic point of view, where the injected liquid was mixed with calibrated particles. The particles are specifically designed for calibration of optical particle counters, produced by BS-Particle GmbH. The individual particles are manufactured from Poly-(styrene-co-divinylbenzene)), and each batch has a narrow particle diameter deviation. The batch used for this experiment is delivered with a certificate of calibration, the particle sizes that were used in the tests are

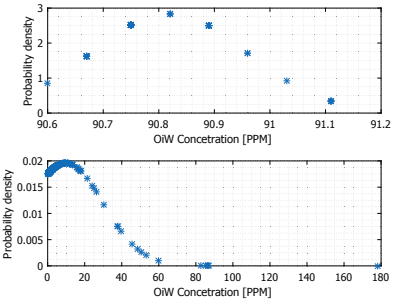

Fig. 10: Normal PDF of the PPM measurements with the Turner (top) and VIPA (bottom).

presented in table I. A series of tests are performed where the

TABLE I: Particle characteristics representing the: particle size, size deviation, standard deviation and relative standard deviation, data is provided by the manufacturer (BS-Partikel GmbH).

Particle size X_N	D X_N	SD X_N	Rel. SD X_N
$9.87\mu m$	$\pm 0.12\mu m$	0.24	2.4%
$19.55\mu m$	$\pm 0.20\mu m$	0.55	2.8%
$40.3\mu m$	$\pm 0.3\mu m$	0.91	2.2%
$75.7\mu m$	$\pm 0.5\mu m$	1.97	2.6%

different particles are circulated through the VIPA instrument using a peristaltic pump, which is used due to its low shearing. The particles as viewed by the VIPA can be seen in figure 11.

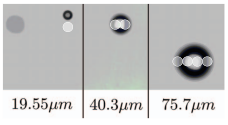

Fig. 11: 3 images captured by the VIPA and compared side by side. The particle sizes are displayed below the photos.

1) Calibration Result with a Particle Size of $9.87\mu m$: A particle size of 9.87μm was introduced into the VIPA instrument, and measured continuously, the result is displayed in figure 12. The top plot in figure 12 illustrates the particle sizes over time, the bottom plot shows the normal PDF of the particle sizes. The first test has a mean size of 12.68μm, which is slightly above the particle size. With that being said, the measurements are very accurate with a small deviation from the real particle size, as is evident in the middle plot from figure 12. This offset is caused by measurement error which could be due to a calibration error, (although the system

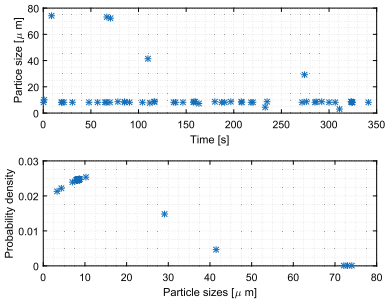

Fig. 12: VIPA results using calibrated particles, size 9.87μm.

was meticulously calibrated between each test). The result also indicates some particles at approximately 40 and 75μm, these are residues in the pumping system from previous tests with the other particle sizes. After every test the circulation system and the instrument were cleaned with soap and rinsed thoroughly with water several times. Other registered particle sizes which occur rarely can be caused by dirt in the system, but statistically they pose a small implication. The concentration plots indicate a very low concentration of particles, as the particles have a small diameter and thus are a small mass concentration in the overall mixture, only when the instrument registers some of the larger particles does the concentration increase.

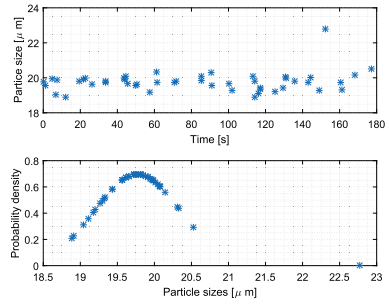

Fig. 13: VIPA results using calibrated particles, size 19.55μm.

2) Calibration Result with a Particle Size of 19.55μ*m:* The test using 19.55μm particles gives a more consistent result than the 9.87μm particle test, where the particles are placed between $\approx$ 18.9 and 20.5μm, only one particle is found outside the range which is $\approx 22.7\mu$m. This consistency is proportionally related to the PPM as can be seen in the two bottom plots. The frequency of occurrence of the particle sizes indicates the peak particle size to 19.7μm, again a slight offset from the injected particle but this is considered a measurement offset caused by calibration offsets and optical distortion caused by fouling. But nevertheless the precision is within $\approx \pm 1\mu$m.

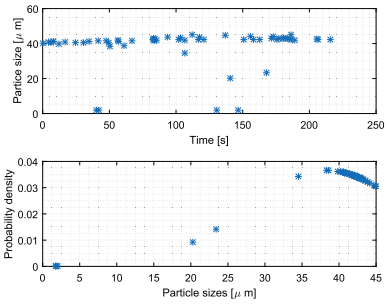

Fig. 14: VIPA results using calibrated particles, size 40.3μm.

3) Calibration Result with a Particle Size of 40.3μ*m:* The test with 40.3μm particles, has a slightly more noisy data, recording some of the 19.55μm particles, which are residual in the mixture as this test was made after the 19.55μm particle test. The main concentration of the particles as seen in middle the plot in figure 14 is between $39 - 45\mu$m, not as consistent as the previous tests and with a larger standard deviation, here $\approx \pm 5\mu$m.

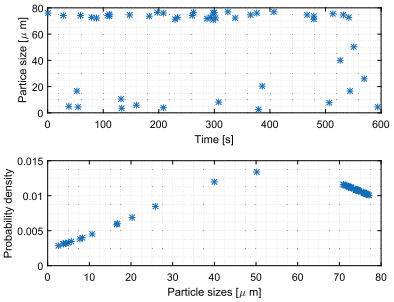

Fig. 15: VIPA results using calibrated particles, size 75.7μm.

4) Calibration Result with a Particle Size of 75.7 μm*:* The 75μm particle test was made after a retrial with all the particle sizes and thus some residue can be traced in the test.

Also some additional particle sizes occur, such as a $50, 26, 17$ and sub 10μm particles, these particles could be due to some external contaminant.

IV. Dynamic OiW Measurements

The dynamic analysis is only concerning the Turner, as the VIPA was proven not to work well in this regard. Two tests were made, one with a low concentration of oil (LCT) and one with a high concentration of oil (HCT) to analyze the system response at different concentrations.

A. LCT (1-20*PPM*)

For the first test the following OiW concentrations were prepared: $[1, 5, 10, 15, 20]$PPM. Each concentration was injected into the view-cell chamber using a syringe over a time period of ≈ 10s. After each injection the test was allowed to settle for ≈ 200s, before the next injection was performed, this enabled us to analyze the consistency of the steady state response.

TABLE II: Mean and variance of the steady state signal from the low concentration test with the Turner.

	1	5	10	15	20
Mean $[\mu]$	1.759	4.901	12.647	15.212	21.198
% D_i	43.2%	2%	20.9%	1.4%	5.7%
Variance $[\sigma^2]$	0.005	0.013	0.112	0.952	0.240

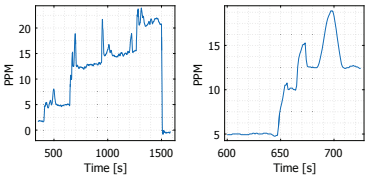

Fig. 16: Turner concentration validation with known oil concentrations diluted in Isopropyl alcohol, low concentrations: from 1-20PPM. Left plot illustrates all the concentration steps and the right plot illustrates a zoom in on one of the steps.

B. LCT Results (1-20*PPM*)

The steady state results from the LCT are presented in table II, which shows the steady state mean and variance data of the individual concentrations. The mean indicates that there is a slight deviation from the measurement, in the case of the 1PPM measurement the mean deviation from the designed concentration is 43.2% and for the 10PPM concentration it is 20.9%. In the 15PPM's case the percentile deviation is only 1.4%. The dynamic response of the LCT is plotted in figure 16. For each injection the instrument overshoots the measurement and oscillates for a varying period of time before settling. Some of the overshoot peaks reach ≈ 5PPM above the steady state value. An example is the 10PPM concentration (a zoomed in version is shown in the left plot of figure 16) which increases the first 10s of the injection time but then it drifts off to 18PPM and oscillates for 40s, after which it settles at a steady state mean value of 12.65PPM, this translates into a 42.32% overshoot.

C. HCT (50-200*PPM*)

For the tests with the (HCT) the following OiW concentrations are used: $[50, 75, 100, 150, 200]$PPM. The the test

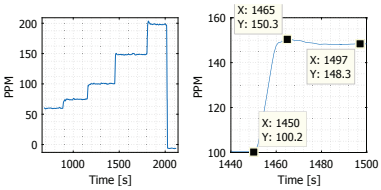

Fig. 17: Turner concentration validation with known oil concentrations diluted in Isopropyl alcohol (HCT): from 50-200PPM. Left plot illustrates all the concentration steps and the right plot illustrates a zoom in on one of the steps.

TABLE III: Mean and variance of the steady state signal from the HCT with the Turner.

	50	75	100	150	200
Mean $[\mu]$	59.849	74.509	100.335	148.476	198.117
% D_i	16.5%	0.66%	0.33%	1.03%	0.95%
Variance $[\sigma^2]$	0.195	0.262	0.234	0.306	0.200

procedure for the HCT is the same as that of the LCT, and the steady state values have been displayed in table III.

D. HCT Results (50-200*PPM*)

Judging from the percentile deviation compared to the one in table II, the steady sate offset has low influence on the HCT, the only instance where the error is above $\approx 1\%$PPM is for the 50PPM test. The percentile deviation of the 50PPM injection is much higher than for the rest of the concentrations in the HCT. The dynamics of the HCT is far more stable than the LCT, best seen in the right plot of figure 17 which illustrates the dynamic response of the concentration increase from 100-150PPM. In the plot the concentration measurement rises to the desired value within $\approx$ 10s, but then it overshoots and stabilizes after $\approx$ 32s, this translates into a 1.2% overshoot. The results are relatively similar for the rest of the injections.

V. Discussion & Conclusion

Through our work we have investigated different OiW measurement equipment for evaluating the efficiency of separation equipment. Through a thorough research, practical and theoretical, we have narrowed the equipment list to two instruments which are described in this article. Our goal was to investigate each of these equipment's ability to measure OiW concentration, particle sizes and to evaluate the precision and accuracy of the measurement both from a static and dynamic perspective, for use in our work with separation. Our findings are discussed in the following.

A. Microscopy

1) Static: The VIPA instrument was successfully able to determine the particle size and concentration of particles using 4 different particle sizes. The results were successful with very high precision of measurement. The issue with this equipment arose when looking at the dynamic behavior, due the design of the chamber and the nature of sampling, this measurement technique works optimally if the data is used in a statistical manner. We have experienced that the best use for this equipment is as a steady state indicator of particle sizes, and their concentration. This is an important task, as particle sizes have a huge impact on the separation efficiency of hydrocyclones. It is although still challenging to measure PPM and particle sizes in an online dynamic manner with the VIPA instrument.

B. Fluorescence

1) Static: The fluorescence based Turner was set to measure various OiW concentrations, ranging from 1-200PPM, which encompasses the range of that the filtration equipment can reach. The samples were injected manually and the dynamic and static response of the equipment was recorded. The static performance varied in the different ranges, especially for the lower concentrations, but the variations are insignificant as the measurement was in most cases within $\pm$1PPM of the desired value. The offset can be caused by several factors besides the embedded accuracy of the instrument, first is the calibration accuracy and second is a precise mixing of the mixture. This especially concerns the lower concentrations, where the amount of oil is one mg per liter of water. Apart from the measurement errors we conclude that the investigated instrument performed to our expectations from the steady state perspective.

2) Dynamic: The dynamic analysis is based on manual injections into the view-cell, and the test data show an increase of concentration the first $\approx$ 10s, which is the approximate injection time. The results indicate that the system can respond to a change in concentration within seconds and that the equipment does measure precisely and consistently. Additionally consistent readings were obtained without using Isopropyl alcohol in the series test, with a mean of 90.8181PPM and a standard deviation of 0.1406, for comparison the VIPA has a mean of 9.7269PPM and a standard deviation of 20.3587, refer to figure 9. This ensures us that the Turner can be successfully used in online measurements of OiW without using Isopropyl alcohol. We finally conclude that both the equipment have their merits, and precise dynamic measurements of the OiW concentrations with the Turner instrument have a big potential, where the VIPA is a good tool for indication of particle sizes but is not suited for online dynamic measurement. Based on the experiments we are prepared to move further and start using the instruments on the separation pilot plant. Future work will involve online injection of different concentrations, which will enable us to precisely measure the response of the equipment and if it is suitable for online measurements.

REFERENCES

[1] J. Robinson, "An overview of produced water treatment technologies," in *14th Annual International Petroleum Environmental Conference, Houston*, 2007.

[2] Danish-Energy-Agency, "Danmarks olie og gasproduktion 2013 - samt anden anvendelse af undergrunden," http://www.ens.dk/, January 2016.

[3] The-Danish-Environmental-Protection-Agency, "Status for den danske offshorehandlingsplan til udgangen af 2009," http://www.mst.dk/, January 2016.

[4] L. Svarovsky and M. Thew, *Hydrocyclones: Analysis and Applications*, ser. Fluid Mechanics and Its Applications. Springer Netherlands, 2013.

[5] G. Young and W. Wakley, "Oil-water separation using hydrocyclones: An experimental search for optimum dimensions," *Journal of Petroleum Science and Engineering*, vol. 11, no. 93, pp. 37–50, 1994.

[6] T. Husveg, O. Rambeau, T. Drengstig, and T. Bilstad, "Performance of a deoiling hydrocyclone during variable flow rates," *Minerals Engineering*, vol. 20, no. 4, pp. 368–379, Apr. 2007.

[7] S. Pedersen, P. D. K. Stampe, S. Pedersen, and Z. Yang, "Experimental study of stable surfaces for anti-slug control in multi-phase flow," *International Journal of Automation and Computing*, 2016.

[8] T. Designs, "Turner designs hydrocarbon instruments, td4100 xd," http://www.oilinwatermonitors.com/products/td-4100xd, January 2016.

[9] J. Limited, "Jorin limited, vipa b hi-flo," http://www.jorin.co.uk/products/b-hf, January 2016.

[10] ARDECA, "Garden oil sae 30," http://www.ardeca-olie.dk, January 2016.

Paper E

Dynamic Oil-in-Water Concentration Acquisition on a Pilot-Scaled Offshore Water-Oil Separation Facility

Petar Durdevic, Chitra S. Raju, Mads V. Bram, Dennis S. Hansen and Zhenyu Yang

Published in:
Journal of Sensors (MDPI), Sensors 2017, 17(1), 124; doi: 10.3390/s17010124

The layout has been revised.

sensors

MDPI

Article

Dynamic Oil-in-Water Concentration Acquisition on a Pilot-Scaled Offshore Water-Oil Separation Facility

Petar Durdevic [1,*,†,‡], Chitra S. Raju [2,‡], Mads V. Bram [1,‡], Dennis S. Hansen [1,‡] and Zhenyu Yang [1,‡]

[1] Department of Energy Technology, Aalborg University, Esbjerg 6700, Denmark; mvb@et.aau.dk (M.V.B.); dsh@et.aau.dk (D.S.H.); yang@et.aau.dk (Z.Y.)
[2] Independent Consultant, Esbjerg 6700, Denmark; chitrasraju@gmail.com
* Correspondence: pdl@et.aau.dk; Tel.: +45-3175-1320
† Current address: Niels Bohrs Vej 8, Esbjerg 6700, Denmark.
‡ These authors contributed equally to this work.

Academic Editor: Vittorio M. N. Passaro
Received: 3 November 2016; Accepted: 4 January 2017; Published: 10 January 2017

Abstract: This article is a feasibility study on using fluorescence-based oil-in-water (OiW) monitors for on-line dynamic efficiency measurement of a deoiling hydrocyclone. Dynamic measurements are crucial in the design and validation of dynamic models of the hydrocyclones, and to our knowledge, no dynamic OiW analysis of hydrocyclones has been carried out. Previous studies have extensively studied the steady state efficiency perspective of hydrocyclones, and have related them to different key parameters, such as the pressure drop ratio (PDR), inlet flow rate, and the flow-spilt. Through our study, we were able to measure the dynamics of the hydrocyclone's efficiency (ϵ) response to step changes in the inlet flow rate with high accuracy. This is a breakthrough in the modelling, control, and monitoring of hydrocyclones.

Keywords: oil in water; oil and gas; offshore; dynamic; on-line monitoring; process control

1. Introduction

In the offshore Oil and Gas industry, instrumentation is kept at a minimum due to several factors, such as reliability, costs of installation, and difficulty of maintenance. Offshore installations are vastly complex and are tightly packed with equipment which require consistent feedback to ensure a satisfying performance. Due to the high costs and safety considerations, the industry avoids installing equipment and updating current control paradigms without concrete evidence that the new equipment can and will perform better and more reliably than the currently operating equipment and methods. Our work focuses on the deoiling hydrocyclone operation, where water and small concentrations of oil are separated, usually below 1% oil-in-water (OiW) concentrations [1]. The hydrocyclone separates oil from water by an enhanced gravity method, where the two phases are injected into a cylindrical chamber which—due to properties inherent in its design—induces the mixture to be spun into a vortex. This motion forces the oil droplets towards the centre of the cylindrical chamber due to the centripetal force, and forces the water towards the cylinder's wall. There is a narrow exit on one side of the cylindrical chamber called the overflow through which the separated oil exits if the separation has been successful; i.e., if the forces were sufficient to force the oil droplets towards the centre. The funnel shape of the cylindrical chamber pushes the water close to the wall, and the water exits through an opening at the end of the funnel called the underflow. The funnel additionally acts to create a back pressure which ensures that some of the liquid—preferably only oil—is pushed through the overflow [2]. The obvious method for controlling such a system would be to measure and use the hydrocyclone's efficiency (ϵ); see Equation (1) [1].

$$\epsilon = 1 - \frac{C_u}{C_i} \tag{1}$$

where C_i and C_u is the OiW concentration in the inlet and underflow of the hydrocyclone, respectively. Yet the current control strategy for hydrocyclones does not consist of direct efficiency measurement, but instead is based on an indirect method, where a pressure drop ratio (PDR) measurement is used for control—refer to Equation (2) [3].

$$PDR = \frac{p_i - p_o}{p_i - p_u} \tag{2}$$

where p_i, p_u and p_o are the pressures in the inlet, underflow and overflow respectively. The PDR control paradigm operates on the empirical evidence that the PDR is almost linearly proportional to the flow split ratio (F_s), refer to Equation (3) [4].

$$F_s = \frac{F_o}{F_i} \tag{3}$$

where F_o is the overflow flow rate and F_i is the inlet flow rate. The flow split has further been empirically linked to the hydrocyclone's efficiency [4]. The problem with using the PDR for ϵ control of the hydrocyclone is that these empirical relations are all made from a steady state perspective and for specific operating conditions. The reason for the common use of PDR is the superior reliability and precision of pressure transmitters compared to most existing technologies.

As far as we know, direct ϵ measurements have not been used as a feedback parameter for efficiency control of hydrocyclones on the North Sea Oil and Gas platforms. This is because a feedback control strategy based directly on the ϵ requires a reliable ϵ measurement with a sufficient sampling rate, but so far no such feedback transmitters are installed on current North Sea installations. Current installations rely on an offline OSPAR reference method ISO9377-2 [5] to measure the OiW concentration based on which the ϵ is calculated. The OSPAR reference method ISO9377-2 requires at least two samples per day to comply with government regulations, and to our knowledge, the samples are taken around three times per day. This low sampling rate has disadvantages, as it could be unrepresentative of the changes that occur through the day. This is not useful as a dynamic controller's feedback parameter, as frequent and reliable samples and measurements are required for dynamic analysis of ϵ. The sampled measurements by the OSPAR reference method could, however, be used as key tuning parameters in a scheduled control paradigm, but this aspect is not considered in this work. Thus, in order to use ϵ as a feedback parameter, it is necessary to find a method of measuring the OiW concentration quickly and reliably.

The aim of this work was to investigate the possibility of using fluorescence-based technology to measure OiW concentrations online under dynamic conditions, such that these measurements could further be used to determine the ϵ of a pilot-scaled offshore deoiling facility. Our earlier work investigated the same OiW monitor—Turner Design TD-4100XDC (TD-4100), a commercially available OiW monitor manufactured by Turner Designs—for its offline steady state and dynamic response [6].

This work indicated that the TD-4100 performed well regarding steady state measurement. Thus, to investigate the performance of the TD-4100 under online dynamic conditions, the TD-4100 was installed on a pilot-scaled plant equipped with two full-sized offshore hydrocyclone liners. One drawback of using optical monitors is the possibility of fouling of the view-cell, which could lead to a drift in the measurement. This aspect has not been addressed in our current work, but in the case of real time applications, this could probably be avoided by using the non-contact falling stream flow cell found in TD-4100XD, where the media is not in contact with the view-cell.

The custom-built pilot-scaled plant (located at Aalborg University, Esbjerg campus, Esbjerg, Denmark) gives the flexibility to emulate realistic offshore scenarios, where parameters such as the volumetric inlet flow rate F_i and the PDR can dynamically be varied in order to affect the ϵ. In addition, by using industrial liners provided by our partners (refer to Table 1), we were able to emulate real scenarios that occur on offshore oil and gas platforms. We measured the ϵ by measuring

the concentration of oil in the inlet and in the underflow, and then calculated ϵ based on the previously introduced Equation (1). To validate the flow rate measurement, the pressure measurement was included and compared to the flow rate measurement.

Table 1. Description of equipment used for the hydrocyclone set-up.

Name	Type	Description	Range/Size
WP	Grundfos CRNE 3	Centrifugal water feed pump	1 L/s at 162.7 m, max 25 bar
OP	Grundfos DDA	Mechanically actuated diaphragm oil feed pump	$(1.94 \times 10^{-7} - 0.0022)$ g/s, max 16 bar
H_n	Vortoil liner	Up to two industrial hydrocyclone liners	1.4″
$P_{in,i,u,o,s}$	Siemens Sitrans P200	Piezo-resistive pressure measuring cell	(0–16) bar
F_{in}	Rosemount 8732	Electromagnetic flow transmitter	DN50 (0–25.966) L/s @ 12 m/s
$F_{i,u}$	Bailey-Fischer-Porter 10DX4311C	Electromagnetic flow transmitter	DN15 (0–1.64034) L/s
F_o	Micro-Motion Coriolis Elite (CMFS010)	Coriolis flow transmitter	DN10 $(1.389 \times 10^{-5} - 0.0033)$ L/s
Mixer	In-house-designed	Venturi based mixer	DN50
$C_{i,u}$	Turner-Design TD-4100XDC	Fluorescence measurement OiW monitor	(5 PPB–500 PPM)
$V_{u,o}$	Bürkert 2301 + 8696	Globe valve	$V_o = 3$ mm $V_u = 15$ mm

Meldrum [3] initiated the investigation of hydrocyclone liners in their early stages of development; the work was done on a full-scale installation (the Murchison field), and involved the analysis of the correlation between F_i and ϵ, F_s and ϵ, and F_s and PDR. The performance evaluation was done solely from the steady state perspective, and the results only proved the potential of the use of hydrocyclones in offshore installations. Similar findings were made in [1,4], where different hydrocyclone types were tested for their steady state performance. The study in [7] involved steady state analyses of a hydrocyclone liner, where investigations of the PDR, flow split, and ϵ were analysed on an in-house hydrocyclone set-up. The work done in [7] is an extension of [1,3,4], but it did not achieve high enough flow rates to achieve sufficient separation. In addition, no control-oriented dynamic models have been developed linking the PDR and ϵ, which could help in the development of model-based control techniques of the hydrocyclone's efficiency. Although the hydrocyclone's ϵ has been extensively researched (as mentioned earlier), it has been done only from the steady state perspective. The reason being that on-line, dynamic measurement of OiW is not straight-forward, due to several factors which are mentioned in the following paragraph.

First, the oil concentrations in the hydrocyclone are often varying, from as low as a few parts per million (PPM) to around 1000 PPM [8]. As the equipment's PPM measurement is only approximately linear, it is calibrated to a certain operating range to assure a nearly linear response [6], and thus large variations in the concentration can result in measurement uncertainties. Second, the OiW equipment can rarely manage the high flows of the hydrocyclone installations, so they are installed instead on side streams with lower flow rates. This poses several difficulties, such as time delay due to the length of the connecting pipelines and the statistical possibility of misrepresentation of the actual flow as only a fraction of the flow enters the view cells for sampling [6]. Third, the inhomogeneous composition of crude oil poses many calibration issues, as one type of oil may require a different calibration curve than a slightly different type of oil [9]. Lastly, even though the OiW equipment has been studied for a long period of time—with the fluorescence-based instruments being the most widespread technique [9]—their use has been limited to monitoring. To our knowledge, they have not been tested as feedback transmitters under dynamic conditions, and verification of their precision still requires further evaluation—especially regarding their ability to measure dynamic changes.

The main achievement of this work was a successful measurement of the system efficiency ϵ using the two fluorescence OiW monitors (TD-4100), where dynamic changes in ϵ could be measured when the system was subjected to a changing F_i.

The article is structured as follows: Section 2 introduces materials, methods, and the experiment design, Section 3 explains the system's operating conditions and the results, Section 4 discusses the results, and Section 5 concludes the article.

2. Materials and Methods

The pilot plant used for the experiments consists of a reservoir tank which has an attached pipeline and riser. The pipeline—which stretches 25 m in length horizontally—ends with a pipeline riser which raises the liquid 6 m up and onto a platform. The platform consists of a three-phase gravity separator and a deoiling hydrocyclone separator. The uniqueness of our pilot plant set-up is its versatility, where each of the mentioned subsystems can be decoupled and can operate individually. The system considered in this work only consists of the hydrocyclone and the reservoir tank. This is to isolate the hydrocyclone, as we wish to investigate the dynamic efficiency of this unit exclusively and to reduce the effects of the inherent dynamics of the other equipment that are not utilised in the current study.

The pilot plant system that was used is illustrated in Figure 1, and the equipment involved is presented in Table 1.

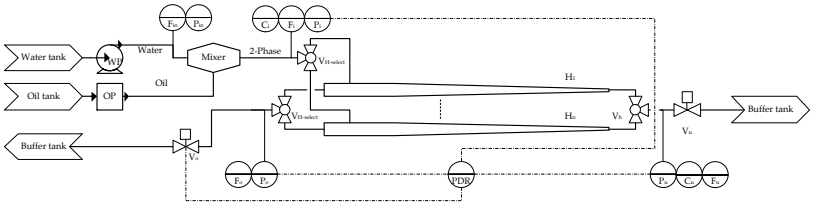

Figure 1. Sketched diagram of the plant, including the feeding system, the hydrocyclone array, and the transmitters used in the study. C_i, C_u: Turner Design TD-4100XDC (TD-4100) fluorescence monitors; F_{in}, F_i, F_u: electromagnetic flow transmitters; F_o: Coriolis flow transmitter; OP: oil pump; P: pressure transmitter; PDR: pressure drop ratio; V: valve; WP: water pump.

2.1. Flow Transmitters

Electromagnetic flow transmitters (Rosemount 8732, Rosemount Inc., Shakopee, MN, USA and Bailey-Fischer-Porter 10DX4311C, ABB Ltd., Zurich, Switzerland) are used for flows with high water concentrations, as they are well suited for measuring flows of conductive material. The electromagnetic transmitters have the following tags: F_{in}, F_i, and F_u; these were placed at points where the oil concentration is less than 1%.

The measurement of multiphase flow (in this case, the two phases are oil and water) or non-conductive phase flow was done with Coriolis flow transmitters. A Coriolis flow transmitter (Micro-Motion Coriolis Elite CMFS010, Emmerson Micro Motion, Boulder, CO, USA) was placed at the hydrocyclone's overflow, as this point has flows with a high oil concentration. The Coriolis flow transmitter has the tag F_o; refer to the diagram in Figure 1 and Table 1.

2.2. Pressure Transmitters

All the pressure transmitters used on the set-up were of the same type (Siemens Sitrans P200, Siemens, Munich, Germany), and use a piezo-resistive measuring cell with a ceramic diaphragm. This type of pressure transmitter has a high step response time of <5 ms. The pressure transmitters used have the following tags: P_{in}, P_i, P_u, P_o, and P_s; refer to the diagram in Figure 1 and Table 1. The PDR was calculated from the values collected from P_i, P_u, and P_o.

2.3. OiW Measurements

The OiW concentration was measured using the fluorescence monitors (Turner-Design TD-4100XDC, Turner-Design, San Jose, CA, USA), which detect the aromatics in the oil and through a calibration curve convert the relative fluorescence unit (RFU) to the related parts per million (PPM)

value. The calibration procedure can be seen in our previous work; refer to article [6]. The equipment promises a refresh rate of 3 s and a detection range of 5 PPB–500 PPM, depending on the calibration [10]. Two TD-4100s were used, one at the hydrocyclone inlet, and one at the hydrocyclone outlet, with the tags C_i and C_u.

2.4. Data Acquisition

The transmitters and actuators were connected to a series of I/O cards (NI PCI-6229, National Instruments, TX, USA) installed in a Simulink xPC Target real-time environment, linked through an Ethernet connection to a computer running Mathworks Simulink. The sampling frequency was kept constant for the entire set-up at 100 Hz, and all the data was stored on the computer. The system was oversampled to allow for high frequency transmitter extensions in the future. This set-up allows for versatile implementation of controller strategies directly in Simulink.

2.5. Materials

The oil and water mixture used for the tests was synthetic and was made of a mixture of tap water and mineral motor oil (ARDECA SAE30, NV Vroman, Vichte, Belgium). The mineral motor oil was chosen, as it is close to the viscosity of crude oil, it was the least purified oil available, and because the use of natural crude oil would pose a fire hazard. The water and oil mixture was kept at room temperature throughout the test, with an average temperature of 20.43 °C. The tests were performed solely with the aforementioned liquids, as no additional chemicals were injected during the test, nor were any present in the buffer tanks.

2.6. Experiment Design

The aim of the experiment was to investigate if the fluorescence-based equipment could track the dynamic changes in OiW concentrations at the hydrocyclone inlet and outlet. In order to achieve an observable response from the ϵ measurement, the system needed sufficient excitation. To achieve this, the inlet flow rate was stepped between four different values. To assure a consistent volumetric flow rate, the pump was controlled using a Proportional-Integral-Derivative (PID) flow controller with the F_{in} flow measurement as the feedback parameter. The chosen F_i step inputs were based on an empirical investigation of the influence of the flow rates on the ϵ. The oil was injected into the mixer where the shear forces dispersed the oil into the water. The flow from the oil pump was controlled using the built-in flow controller. The PDR was kept stable using a PID controller to reduce its impact on the system performance; the resulting PDR that was measured is illustrated in the bottom plot of Figure 2 together with F_s. The valve used in the control of the PDR has an inbuilt PID controller which aims at achieving the desired valve opening position. The PID controller was tuned using a trial and error method until a satisfactory performance was achieved; i.e., the dynamics of the valve are faster than the other dynamics of the system, such as the pressures and the flows. Operating conditions for this experiment are shown in Table 2. The collected data was filtered using a low-pass filter with a 0.2 Hz cut frequency to reduce unwanted sensor and measurement noise.

Table 2. Experimental operating conditions.

Parameters	Set-Points	Units
PDR	≈2	$\frac{\Delta p_u}{\Delta p_o}$
F_{in}	$0.22 - 0.27 - 0.33 - 0.39$	[L/s]
P_{in}	≈9.5	[bar]
C_i	≈400	[PPM]

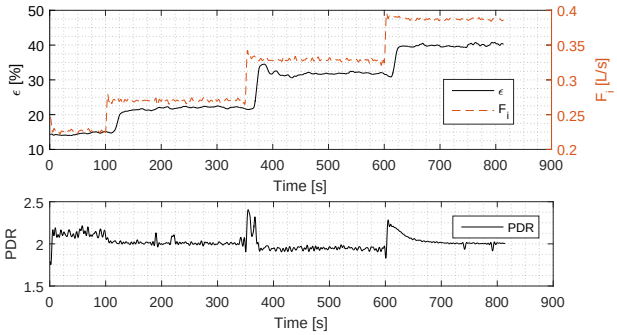

Figure 2. Experimental results: the (**top**) plot illustrates the calculated ϵ and F_i; The (**bottom**) plot illustrates the PDR.

3. Results

3.1. Operating Conditions

The comparison of F_i and the system efficiency represented by ϵ is shown in the top plot of Figure 2. The requirement for good results is that F_i has a step input amplitude which should produce a corresponding step deviation in ϵ, and as seen from the results, this has been achieved.

Secondly, in order to remove any steady state bias from F_i, it is crucial that F_i closely tracks its reference. The F_i has an average standard deviation from its mean of $\sigma = 0.0014$ L/s, which is a small deviation considering that the mean of the three individual steps is 0.2704 L/s, 0.3289 L/s, and 0.3871 L/s, and F_i is thus considered suited for the experiment. The PDR—plotted in the bottom plot of Figure 2—stays close to its reference of 2, with small deviations from steady state around the step inputs. During the second step, the PDR is offset with 0.05 from the PDR set-point, which is caused by the internal valve hysteresis. Based on previous experience, small deviations in the PDR do not have much significance on system ϵ, as long as the PDR is kept within a safe boundary; therefore the PDR that was used is considered well-suited for the experiments.

3.2. Results

The impact of each step input in F_i on ϵ is presented in Table 3, which shows the time of each individual step, steady state mean amplitude, steady state standard deviation, percentile increase from previous step's steady state mean to current steady state mean, percentile deviation of the two signals' step increase, and time delay between the two signals' response and rise-time, where the rise-time is the time from which the step goes from 10% to 90% of its steady state value [11]. Table 3 also includes the percentile deviation of the two signals' rise-time and the percentile overshoot of the signal, which is measured for the largest value's percentile deviation from the new steady state mean. ϵ reacts to every step input of F_i with an approximate time delay of 10 s. The response of F_i is consistent with a rise-time between 1.83 s and 1.96 s, and a steady state mean increase of roughly 20%. The response of ϵ to the F_i step input is not as consistent, where a steady state amplitude response of ϵ decreases for each step: 25.76 %, 20.18 %, and 6.49 % for the first, second, and the third step respectively.

To analyse the dynamics of the two signals in further detail, the signals from the third step are enlarged and shown in Figure 3. From this plot, the delay in the rise time of ϵ is evident, and by analysing the rise-time, it was found to be 7.9 s for ϵ and 1.96 s for F_i, which makes F_i four times faster. This is also observable in the plot, where the trend of ϵ is less steep. A rise-time offset was consistently measured in the other steps, where it was slightly shorter in the second step, as ϵ exhibited

an overshoot of 2.8% when compared to virtually no overshoot in step one, and an insignificant overshoot in step three. The overshoot in ϵ is consistent with an overshoot in F_i, which at this point is 0.0134 L/s compared to the overshoot value of 0.089 L/s and 0.086 L/s for the first and the third steps, respectively, thus making the second step's overshoot ≈65% larger than the other two steps' overshoot. The overshoot also means that the settling time for ϵ changes slightly, reaching its steady state within ≈80 s, ≈110 s, and ≈20 s for the first, second, and the third steps, respectively. The rise-time regarding ϵ in step one is slow compared to step two and step three, where the rise-time of F_i is 1125.68% faster.

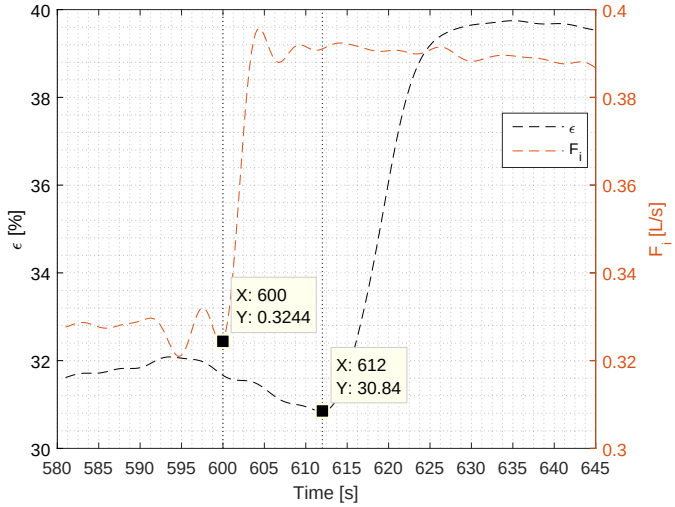

Figure 3. Zoomed view of the third step from Figure 2, illustrating the dynamic behaviour of ϵ and F_i. The dotted lines indicate the time of step input of F_i and the approximate step response of ϵ.

To confirm the validity of the F_i, it is compared to the pressure measurement, and if the measurements have consistent dynamics and steady state behaviour, F_i can be considered valid. The result is shown in Figure 4, where the two pressures (P_u and P_o) are chosen. These two pressures are the ones that get affected most by a change in F_i, in comparison to Pi, due to the back pressure over the two valves V_u and V_o, which are located directly downstream of P_u and P_o. The values are normalized, and their gain is adjusted to fit them on top of each other for easier comparison of the time delays. The step delay regarding the F_i and P_o is less than 0.1 s, and if F_i and P_o are compared, the delay is ≈0.45 s with a close to identical rise-time for all the measurements. A comparison of the rise-time of F_i and P_o is shown in Figure 5.

Table 3. Step response and steady state analysis of ϵ and F_i; for more details, refer to Section 3.2.

Signal-Name	Step-Time	Steady State Mean (Steady State Standard Deviation)	Increase from Previous Mean	Deviation of F_i from ϵ Mean	Step Delay	Rise-Time	Δ Rise-Time	Overshoot
Initialisation								
F_i	-	0.2264 L/s (0.0014) L/s	-	-	-	-	-	-
ϵ	-	0.1444 PPM (0.0033) PPM	-	-	-	-	-	-
Step 1								
F_i	100 s	0.2704 L/s (0.0029) L/s	119.43%	25.76%	-	1.83 s	1125.68%	3.2943%
ϵ	≈110 s	0.2169 PPM (0.0020) PPM	150.2%	-	≈10 s	20.6 s	-	0%
Step 2								
F_i	350 s	0.3289 L/s (0.0013) L/s	121.67%	20.18%	-	1.87 s	263.1%	4.0729%
ϵ	≈360 s	0.3171 PPM (0.0023) PPM	146.22%	-	≈10 s	4.92 s	-	8.8345%
Step 3								
F_i	600 s	0.3871 L/s (0.001) L/s	117.68%	6.4931%	-	41.96 s	403.06%	2.2187%
ϵ	≈612 s	0.3974 PPM (0.0037) PPM	125.32 %	-	≈12 s	7.9 s	-	0%

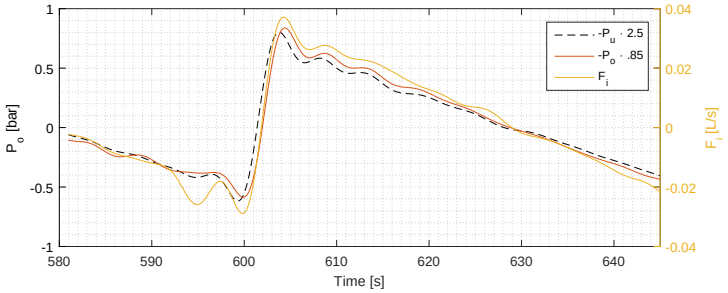

Figure 4. Comparison of F_i, P_u, and P_o.

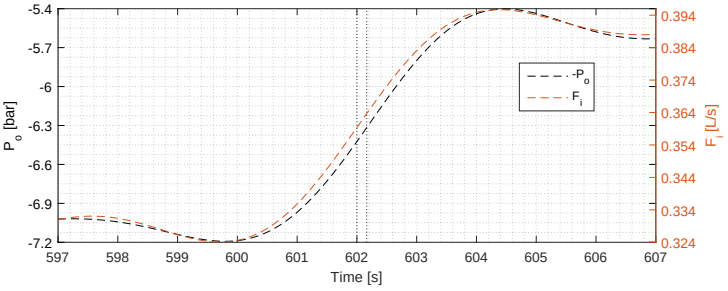

Figure 5. Comparison of F_i and P_o; the dotted lines illustrate the delay between the two measurements, measured to be 0.165 s.

4. Discussion

The goal of the study was to analyse the ability of the TD-4100 to measure the dynamic changes in the hydrocyclone's ϵ, where the changes were created by incrementing the inlet flow rate F_i several times. The increments had to be sufficient to cause ϵ to change significantly enough to be measured, and this was achieved as ϵ responds to every step input of F_i, as seen in the top plot of Figure 2. In addition, the F_i measurement was required to remain at a consistent steady state value; although small variations in the steady state were observed, the average coefficient of variation was <1%, indicating a high signal-to-noise ratio (SNR). The fluctuations were caused by small variations in the control signal to the pump being discretised by the pump frequency converter, and the discretisation of the flow measurement used for the pump controller feedback signal. Thus, the F_i could be used as an excitation signal (due to the high SNR), without considerable influence on the dynamics of ϵ.

The F_i step input was observed to have a direct impact on the ϵ, with a consistent delay of $\approx$10 s at each step. There are several factors which could contribute to this phenomenon; the first being the positioning of the TD-4100. The TD-4100 was connected on a side stream to the inlet and to the underflow of the hydrocyclone with pressure hoses, each of which were 3 m long and of a smaller diameter than the inlet and the underflow. The length of the hoses and the reduction in diameter (which introduces a pressure drop) affects the flow of the liquid, thus affecting the time it takes for the fluid to reach the equipment from the main line. Shorter hose connections to the equipment could reduce the delay of liquid entering the test chamber. The second reason is the response time of the TD-4100, which is estimated to be 3 s by the manufacturer [10]. It is expected that the delay is

solely caused by the two mentioned reasons, but further research will investigate what causes this consistent delay.

The rise-time delay (as seen in Figure 3) has a more complicated explanation than the time delay, and we assume that it was caused by the dynamics of the separation, and our future work will aim to uncover the exact cause for it. Judging from the top plot in Figure 2, the rise-time—and thus the tangential of the ϵ—is similar for all three steps, which means that the TD-4100 is measuring consistently each time. We can observe from the overshoot in the second step—which occurs both in F_i and ϵ—that the TD-4100 is able to track the dynamic behaviour of ϵ. As in the first and the second step where F_i has considerably less overshoot, ϵ follows suit with no overshoot. Due to the complexity of the separation dynamics inside the hydrocyclone, it is hard to predict the exact behaviour of ϵ, and thus predict the outcome. However, our measurements do uncover a consistent relationship between F_i and ϵ, which follows the theory of droplet separation formulated by Stokes' law [12]. To validate our F_i measurement, we have used the pressure measurements as a comparison, and the two measurements agree well with each other, which increases the validity of the flow measurements.

5. Conclusions

Our conclusion is thus that the fluorescence-based measurement monitor (the TD-4100) can successfully measure dynamic response of the hydrocyclone's ϵ. In addition, the steady state and dynamic measurements of ϵ were consistent, and responded to the flow input in accordance to established laws of physics. The time delay and slower rise-time phenomena in the ϵ measurement—although a common effect in such systems—requires further investigation.

We propose that additional instruments be placed in series with the current instruments to enable further validation of the TD-4100. In addition, a reliability study of the fluorescence monitors should be done to evaluate their performance in a long term perspective. Finally, a different type of equipment should be introduced, preferably based on a different sensing paradigm, as an additional validation of the OiW measurement by the TD-4100.

Acknowledgments: This project is funded by: Danish National Advanced Technology Foundation, Maersk Oil A/S and Ramboll Oil & Gas A/S.

Author Contributions: Petar Durdevic and Zhenyu Yang conceived and designed the experiments; Mads V. Bram and Dennis S. Hansen performed the experiments; Petar Durdevic and Chitra S. Raju analysed the data; Zhenyu Yang contributed reagents/materials/analysis tools; Petar Durdevic wrote the paper.

Conflicts of Interest: The authors declare no conflict of interest.

Abbreviations

The following abbreviations are used in this manuscript:

PDR	Pressure Drop Ratio
OiW	Oil in Water
PPM	Parts Per Million
RFU	Relative Fluorescence Unit
SNR	Signal to noise ratio
PID	Proportional–Integral–Derivative Controller

References

1. Thew, M. Cyclones for oil/water separation. *Encycl. Sep. Sci.* **2000**, *4*, 1480–1490.
2. Sinker, A.; Humphris, M.; Wayth, N. Enhanced deoiling hydrocyclone performance without resorting to chemicals. In Proceedings of the Offshore Europe Oil and Gas Exhibition and Conference, Aberdeen, UK, 7–10 September 1999; Society of Petroleum Engineers: Richardson, TX, USA, 1999.
3. Meldrum, N. Hydrocyclones: A Solution to Produced-Water Treatment. *SPE Prod. Eng.* **1988**, *3*, 669–676.
4. Thew, M. Hydrocyclone redesign for liquid-liquid separation. *Chem. Eng.* **1986**, *427*, 17–23.

5. Methodology for the Sampling and Analysis of Produced Water and Other Hydrocarbon Discharges. Available online: https://www.gov.uk/guidance/oil-and-gas-offshore-environmental-legislation (accessed on 3 November 2016).
6. Durdevic, P.; Pedersen, S.; Yang, Z. Evaluation of OiW Measurement Technologies for Deoiling Hydrocyclone Efficiency Estimation and Control. In Proceedings of the Oceans' 16 MTS/IEEE Shanghai, Shanghai, China, 10–13 April 2016.
7. Husveg, T.; Rambeau, O.; Drengstig, T.; Bilstad, T. Performance of a deoiling hydrocyclone during variable flow rates. *Miner. Eng.* **2007**, *20*, 368–379.
8. Young, G.; Wakley, W. Oil-water separation using hydrocyclones: An experimental search for optimum dimensions. *J. Pet. Sci. Eng.* **1994**, *11*, 37–50.
9. Yang, M. Measurement of oil in produced water. In *Produced Water*; Springer: New York, NY, USA, 2011; pp. 57–88.
10. TD-4100XDC. Available online: http://www.oilinwatermonitors.com/portfolio-items/td-4100xdc/ (accessed on 3 November 2016).
11. Franklin, G.F.; Powell, J.D.; Emami-Naeini, A.; Powell, J.D. *Feedback Control of Dynamic Systems*; Addison-Wesley: Reading, MA, USA, 1994; Volume 2.
12. Wolbert, D.; Ma, B.F.; Aurelle, Y.; Seureau, J. Efficiency estimation of liquid-liquid Hydrocyclones using trajectory analysis. *AIChE J.* **1995**, *41*, 1395–1402.

Paper F

Application of H_∞ Robust Control on a Scaled Oil&Gas De-Oiling Facility

Petar Durdevic, Simon Pedersen, Zhenyu Yang

The paper has been submitted to:
IEEE Transactions on Control Systems Technology, march 2017.

Application of H_∞ Robust Control on a Scaled Oil&Gas De-Oiling Facility

Petar Durdevic and Simon Pedersen and Zhenyu Yang

***Abstract*—Oil and water separation in offshore Oil and Gas installations is usually performed by a de-oiling system consisting of a gravity separator and a hydrocyclone. The hydraulic coupling in this system makes it susceptible to poor efficiency, especially during fluctuating input flows, where the input flow is unmeasured and is considered a disturbance. The study showed that the disturbance and the coupling had a significant effect on the de-oiling system's performance and that the current PID control solution that includes two decoupled PID controllers, worsens the effect. A MIMO process model that included a novel hydrocyclone model and a gravity separator model was derived and based on this a robust suboptimal H_∞ control solution was designed. The H_∞ control solution was applied to the de-oiling system and compared to a benchmark PID control solution, both in simulations and in experiments performed on a scaled pilot plant. In simulations, the H_∞ control solution performs better than the PID control solution, where its disturbance rejection and the MIMO structure improves the overall performance especially during an oscillating disturbance. During the experiments on the scaled pilot plant, the H_∞ control solution kept the system stable and outside saturation, a feat which was not achieved with the PID control solution. In addition the relaxed reference tracking by the H_∞ control solution filtered the transmission of the fluctuating inlet flow from the gravity separator to the hydrocyclone, which based on previous studies is known to improve the de-oiling efficiency.**

***Index Terms*—Oil & Gas, Separation, Control, separation efficiency, OiW measurement**

NOMENCLATURE

Name	Description	Unit
PDR	Pressure Drop Ratio	-
l	Water level	[mm]
in	Inlet to the gravity separator	-
i,u,o	Hydrocyclone inlet, underflow and overflow	-
$V_{i,u,o}$	Opening percentage of controllable valves	[%]
$P_{i,u,o}$	Pressure	[bar]
$F_{in,i,u,o}$	Volumetric flow-rate	[l/s]
$C_{i,u}$	Oil in water concentration	%
R_f	Flow split inside the hydrocyclone	%
ϵ	Hydrocyclone separation efficiency	%
ref_l	Interface level reference	[mm]
ref_{PDR}	PDR reference	[mm]

I. INTRODUCTION

Since the late $1960's$; the North Sea has been home to a booming Oil and Gas industry and has provided substantial quantities of petroleum products [1]. The reservoirs which are located beneath the seabed were initially pressurized with high concentrations of oil and gas and relatively small amounts of water. The long period of oil exploration has had its toll on the reservoirs, wherein natural water leakage into the reservoirs and water re-injection have changed the balance between oil, gas and water, [2]. The liquid pumped from the reservoirs has in many cases a 98% water fraction and due to conveyance costs the water must be separated from the product on the offshore facilities, [3], [4] and [5]. In the Danish sector the water fraction has increased by 350% in the period between 2005-2015, [6], resulting in an ever increasing strain on the separation facilities, which must adhere to discharge regulations The current regulation for the Oil in Water (OiW) concentration in the discharge into the North Sea is 30mg/l [7]. This article focuses on the most common de-oiling unit processes, namely the three phase gravity separator and the de-oiling hydrocyclone separator, while paying specific attention to gravity separator's water outlet which is connected to the downstream de-oiling hydrocyclone and the performance of the system with respect to the hydrocyclone's efficiency ϵ, [8], [9], [10] and [11]. A typical system layout is presented in figure 1: the three phase gravity separator has one inlet, where the mixture of water, oil and gas enters, and three outlets, one each for water, oil and gas. In the gravity separator the oil and gas float on the top of the water due to buoyancy, the gas separates and collects in the headspace and the oil flows over the weir into a separate chamber. The remaining water should ideally contain almost no oil, but due to short residence times in this unit process, some of the dispersed oil droplets remain in the water phase. [12]. These droplets are thereafter removed in the downstream water treatment facility which consists of a stack of hydrocyclone separators. This mixed water/oil phase flows through a pipe located at the bottom of the gravity separator into the hydrocyclone. The hydrocyclones work on the principle of centripetal/centrifugal force, which is created by the cyclic motion of the liquid inside the hydrocyclone. The centripetal force pushes oil droplets towards the center of the hydrocyclone and out through a narrow outlet on one side of the hydrocyclone called the overflow, and the water exits through a larger outlet called the underflow, [13]. In general the gravity separator separates oil droplet sizes until 150μm, and the hydrocyclone can separate droplet sizes until 12 μm, [14]. The separation process is controlled using two valves, one on each outlet of the hydrocyclone. The underflow valve (V_u) is used to maintain the correct water/oil interface level (l) inside the gravity separator and the overflow valve (V_o) is used to maintain the correct pressure drop ratio (PDR) inside the hydrocyclone, refer to equation 2. The l controller assures the correct residence time for the droplets to separate and prevents

Petar Durdevic and Simon Pedersen and Zhenyu Yang are with the Department Energy Technology, Aalborg University, Esbjerg, 6700 Denmark e-mail: pdl@et.aau.dk.

Manuscript received March 22, 2017; revised Month day, year.

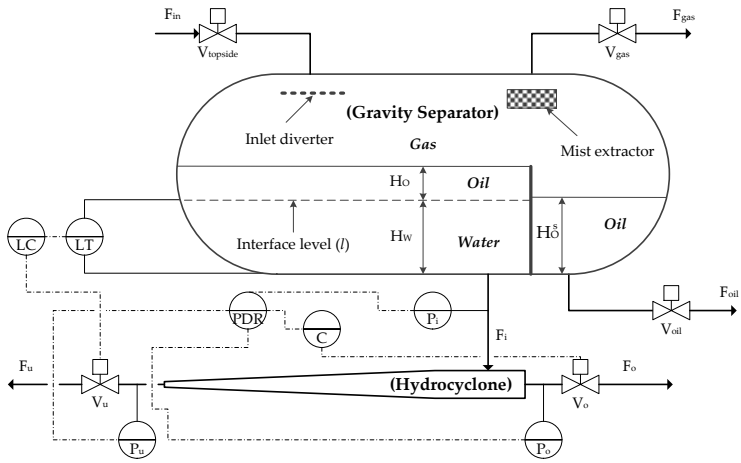

Fig. 1. P&ID of an offshore de-oiling facility, including the control loops.

the water from crossing the weir into the oil chamber.

$$R_f = F_u/F_i \tag{1}$$

$$PDR = \frac{\Delta P_o}{\Delta P_u} = \frac{P_i - P_o}{P_i - P_u} \tag{2}$$

The PDR controller operates on the principle that the PDR is approximately linearly proportional to the flow split ratio (R_f) which is the ratio of the inlet volumetric flow rate (F_i) to the underflow volumetric flow-rate (F_u), shown in equation 1, [15], [16], [17], [11] and [18]. This ensures the correct amount of liquid to pass through the overflow and the underflow. In [17] [19], [11], steady state analysis have related the R_f to the hydrocyclone's efficiency (ϵ) see equation 3 ([15]).

$$\epsilon = 1 - \frac{C_u}{C_i} \tag{3}$$

Where C_i is the concentration of oil in the inlet to the hydrocyclone and C_o is the concentration of oil in the underflow of the hydrocyclone. This relationship is strictly dependent on the F_i, which ensures the correct centrifugal/centripetal force required for separation of oil droplets from the water phase [13]. Thus to ensure a high ϵ, F_i must be kept within a certain operating range, which is in turn specific to each individual platform [17]. This implies that the dynamic changes in F_i, such as an oscillating F_i, influences ϵ in certain operating ranges, as shown in [20]. Therefore the use of PDR does not strictly ensure an optimum ϵ. The obvious factor that could be used as a feedback for control is ϵ, however, this is not the case as it has been difficult to measure the required OiW concentrations under dynamic conditions. Hence PDR, despite its drawbacks, is still being used as the feedback parameter as it is easily estimated using measurements from pressure transmitters that are quite reliable and simple. The most common controller strategy is to use two separate PID controllers for the two control loops. By analysing the P&ID diagram in figure 1, a possible issue can be observed due to the physical coupling of the two valves, as discussed in [21].

A preliminary study was performed to evaluate the current controller structure's performance, as it is believed that the coupling of the two unit processes may affect the control structures performance. The preliminary study was based on data collected from an offshore plant, which was then compared to an emulated scenario performed on a scaled pilot plant. The PDR control loop was in addition investigated from the perspective of ϵ to uncover any further drawbacks. Based on the study a new control solution was proposed.

II. Preliminary Investigation

An investigation of the offshore data as shown in figure 2 shows that the conventional de-oiling controller, consisting of two individual PID controllers; an l and a PDR controller as shown in figure 1, aim at tracking the two individual references ($l = 1200$mm & PDR $= 2.1$).

During nominal operation (13:00h-13:50h), the PID controller tracks the reference of both the output parameters: l and PDR. The operating conditions change after 13:50h, due

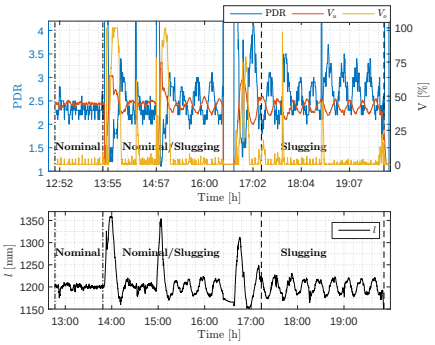

Fig. 2. Real time data collected from one North Sea Danish installation.

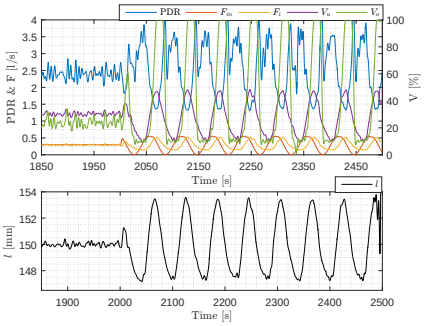

Fig. 3. Tests performed on the scaled pilot plant representing two operating conditions, steady F_{in} and severely oscillating F_{in}.

to a fluctuating F_i which is often a result of slugging flow, [22], [23] and [24]. On the offshore platform that is under consideration, F_i is not measured, as is the case with many of the North Sea installations. From 13:50h and until the 20:00h, the system does not consistently track its reference which results in a varying l, especially where consistent slugging behavior occurs between (17:12h-20:00h). Each time l starts rising the l controller reacts by closing V_u, and by doing so disrupts the PDR value. The PDR controller compensates at times by large adjustments of V_o but most of the time it chatters at almost fully closed position. This results in a PDR value which reaches values as high as 65 and as low as 1. Where a low opening of V_o, i.e. where PDR values are high, results in excess oil being sent through the underflow along with the water. And if this is not recirculated through the de-oiling system, the oil will be lost into the ocean. In the opposite case when V_o is fully open and the PDR moves towards 1, and large quantities of water are sent through the overflow, which, again, necessitates recirculation in order to purify the overflow.

It is assumed that the performance issues presented by the PID controller in the offshore scenario are predominantly caused by the physical coupling of the valves, V_u and V_o, which are the manipulated variables of the l and PDR control loop. Thus any adjustment of one valve will affect the pressure/flow at the other valve due to this hydraulic coupling. With respect to the Coleman Thew hydrocyclone design, described in [13], the cross sectional area of V_u is 25 times larger than that of V_o which makes V_u the dominant manipulative variable. To further analyse this phenomena the scenario illustrated in figure 2 is emulated on a scaled pilot plant described in section VI.

A. Emulation of the Offshore Scenario

The flow fluctuations were emulated to see if the scaled pilot plant when maintained by a PDR controller responded the same way as the offshore system and to see if the coupling issue could be emulated, figure 3 shows the results. Nominal operation was achieved with a steady inflow to the gravity separator F_{in} between $(1850s - 2000s)$ followed by severe flow conditions where F_{in} was fluctuated between 0 and 0.6l/s with a frequency of 1/60 Hz, in the time interval $(2000s - 2500s)$.

The results from emulated test on the scaled pilot plant are similar to what is observed in the offshore case. During the nominal operation, V_u remains steady with small variations, whereas the small variations are amplified in the case of V_o. As the severe slugging flow condition is introduced, the l controller actuates V_u in order to continue tracking ref_l, this has a huge impact on the PDR which reaches values above 4 PDR, due to a fully open V_o and a PDR of 1.3 while V_o is around 0.1 %. This oscillating behavior resembles the offshore case between (17:00h-20:00h), during which the system is believed to be facing slugging flow regime.

Based on this preliminary investigation it was observed that conventional PDR based control structure has a weakness when it is subjected to an oscillating F_{in}. The l tracking results in excessive actuation of V_u which has a negative effect on the PDR controller. This can lead to saturation of the valves, which can reduce ϵ and induce wear and tear on the valves. It is well known from literature [17], [10] that a hydrocyclone operates at high efficiency as long as the PDR and the F_i are kept within certain boundaries; (1.5-3) for the PDR [25], while the F_i value is specific to individual hydrocyclone set-ups [17]. In addition, fluctuations in F_i influence the hydrocyclone's ϵ, as was shown in [26], [11], [18] and [20].

To conclude this investigation, the issue was that the current PID control solution lacks disturbance rejection which is further worsened by the lack of a methodologically derived MIMO control structure. In addition the explicit reference tracking of the PID control structure, amplifies the disturbance transmission through the system, which affects the de-oiling systems performance. The control solution chosen for this problem is based on robust sub-optimal H_∞ control, such that the disturbance rejection and the MIMO structure can

be explicitly handled. A sub-optimal H_∞ control solution which sacrifices the minimum H_∞ norm is chosen, as optimal reference tracking is not beneficial for the de-oiling system.

III. De-oiling Process' Model

To enable the design of the proposed controller, a model of the de-oiling process is required. The de-oiling process model included a SISO gravity separator model, $\mathbf{G}_1$, and the hydrocyclone was modelled using two SISO models, $\mathbf{G}_2$ and $\mathbf{G}_3$. With respect to the $\mathbf{G}_1$, l is controlled by the manipulated variable V_u, which is thus allocated as the input to the gravity separator subsystem. As V_o has a small impact on the total output flow from the gravity separator, it is ignored in the $\mathbf{G}_1$. $\mathbf{G}_1$ consists of a mass balance model where the inlet flow rate to the gravity separator F_{in} is a disturbance, denoted by d, and the outlet flow from the gravity separator F_{out} is converted into the water level l by a trigonometric function. Where the F_{out} is governed by a valve equation, refer to [27] for more information. The hydrocyclone's hydrodynamics are complicated, and often require high order partial differential equation (PDE) models to recreate the important aspects of two phase flow and phase separation in such a highly turbulent system. A black box model is thus proposed, refer to [28] and [29], where the model is designed from the PDR perspective as this is the sole observable parameter in the installations. As the dynamics of the hydrocyclone are affected by both the V_u and V_o, it is modeled by two second order transfer function models denoted as $\mathbf{G}_2$ and $\mathbf{G}_3$, where $\mathbf{G}_2$ takes V_u as an input and returns PDR as the output and $\mathbf{G}_3$ takes V_o as an input and returns PDR as the output. Due to the highly non-linear dynamic of the hydrocyclone, $\mathbf{G}_2$ and $\mathbf{G}_3$ are identified around a small operating range.

The final model of the entire system, $\mathbf{G_s}$, is a MIMO model, with two inputs $\begin{bmatrix} V_u \\ V_o \end{bmatrix}$, and two outputs $[l, \text{PDR}]$, presented in the block diagram in figure 4. A disturbance d is added through a weighting matrix E to the gravity separator subsystem through a scaling factor E which is adjusted through an ad-hoc method to account for the algebraic conversion from valve openness to volumetric flow rate.

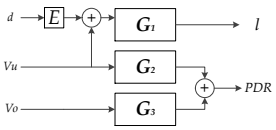

Fig. 4. Cooperative model structure of the separation system, where the three individual system models ($\mathbf{G}_1$, $\mathbf{G}_2$ and $\mathbf{G}_3$) are combined into a MIMO model structure for the entire separation system represented by $\mathbf{G}_s$.

Following the standard state space representation, the system parameters are structured and shown in equation 4. The model consists of five states, one state for the gravity separator (l) and two states for each of the two second order models of the hydrocyclone.

IV. Robust Control

Our system consists of a linear interconnected plant P, with the un-modeled disturbance d, and can be represented as a closed loop system by the block diagram shown in figure 6 which follows the general closed-loop inter-connection shown in figure 5, where:

$$w = \begin{bmatrix} \Delta ref \\ \Delta d \end{bmatrix} = \begin{bmatrix} \begin{bmatrix} \Delta ref_l \\ \Delta ref_{\text{PDR}} \end{bmatrix} \\ \Delta d \end{bmatrix} \tag{5}$$

$$u = \begin{bmatrix} V_u \\ V_o \end{bmatrix} \tag{6}$$

$$z = \begin{bmatrix} l \\ \text{PDR} \end{bmatrix} \tag{7}$$

$$y = \begin{bmatrix} \Delta e_l \\ \Delta e_{\text{PDR}} \end{bmatrix} \tag{8}$$

The external inputs to the system defined by w, see equation 5, are the reference Δref and the disturbance Δd and the Δ represents the linear model's deviation from the real value. The output signals are defined as z, see equation 7, consists of l and PDR. The vector of control signals defined as u, see equation 6 consists of the input variables V_u and V_o. The vector of the available measurements defined as y, see equation 8, consists of the error signals Δe_l and (Δe_{PDR}). This system presented in the block diagram shown in figure 5 has the state space representation as shown in equation 9.

$$\begin{aligned} \dot{x}(t) &= Ax(t) + B_1 w(t) + B_2 u(t) \\ z(t) &= C_1 x(t) + D_{11} w(t) + D_{12} u(t) \\ y(t) &= C_2 x(t) + D_{21} w(t) + D_{22} u(t) \end{aligned} \tag{9}$$

And can be denoted by:

$$P = \begin{bmatrix} \dot{x} \\ \hline z \\ y \end{bmatrix} = \left[\begin{array}{c|cc} A & B_1 & B_2 \\ \hline C_1 & D_{11} & D_{12} \\ C_2 & D_{21} & D_{22} \end{array}\right] \begin{bmatrix} x \\ \hline w \\ u \end{bmatrix} \tag{10}$$

which leads to the following matrix representation of our system's interconnected plant P, see equation 11.

$$P = \begin{bmatrix} \dot{x} \\ \hline \begin{bmatrix} z_1 \\ z_2 \end{bmatrix} \\ y \end{bmatrix} = \left[\begin{array}{c|cc} A & [0\ B] & B \\ \hline C & [0\ 0] & 0 \\ -C & [1\ 0] & 0 \end{array}\right] \begin{bmatrix} x \\ \hline \begin{bmatrix} r \\ d \end{bmatrix} \\ u \end{bmatrix} \tag{11}$$

$$\begin{bmatrix} \dot{l} \\ \dot{x_{V_u}} \\ \dot{x_{V_u}} \\ \dot{x_{V_o}} \\ \dot{x_{V_o}} \end{bmatrix} = \begin{bmatrix} -1.23 \times 10^{-05} & 0 & 0 & 0 & 0 \\ 0 & -0.97 & -0.76 & 0 & 0 \\ 0 & 1 & 0 & 0 & 0 \\ 0 & 0 & 0 & -0.93 & -0.65 \\ 0 & 0 & 0 & 1 & 0 \end{bmatrix} \begin{bmatrix} h \\ x_{V_o} \\ x_{V_o} \\ x_{V_u} \\ x_{V_u} \end{bmatrix} + \begin{bmatrix} -14 \times 10^{-04} & 0 \\ -1 & 0 \\ 0 & 0 \\ 0 & 1 \\ 0 & 0 \end{bmatrix} \begin{bmatrix} V_u \\ V_o \end{bmatrix}$$

$$\begin{bmatrix} y_l \\ y_{\text{PDR}} \end{bmatrix} = \begin{bmatrix} 1 & 0 & 0 & 0 & 0 \\ 0 & 0 & 2.72 & 0 & 1.69 \end{bmatrix} \begin{bmatrix} h \\ x_{V_u} \\ x_{V_u} \\ x_{V_o} \\ x_{V_o} \end{bmatrix} + 0 \tag{4}$$

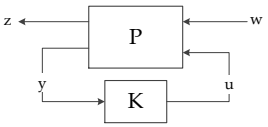

Fig. 5. The standard representation of the Robust H_∞ control solution.

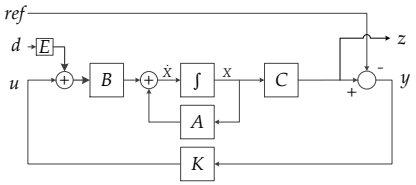

Fig. 6. Interconnected plant P with the reference, disturbances and the controller K

A. Robust Controller Design

For an interconnected plant P, see equation 11, we find all rational internally stabilizing feedback controllers K, which satisfies that the norm of the closed loop function $||F_l(P,K)||_\infty$ is smaller than a given γ, refer to [30] and [31], that is:

$$||F_l(P,K)||_\infty < \gamma \tag{12}$$

Before the controller is obtained the interconnected system P has to satisfy several assumptions listed below, [31]:

1) (A, B_2) must be stabilisable and (C_2, A) must be detectable,
2) $D_{12} = \begin{bmatrix} 0 \\ I \end{bmatrix}$ and $D_{21} = \begin{bmatrix} 0 & I \end{bmatrix}$.
3) $\begin{bmatrix} A - j\omega I & B_2 \\ C_1 & D_{12} \end{bmatrix}$ has full column rank for all ω.
4) $\begin{bmatrix} A - j\omega I & B_1 \\ C_2 & D_{21} \end{bmatrix}$ has full row rank for all ω.

The considered system P has been found to satisfy the four given assumptions. The controller is numerically solved using the D-K iteration, for more information refer to [30], [32] and [33]. The calculation of the controller K was done using commercial software, using the `hinfsyn` function in Matlab's Robust Control Toolbox, refer to [32] and [34].

V. Performance Analysis via Simulation

This section presents a comparison of the performances of the H_∞ control solution and the benchmark PID control solution in simulations. The comparisons were made for the following performance aspects: (a) reference tracking (b) disturbance rejection (both steady state and dynamic) and (c) parametric disturbance by introducing an error in the model's dynamic and static part.

A. Benchmark PID control solution

The PID control solution was structured as shown in figure 1, where there are two individual PID controllers for the two manipulated variables, V_u and V_o, using the two feedback parameters, l and PDR. This is, to our knowledge, the most common controller structure used in the North Sea. The individual PID controller's gains, i.e. K_p, K_i and K_d, were tuned using a trial and error method. The PID controller with respect to l was tuned first as it is dominant and has a strong influence on the PDR controller. The two controllers were simulated using the system model introduced in equation 4. Anti-windup was added to make sure that the controller did not accumulate error during saturation of the control parameters.

B. Description of the Testing Scenarios

Two testing scenarios were performed, first the **V1** scenario which consist of 4 sub-scenarios presented in table I and the second **V2** scenario which is a severe scenario consisting of 2 sub-scenarios presented in table II .

*1) Scenario **V1**: l reference (ref_l) step **LRS**:* This scenario aims at testing both the controllers' step response and their steady state reference tracking performance, by subjecting ref_l to a step change.

*2) Scenario **V1**: PDR reference (ref_{PDR}) step **PRS**:* This scenario aims at investigating both the controllers' step response and their steady state performance towards a step input on the ref_{PDR}.

TABLE I
DESCRIPTION OF THE SIMULATION SCENARIO **V1**

Name	Value & time	Description	Figure
LRS	[230mm - 225mm] @ t = 3000s	ref_l step	7
PRS	PDR = [1.8 - 2] @ t = 4000s	ref_{PDR} step	7
DIO	ω = 0.104 rad/sec $\hat{U}$ = 7×10^{-05} @ t = 7000s	$sine_{dist}$ input	7
MOE	$A \cdot 0.7$ $B \cdot 0.7$ @ t = 6500s	Modeling error	8

TABLE II
DESCRIPTION OF SIMULATION SCENARIO **V2**

Name	Value & time	Description	Figure
SPRS	PDR = [2-2.4] @ t = 4000s	ref_{PDR} step	9
SDIO	ω = 0.104 rad/sec $\hat{U}$ = 7×10^{-05} @ t = 5000s	$sine_{dist}$ input	9

*3) Scenario **V1**: Sine-Wave Disturbance **DIO**:* This evaluates both controllers' robustness towards additive disturbances, in this case the disturbance is set to emulate a severe slugging scenario which impacts the gravity separator's l and thus affects both the valves due to the coupling. The aim of this test is to evaluate both controllers' dynamic disturbance rejection and identify the controller that has an advantage in reducing the impact of fluctuating flows to the system.

*4) Scenario **V1**: Multiplicative error **MOE**:* This scenario introduces a multiplicative error on the state matrix A and B, the aim is to evaluate the two controllers' robustness toward a modeling error. This is important as our model represents a complicated nonlinear system with multiple uncertainties which are hard to model.

*5) Scenario **V2, SPRS, SDIO**:* In **SPRS** scenario, the ref_{PDR} is stepped from 2 to 4, the aim is to move the system away from its nominal operating point of 2PDR, which could potentially lead the two controllers' to saturate. During the **SDIO** scenario the system is subjected to a oscillating disturbance, while the ref_{PDR} is kept at 4. The goal is to investigate the two controllers' disturbance rejection outside nominal operating conditions.

C. Simulation Results

The two controllers are simulated using the linear model presented in equation 4, and the results of **V1** and **V2** are plotted in figures 7 and 9, respectively. Each figure consists of four individual plots where: the top two plots from left to right show l and the PDR, in both plots the reference value is indicated with a dotted line. The bottom two plots, from left to right show the V_u and the V_o. Each of the individual plots show the output of the two respective controllers, which have been simulated using the four individual testing scenarios as described in tables I and II. The simulations results shown in figure 7 are set to run for 3000s to initialise the system and allow it to reach steady state, the results shown in figure 8 are a continuation of the simulations in figure 7. The last simulation results shown in figure 9 are set to run for 4000s to initialise the system and allow it to reach steady state

*1) Simulation results of Scenario **LRS**:* The tracking performance of the PID control solution with respect to ref_l is perfect in the initialisation phase, when **LRS** is applied, V_u is actuated to compensate for the step change. V_u is increased instantaneously from its steady state of 11.48% to 17.48% after which it reaches its steady state of 11.49% again at 3900s, with an undershoot of 0.4%. The actuation of V_u reduces l to its steady state or ref_l of 225mm after 3874s, with an undershoot of 1mm.

The H_∞ control solution does not track ref_l prior to the application of **LRS**, and the steady state value up until this point is 419.4mm, which equals steady state error of 189.4mm. After the application of **LRS**, the H_∞ control solution actuates V_u with an overshoot that is ≈ 4 times smaller than that of the PID control solution but reaches its steady state around the same time as the PID control solution. Thus with the H_∞ control solution, l decreases according to a first order response, reaching a steady state value of 414.4mm at 3880s, with a steady state error of 189.4mm. The steady state error is thus the same before and after **LRS**.

The aggressive actuation of V_u by the PID control solution, results in a spike in the PDR, which moves away from ref_{PDR} of 1.8 to 1.61 and reaches steady state of 1.8 again after 300s. The response to the change in PDR is aided by the PID control solution's actuation of V_o from 85.69% to 92.3% within a time-period of 24s. The relatively more relaxed actuation of V_u by the H_∞ control solution combined with its lower and slower actuation of V_o 72.27% to 74.06% within 110s, results in a relatively unchanged PDR. In addition, the H_∞ control solution does not track ref_{PDR} and stays around a steady state point of 1.46 before and after **LRS** with a steady state error of 0.34PDR before and after **LRS**.

*2) Simulation results of scenario **PRS**:* The simulations results for the **PRS** scenario are shown in figure 7. ref_{PDR} step has no observable impact on the l, with regards to the PID control solution, and accordingly the PID control solution does not actuate V_u. The H_∞ control solution reacts to the step in ref_{PDR} by adjusting both valves, which results in l to raise from 414.4mm to 431.7mm within 700s, which results in a steady state error of 206.7mm.

The PID control solution actuates V_o from a steady state value of 85.69% with a first order response, reaching the steady state value of 93.44% after 70s. Correspondingly the PDR reaches its steady state value of 2 after 59s, from a steady state value of 1.8, demonstrating the same first order behavior.

The PDR value controlled by the H_∞ control solution, has a similar dynamic response as the PDR value controlled by the PID control solution, but the ref_{PDR} has a steady state error of 0.377 with respect to the H_∞ control solution.

*3) Simulation results of scenario **DIO**:* The simulations results for the **DIO** scenario are shown in figure 7. The sine-wave disturbance has a direct impact on l with respect to the PID control solution which reacts by actuating V_u, however, due to the severity of the disturbance the tracking of ref_l is

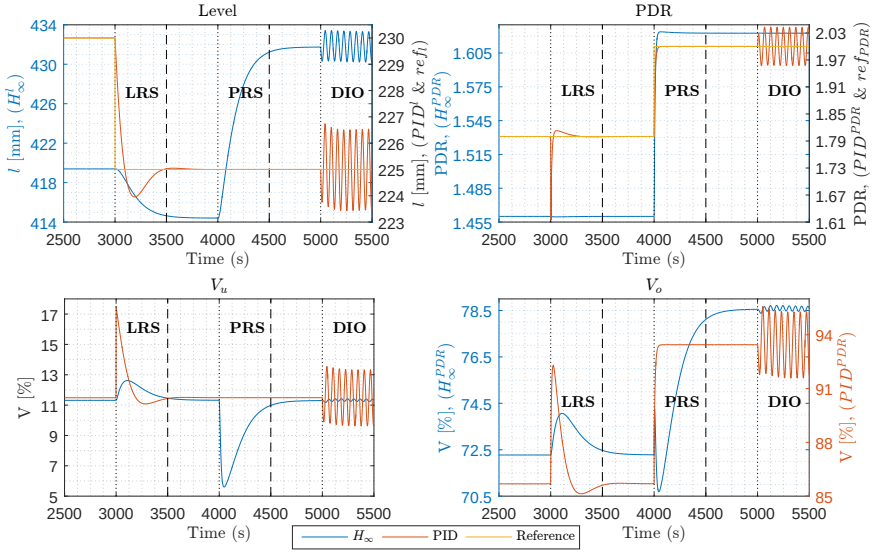

Fig. 7. **VI LRS, PRS, DIO**: Simulation of the two controllers' performance under different operating conditions. Individual scenarios are separated with horizontal dotted lines. The initialisation of the simulations occurs in the initial 3000s of the run-time.

not achieved. This directly influences the PDR and accordingly the PID control solution actuates V_o to compensate, but does not succeed at tracking ref_{PDR}. The impact on l is less severe in case of the H_∞ control solution, where l oscillates with an amplitude of 3mm. In comparison l oscillates with an amplitude of to 3.3mm when the PID control solution is used. In addition l with respect to the H_∞ control solution has a steady state value of 431.8mm, which is a steady state error of 206.8mm. The H_∞ control solution actuates V_o with an amplitude that is $\approx 21\%$ lower than that of the PID control solution. The PDR with respect to both controllers, oscillates with the same frequency, i.e. the frequency of the disturbance 0.104rad/s. The lower actuation of both valves by the H_∞ control solution results in a more steady PDR value, which has a peak-to-peak amplitude of 0.005 when compared to 0.043 with respect to the PID control solution.

*4) Simulation results of scenario **MOE**:* The simulations results for the **MOE** scenario are shown in figure 8. PID control solution, which tracks ref_l, actuates V_u more aggressively than the H_∞ control solution, thus influencing l to rise fast and oscillate twice before reaching steady state at ref_l at 7500s. With respect to the H_∞ control solution, l has a first order response, resembling that of V_u. The rise-time of l with respect to the the H_∞ control solution is approximately 10 times slower than the rise time of l with respect to the PID control solution, 760s vs. 76s respectively. l, with respect to both controllers reaches steady state around 7500s, where l with respect to the H_∞ control solution has a steady state offset of 221.2mm from ref_l, similar to previous scenarios The more aggressive actuation of V_u by the PID control solution, affects the PDR which drops rapidly until it is corrected by an additional aggressive actuation of V_o. The PID control solution's reference tracking of PDR results in the saturation of V_o at 250s after the introduction of **MOE**. The saturation of V_o results in a discontinuation of the PDR's increase towards ref_{PDR}. 230s after the introduction of **MOE**, at which time the PID control solution starts reducing V_u, the PDR starts increasing again. The PDR with respect to the PID does not reach ref_{PDR} due to the saturated V_o.

*5) Simulation results of scenario **SPRS**:* The simulations results for the **SPRS** scenario are shown in figure 9. As with scenario **(PRS)**, the ref_{PDR} step does not impact l with respect to the PID control solution. The PDR is affected and the PID control solution actuates V_o to compensate for the change in ref_{PDR} with a fast response only to saturate the valve after 2s.

With respect to the H_∞ control solution, **SPRS** scenario impacts l and the PDR as the H_∞ control solution adjusts both valves to compensate for the step of ref_{PDR}. During the **SPRS** scenario the H_∞ control solution does not saturate V_o, but as in **(PRS)**, it sacrifices its tracking performance in order to keep both valves within a safe boundary.

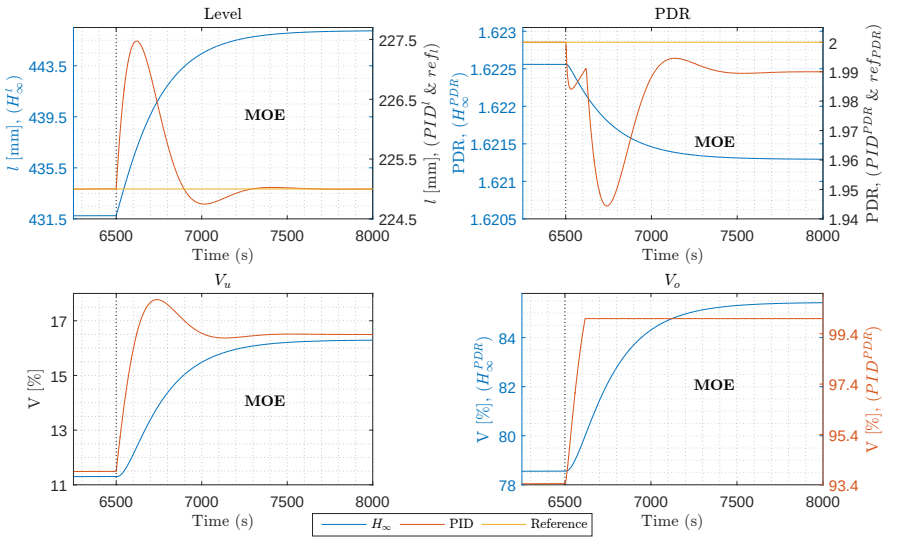

Fig. 8. **V1 MOE**: Simulation of the two controllers under the introduction of a modeling error, the error is marked by a vertical dotted line.

*6) Simulation results of scenario **SDIO**:* The simulations results for the **SDIO** scenario are shown in figure 9. After the introduction of the oscillating disturbance, the PID control solution oscillates l while aiming at tracking ref_l, resembling its behavior in scenario **(DIO)**. This is directly translated into an oscillation of the PDR, as V_o is saturated, and thus cannot control the PDR.

The H_∞ control solution, on the other hand, actuates V_o with small adjustments, enough to keep the PDR stable, and meanwhile does not saturate V_o, resembling its behavior in scenario **(DIO)**.

VI. Scaled Pilot Plant Implementation

A scaled pilot plant of an offshore de-oiling facility was designed and constructed at our laboratory in Aalborg University, Esbjerg, Denmark [35].The de-oiling facility, consisting of a three phase gravity separator and industrial hydrocyclone (Vortoil 1.4"), separates the three phases of oil, gas and water. The scaled pilot plant is equipped with sensors and actuators which replicate the offshore installation, and gather the generated data into a cross-platform data file. The platform has the capability to inject oil, gas and water into the system and as shown in figure II-A in section II it has the ability to recreate offshore scenarios. This scaled pilot plant was a crucial tool in the model and control development; implementation and evaluation. The scaled pilot plant is operated through Simulink Real-Time™ environment, which gives the opportunity to use Simulink ® for implementation of controllers onto the system.

A. PID control solution Implementation

The PID control solution used for the experimental tests is the same as explained in section V. The PID control solution was fine tuned by a trial and error method, to achieve the best performance on our scaled pilot plant. The PID control solution was implemented using Simulink® environment, by applying a standard PID block.

B. H_∞ control solution Implementation

The H_∞ control solution was implemented onto the scaled pilot plant through the Simulink® environment. The input to the H_∞ control solution is the error calculated from the reference and the measured l and the PDR (calculated from the pressure measurements). The H_∞ control solution outputs control the two manipulated variables, the V_u and V_o.

C. Auxiliary Controllers

A series of auxiliary controllers ensured that the setup could be operated safely while achieving the desired operating conditions. The controllers that are important for system dynamics, i.e. the gravity separator pressure P_s controller and the inlet feed pump volumetric flow-rate F_{in} controller, are presented in this section. The limits for the gravity separator water level are as follows; the minimum level is 30mm and the maximum level is 330mm, which is the level of the weir and an increase in the level after this point will flood the oil. If $P_s > 10.5$bars the system will shut down due to safety reasons.

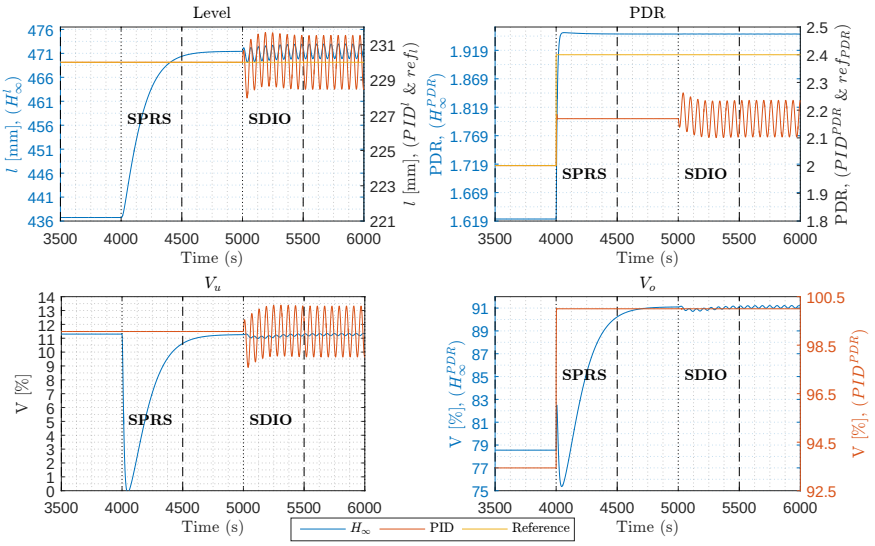

Fig. 9. **V2, SPRS, SDIO**: Simulation of the two controllers under different operating conditions, in which the ref_{PDR} step forces a saturation of V_o. Individual scenarios are separated with horizontal dotted lines. The initialisation of the simulations occurs in the initial 4000 of the run-time.

1) Gas Flow-Rate Into the Gravity Separator: The separator inlet gas pressure is controlled at 8 bar constantly, this is 1 bar above P_s and is to ensure that there is a flow into the gravity separator.

2) Gravity Separator Pressure: V_s controls P_s using a feedback from the gravity separator's pressure transmitter located on the gravity separator's gas outlet. The valve that was used has a fast dynamic, as does the pressure transmitter, and the controller that was used was a PID controller. The controller was tuned using a recursive trial and error method, where the goal was to achieve the fastest possible dynamic.

3) F_{in} Controller: As the outlet flow from the separator is pressure driven, the inflow of liquid should be kept proportionally lower than the pressure thus ensuring that the separator is not overfilled with liquid. Thus in the initialization phase the pressure of the water pump *WP* is controlled, where the feedback signal is the P_s and the pump control signal is WP_V. During the nominal operation the pump is controlled using a volumetric flow transmitter.

D. Scaled Pilot Plant Experiment Description

The PID and the H_∞ controllers were implemented on the scaled pilot plant and tested under different operating conditions, similar to the conditions tested during the simulations in section V. In addition, the start-up and shutdown procedures were emulated, as these are crucial to offshore operations. The experimental scenarios are presented in table III. The desired operating conditions of the two control parameters, the PDR and the l for the scaled pilot plant are presented in table IV.

TABLE III
EXPERIMENTAL SCENARIOS, THE OCCURRENCE OF THE SCENARIOS ARE MARKED WITH DOTTED VERTICAL LINES IN THE SIMULATION PLOTS

Name	Value & time	Description	Figure
ST$_e$	l = 130mm PDR = 2 @ t = 0s	Start up	10
LRS$_e$	l = [130mm - 150mm] @ t = 1500s	ref_l step	11
PRS$_e$	PDR = [2 - 2.4] @ t = 1800s	ref_{PDR} step	11
DIO$_e$	ω = 0.104 rad/s $\hat{U}$ = 0.6 l/s μ = 0.3 l/s @ t = 2000s	$sine_{dist}$ input	11
SD$_e$	l = 130mm PDR = 2 @ t = 1300s	Shut Down	12
SEV$_e$	PDR = 2 $\hat{U}$ = 0.8 l/s μ = 0.41 l/s	Severe scenario	13

*1) Experiment Description for **ST**$_e$:* In this test we ran the setup from its initial state, i.e. all pressures and flows were 0. The initialization cycle is as explained in the implementation section VI-C3. The goal of this test was to emulate the system

TABLE IV
ALLOWED OUTPUT OPERATING CONDITIONS.

Parameter	Value	Unit
PDR	1.5-3	PDR
l	30-330	[mm]

during start-up, which is a common offshore scenario that causes long dead time periods resulting in low production and thus reduced profit. It is therefore crucial that the start-up periods be reduced such that the system can achieve nominal operation as soon as possible.

2) Experiment Description for ***LRS***$_e$, ***PRS***$_e$, ***DIO***$_e$*:* The aim of the following scenarios, **LRS**$_e$, **PRS**$_e$, **DIO**$_e$, is similar to that of the simulation scenarios (**LRS**, **PRS**, **DIO**) in section V-B, refer to table III. Due to the differences between the linear MIMO model of the de-oiling facility and the physical de-oiling facility (scaled pilot plant), the operating conditions are slightly changed, refer to table III.

3) Experiment Description for ***SD***$_e$*:* In this test the liquid inflow was set to 0 to simulate a shut down scenario. The goal of this test was to investigate the PID and H_∞ control solutions' robustness towards system shutdown which is a common offshore scenario and like the start-up, results in long zero production periods which affect the production and the profit of the facilities. The desired performance for the PID and H_∞ control solutions is that they should maintain the system operational as long as possible, i.e. the levels within the safe region and the PDR within the recommended range (this range can alter for individual installations).

4) Experiment Description for ***SEV***$_e$*:* In the severe scenario the F_i is oscillated with a random frequency and amplitude that are generated using a sampled Gaussian Noise with a frequency of 0.06Hz, μ0.5, σ0.2 and a seed of 1, the generated signal is identical for both tests). The goal of this experiment is to test the system's robustness towards severe slugging emulated by manipulating the F_{in} such that large fluctuations as experienced by offshore de-oiling systems were formed, refer to figure 2. For comparison, one cycle lasts 60s in **DIO**$_e$, where the long surges in **SEV**$_e$ last for approximately 250s. This experiment in addition tests the controller's robustness towards long drought periods where F_{in} is 0l/s for up to 35s.

E. Experimental Results Performed on the Scaled Pilot Plant

1) Experiment results for ***ST***$_e$*:* The result of the start-up experiment is plotted in figure 10 where the dotted lines represent the changes under different operating conditions. During start-up, l is 0mm which leads to a large measurement error to the PID control solution, to which the PID control solution compensates by closing V_u. This has an immediate impact on the PDR which goes to zero, and PID control solution reacts by setting $V_o = 100\%$. This continues until $\approx$ 150s where PID control solution starts opening V_u as l increases and reaches its steady state value of 130mm at 225s. This occurs as P_s, during the start-up phase, is not large enough to ensure the required flow through V_u. To compensate the PID control solution opens V_u up to 90% at 275s and then slowly decreases it to 63% at 650s, which is the transition into the nominal operating phase. The relatively large opening of V_u results in a low PDR value, which the PID control solution handles by saturating V_o in a fully open position, even so ref_{PDR} cannot be maintained during the start-up phase. The effect of the relatively large openings of V_u and V_o is reflected in the time it takes the pressure to reach its nominal operating pressure of 7bars, as the large valve openings constantly let out liquid, thereby reducing the pressure.

H_∞ control solution does not track ref_l and during the first 125s, it holds V_u and V_o 100% open, which results in a PDR value of approximately 0.75 and $l = 0$mm. After 125s the V_u's and after 175s the V_o's opening is reduced resulting in the PDR slowly moving towards ref_{PDR}. At 300s, V_u and V_o are open within a region of $15 - 50\%$ till the end of the experiment. The relatively fast actuation of the valves towards a more closed position, results in a quick pressurization of the tank and thus the system reaches nominal operating condition. The nominal pressure is reached 200s faster with the H_∞ control solution, in comparison to the PID control solution, which is an improvement by $\approx 31\%$.

2) Experiment results for ***LRS***$_e$*,* ***PRS***$_e$ *and* ***DIO***$_e$*:* The result of the nominal operation experiment is plotted in figure 11, where the dotted lines represent the changes in different operating conditions and the dashed lines separate the three different scenarios.

Experiment results for ***LRS***$_e$*:* The step in ref_l causes the PID control solution to fully choke V_u, causing the PDR to increase rapidly to high values (with a peak of 415). This leads the PID control solution to fully open the V_o. This state of PDR instability lasts for 50s, and stabilizes when l reaches its new set-point, after 150s. The H_∞ control solution, however, manages to keep the PDR steady, by cooperatively adjusting both V_u and V_o. In order to do so it sacrifices the level slightly which stays well within the allowed operating conditions, with a maximum steady state deviation of 28mm before, and 24.2mm after **LRS**$_e$ respectively.

Experiment results for ***PRS***$_e$*:* PID control solution reacts to the change in ref_{PDR} with a small adjustment of V_o from a steady state gain of 17.40% to 20.46%. PID control solution closes V_u slightly during the step change in ref_{PDR} so as to compensate for the small amount of water which escapes through V_o. l is unchanged during **PRS**$_e$.

H_∞ control solution reacts to the step change in ref_{PDR} by adjusting both V_o and V_u, which results in a faster increase of the PDR compared to the PID control solution. The new ref_{PDR} of 2.4 is not tracked by H_∞ control solution and it has a steady state offset of approximately 0.1PDR, but with less oscillations than the PID control solution. The peak-to-peak amplitude of the two signals is; $2\hat{U} = 0.07$PDR and $2\hat{U} = 0.23$PDR for the H_∞ and the PID control solution respectively. l with respect to H_∞ stays unchanged during **PRS**$_e$.

Experiment results for ***DIO***$_e$*:* During the oscillating inflow the PID control solution tracks ref_l with relatively small oscillations, with a peak-to-peak amplitude of $2\hat{U} = 2.1$mm and a steady state amplitude of 150mm. The consequence of the tracking is oscillations of V_u with a peak-to-peak amplitude of $2\hat{U} = 12.54\%$. The oscillation of V_u is directly translated into an oscillating PDR value which at times reaches 4, with a

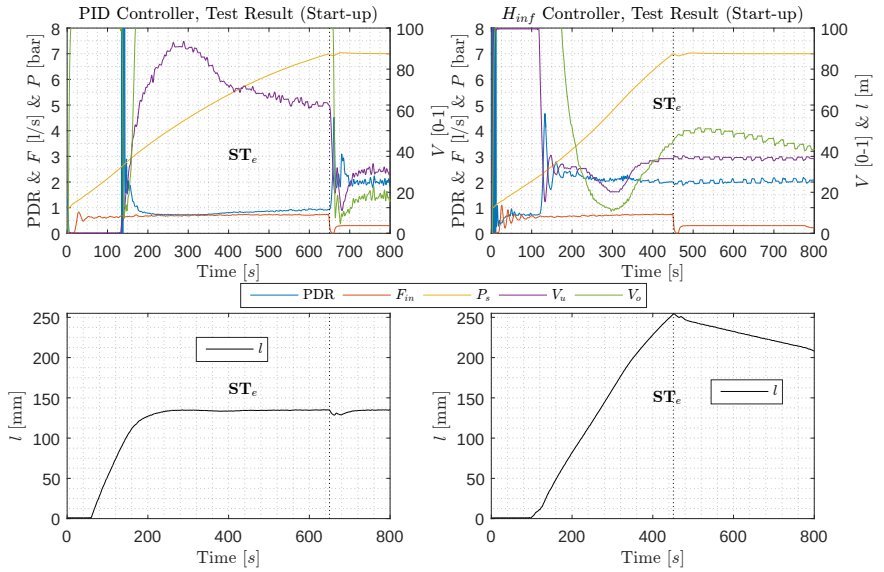

Fig. 10. Test result, start-up **ST**$_e$. The dotted line shows the achievement of the nominal operating pressure.

peak-to-peak amplitude of $2\hat{U} = 1.32$PDR and a steady state amplitude of 2.54PDR. The PID control solution compensates by adjusting V_o, which results in an oscillating V_o with a peak-to-peak amplitude of $2\hat{U} = 37.1\%$

V_u with respect to H$_\infty$ control solution has no oscillations. As a result the PDR is not affected and is stable throughout the test, with a peak-to-peak amplitude of $2\hat{U} = 0.06$ and a steady state amplitude of 2.51.

3) Experiment results for ***SD***$_e$*:* The results of the shutdown experiment is plotted in figure 12, and the dotted lines represent the changes in different operating conditions. At the shutdown point of 2000s, l starts to decrease which results in the PID control solution closing the V_u in order to stop the remaining liquid in the tank from exiting, and shutting down the process after 21s when V_u is fully closed. As the H$_\infty$ control solution does not track ref_l the l decreases until 90mm at which point it decreases V_u and V_o to 0%, this occurs at 2157s. This action results in the system running with a PDR above 1.5 until it shuts down the system. The effective run time of the PID control solution is 31s compared to 166s of the H$_\infty$ control solution, which is approximately five times longer.

4) Experiment results for ***SEV***$_e$*:* Figure 13 illustrates the response of the system when subjected to severe random input flow, which oscillates between $[0-0.8]$l/s at 8 bars of pressure. In this test the PID control solution again saturates V_o at a fully open position as in (DIO_e). The V_o saturation in **SEV**$_e$ accounts for 45% of the experiment time and has a continuous saturation for as long as 174s in one instance. This has a severe impact on the PDR which oscillates with values as low as 1, during $V_o = 100\%$, and as high as 21PDR. The oscillation of V_u between 0% and 60% throughout the experiment, directly impacts V_o. The reason is l tracking by the PID control solution, with a resulting standard deviation of $\sigma = 24$mm and a steady state amplitude of 150mm which is equal to ref_l. The H$_\infty$ control solution has a low fluctuating V_u. The effect of the stable V_u is translated into a relatively stable V_o which stays within a boundary of [25% - 59%]. The result is a steady PDR value, with a standard deviation of $\sigma = 0.06$PDR and a mean of $\mu = 2.02$ which is relatively close to $ref_{\text{PDR}} = 2$. The H$_\infty$ control solution sacrifices the ref_l, and l has a standard deviation of σ23.1mm, with a mean of $\mu = 242.9$mm and thus a mean steady state error of 92.9mm. The level stays within the minimum and maximum level of $[184.5-282.6]$mm which is within the allowed operating conditions.

VII. Discussion

A. Simulation Results

As seen throughout the simulation results, the H$_\infty$ control solution has a reduced reference tracking which kept the

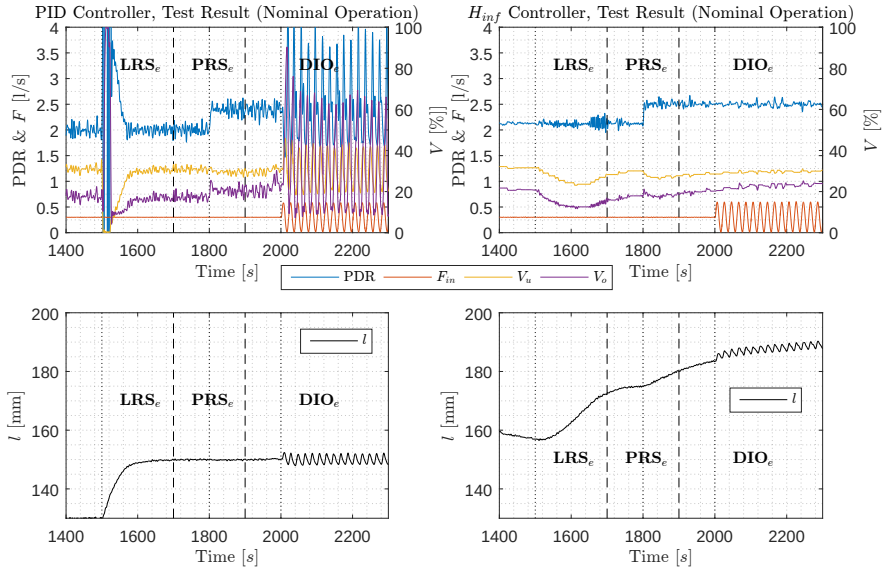

Fig. 11. Nominal operation, the scenarios **LRS**$_e$, **PRS**$_e$, **DIO**$_e$ are separated into 3 segments divided by dashed lines, the scenario changes are indicated by dotted lines.

controllable parameters V_u and V_o from saturating. The benchmark PID control solution saturated V_o in favor of the PDR reference tracking in the **V2** scenarios. With the H$_\infty$ control solution, the MIMO control structure leads to cooperation of both the controllable parameters. The result is a more relaxed valve actuation, which benefits the PDR value in particular, unlike the PID control solution where each valve is actuated independently and more aggressively as the two sub-systems work against each other resulting in a more oscillating PDR.

With respect to the **DIO** scenario the H$_\infty$ control solution's reference tracking is sacrificed which results in the controlled variables being within safe ranges. In comparison, the PID control solution saturates the V_o. During the severe scenarios **V2** the strength of the H$_\infty$ control solution is even more evident. Where the cooperative actuation of V_u and V_o results in a more relaxed PDR after the step of ref_{PDR}.

While under similar conditions the PID control solution saturates V_o thus rendering the system uncontrollable from the PDR perspective. The sacrifice which the H$_\infty$ control solution makes is a fluctuating l, which if kept within certain bounds, is inconsequential for this type of system as discussed in section I. Although the relaxed PDR response does not directly result in a better de-oiling efficiency under specific operating conditions, the reduced actuation of the valves especially of V_u will result in a smoother F_i and thus an overall increased de-oiling efficiency.

The saturation of valves, as in the case of the PID control solution, renders the system uncontrollable and l can as a result exceed its minimum or maximum level which would lead to system instability.

B. Experimental Results Performed on the Scaled Pilot Plant

The reference tracking of the PID control solution and the lack of cooperation between the two sub-controllers for l and PDR, affects the performance of the PID control solution throughout the experiments. The reference tracking often results in saturation of V_u which is of great consequence for the PDR, as the V_o is less dominant and PID control solution cannot compensate for this effect due to the saturated V_o. While the tracking of the ref_{PDR} at time 1800s, in figure 11, appears to be managed well by the PID control solution, tracking of ref_l at time 1500s has a negative effect on the PDR, due to the reasons mentioned. The result of this behavior is specifically expressed during the oscillating F_i, in the **DIO**$_e$ scenario at 2000s in figure 11, where large fluctuations of V_u saturate V_o thus creating unfavorable PDR values, all in favor of maintaining the ref_l.

During **DIO**$_e$, the peak-to-peak amplitude of PDR with respect to the PID control solution was $2\hat{U} = 1.31$, while under the same conditions the PDR with respect to the H$_\infty$ control

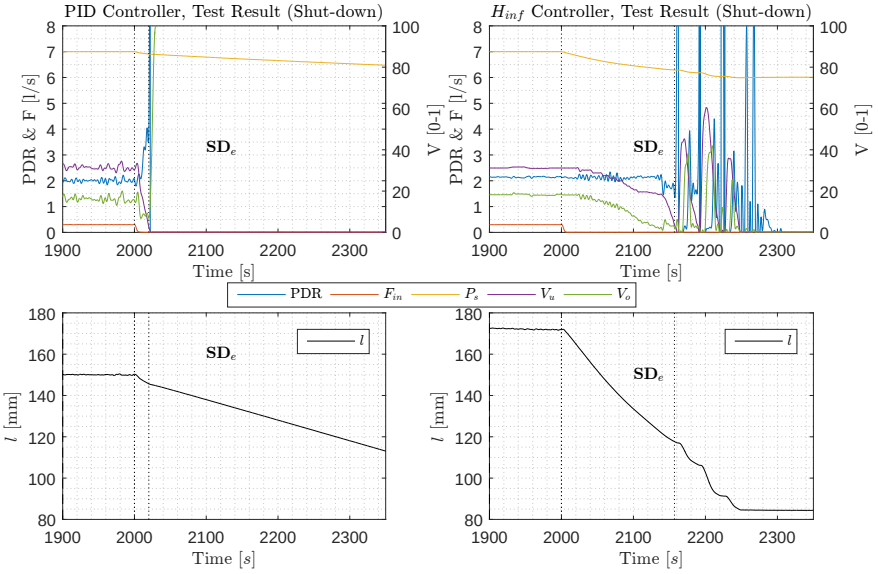

Fig. 12. Test results of the the shut-down $\mathbf{SD}_e$ scenario, the shut-off of F_{in} (2000s) and system shut down are indicated with two separate vertical dotted lines.

solution had a peak-to-peak amplitude $2\hat{U} = 0.06$, which is a considerable 22 times lower oscillating amplitude. At times the PDR even reaches values of 22, which is comparable to the real offshore scenario shown in figure 2, section I. This is far outside the operating range, see table IV, and such a performance will result in large concentrations of water in the overflow, which then necessitates recirculation through the separation process. In addition, the reference tracking, performed by the PID control solution affects the system during start-up and shut-down where drastic V_u openings, caused by the PID control solution tracking the l, results in undesirable system performance, see figure 10 and 12 for start-up and shut-down respectively. During start-up the system sacrifices fast pressurization of the tank, necessary for nominal system operation, in favor of tracking ref_l which in this case is not crucial as long as it is kept within a certain safety margin. In comparison, the H_∞ control solution reaches nominal operating pressure 31% faster. During shut-down, where $F_{in} \to 0$, the PID control solution's reference tracking seeking to maintain the desired ref_l saturates the valves and thus disables the system from operating. The H_∞ control solution under the same shut-down scenario maintains the system operational five times longer.

In article [20] it was shown that F_i has a direct impact on ϵ from a dynamic and static perspective and steps of an amplitude of 0.06 L/s were shown to have an impact on ϵ in experiments performed on the same scaled pilot plant that was used in this work. Figure 14 is an analysis of the the volumetric flow rate into the gravity separator F_{in} and the volumetric flow-rate from the gravity separator and into the hydrocyclone F_i. It can be observed that F_{in} is conveyed directly to F_i and in this case the step's peak amplitude is far greater, up to ≈ 0.7 L/s when controlled by the PID control solution. Its frequency is lower and thus the dynamic impact may be reduced but according to analysis done in [17], having such deviations in flow will affect the static ϵ. Reducing the transmission of these oscillations from F_{in} to F_i is therefore crucial. This has been successfully achieved using the H_∞ control solution, where the transmission has been filtered significantly. The result is a lower DC gain, which is caused by the integration of the peaks by the gravity separator, by operating as an analogue low pass filter where the oscillations' peaks are stored in the vessel as volume instead of being transmitted to the hydrocyclone. This is further illustrated in the frequency analysis, presented in the bottom plot of figure 14, where H_∞ control solution has zero amplitude above 2 Hz, and 1/6th DC gain in comparison to PID control solution.

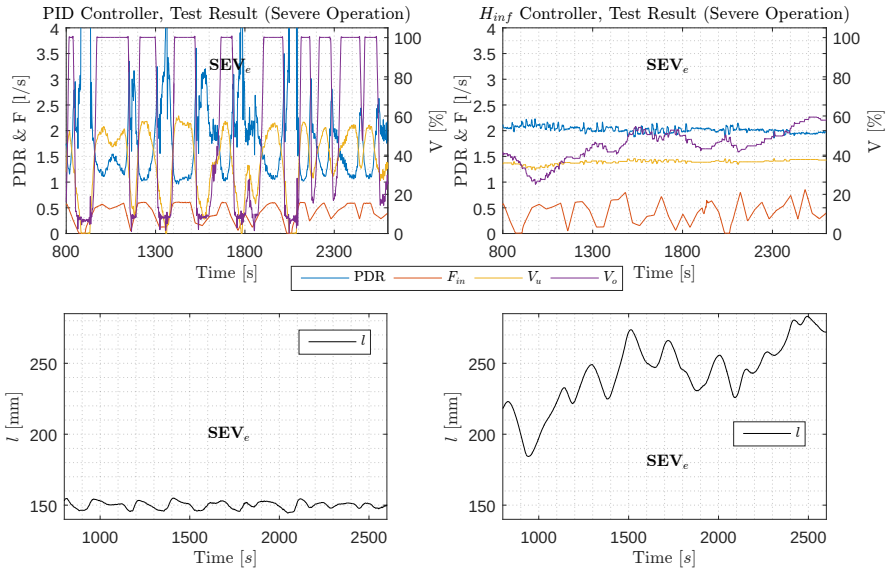

Fig. 13. Test results for severe operation (**SEV**$_e$), where F_{in} is fluctuating between [0-0.8] l/s.

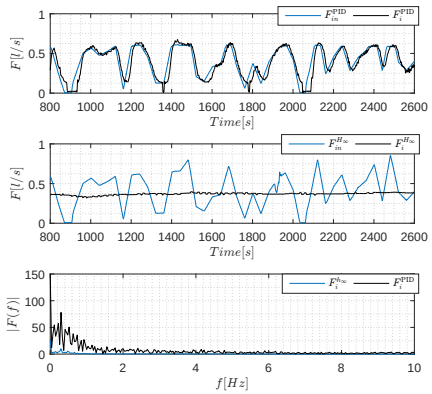

Fig. 14. Comparison of flow propagation through the de-oiling system, from F_{in} to F_i from a time and frequency perspective. (Analysis is based on the experimental data from figure 13, i.e. scenario (**SEV**$_e$))

VIII. Conclusion

Slugging flow, which causes the inlet flow rate F_{in} into the offshore de-oiling facilities to fluctuate severely, is an unmeasurable disturbance and has negative effects on the de-oiling process. The controllable parameters in the de-oiling system are the level of the gravity separator l and the pressure drop ratio (PDR) of the hydrocyclone, which are controlled by the actuation of the underflow valve (V_u) and overflow valve (V_o) respectively. In this study we have investigated the benefit of a robust sub-optimal H_∞ control solution in comparison to a benchmark PID control solution that is used for offshore de-oiling. The initial investigation showed that the current PID control paradigm, and the inherent coupling of the unit processes of the de-oiling facilities, the gravity separator and the hydrocyclone, results in a system which has poor disturbance rejection. The investigation also revealed the strong dominance of V_u with respect to the performance of the de-oiling system in comparison to V_o.

The slugging flow was emulated on a scaled pilot plant and was observed to propagate through the gravity separator and to the downstream hydrocyclone. This resulted in an oscillating hydrocyclone inlet flow rate F_i which in previous studies was shown to have a direct impact on the hydrocyclone's de-oiling efficiency ϵ unless the PDR was kept within a certain range. Thus it was concluded that the de-oiling system would perform

better if its disturbance rejection was improved.

A MIMO model of the de-oiling process was developed, based on which a robust suboptimal H_∞ control solution was designed. The H_∞ control solution was tested in simulations and then implemented and tested on the scaled pilot plant. In the simulations, where the H_∞ control solution was compared to a benchmark PID control solution, the H_∞ control solution facilitated disturbance attenuation and provided a more relaxed actuation of V_u and V_o. The conventional PID control solution, however, saturated the V_o while trying to track the level reference ref_l, a scenario similar to what was observed in data from offshore facilities during slugging flow.

The results from the experiments performed on the scaled pilot plant further proved that the H_∞ control solution was better at handling various disturbances, and in all the circumstances that were tested, it kept the system stable. The benchmark PID control solution once again under certain circumstances saturated the controllable parameters. The reduced reference tracking of the ref_l by the H_∞ control solution, resulted in almost perfect damping of the transmission of the disturbance F_{in} into F_i, as shown in figure 14. This is further shown in the frequency analysis in the bottom plot in figure 14, where the H_∞ control solution shows a considerable reduction of all frequencies above 0.2 Hz. An added advantage was that the H_∞ control solution needed no tuning after implementation, which was not the case with the PID control solution, which required extensive trial and error tuning both in the dynamic and steady state perspectives. The H_∞ control solution also offered shorter start-up and longer shut-down time periods In addition, in real life scenarios the reduced valve actuation by the H_∞ control solution could reduce the wear and tear on the system.

In future work, the model of the de-oiling system will be extended to include the ϵ in the model and control design.

ACKNOWLEDGMENTS

The authors would like to thank the support from the Danish Innovation Foundation (via PDPWAC Project (J.nr. 95-2012-3)). Thanks also go to colleagues J.P. Stigkær, A. Aillos, K. G. Nielsen and T. I. Bruun from Mærsk Oil A/S, colleagues P. Sørensen, A. Andreasen and Jakob Biltoft from Ramboll Oil & Gas A/S, for many valuable discussions and supports. Thanks also go to AAU colleagues: C. Mai, K. Jepsen, L. Hansen, M. Bram and D. Hansen for their contributions to this project.

REFERENCES

[1] J. Bamberg, *British Petroleum and Global Oil 1950-1975: The Challenge of Nationalism*, ser. British Petroleum series. Cambridge University Press, 2000.

[2] P. Ekins, R. Vanner, and J. Firebrace, "Zero emissions of oil in water from offshore oil and gas installations: economic and environmental implications," *Journal of Cleaner Production*, vol. 15, no. 13–14, pp. 1302 – 1315, 2007, approaching zero emissions.

[3] M. Stephenson, "A survey of produced water studies," in *Produced water*. Springer, 1992, pp. 1–11.

[4] B. Bailey, M. Crabtree, J. Tyrie, J. Elphick, F. Kuchuk, C. Romano, L. Roodhart *et al.*, "Water control," *Oilfield Review*, vol. 12, no. 1, pp. 30–51, 2000.

[5] J. A. Veil, M. G. Puder, D. Elcock, and R. J. Redweik Jr, "A white paper describing produced water from production of crude oil, natural gas, and coal bed methane," *Argonne National Laboratory, Technical Report*, vol. 63, 2004.

[6] "Danish production of oil, gas and water (danish energy agency)," https://ens.dk/en/our-services/oil-and-gas-related-data/monthly-and-yearly-production, Acssessed (09-11-2016).

[7] Miljoestyrelsen, "Status for den danske offshorehandlingsplan til udgangen af 2009," *Miljoestyrelsen*, Acssessed (01-11-2016).

[8] W. D. Monnery and W. Y. Svrcek, "Successfully Specify 3-Phase Separators," *Chemical Engineering Progress*, vol. 90, no. 9, pp. 29–40, 1994.

[9] A. F. Sayda and J. H. Taylor, "Modeling and control of three-phase gravilty separators in oil production facilities," in *American Control Conference, 2007. ACC'07*. IEEE, 2007, pp. 4847–4853.

[10] M. Thew, "Hydrocyclone redesign for liquid-liquid separation," *Chemical Engineer (London)*, no. 427, pp. 17–23, 1986.

[11] T. Husveg, O. Rambeau, T. Drengstig, and T. Bilstad, "Performance of a deoiling hydrocyclone during variable flow rates," *Minerals Engineering*, vol. 20, no. 4, pp. 368–379, Apr. 2007.

[12] S. Mokhatab, W. Poe, and J. Speight, *Handbook of Natural Gas Transmission and Processing*, ser. Chemical, Petrochemical & Process. Gulf Professional Pub., 2006.

[13] D. Wolbert, F. Ma, B, Y. Aurelle, and J. Seureau, "Efficiency estimation of liquid-liquid hydrocyclones using trajectory analysis," *AIChE Journal*, vol. 41, no. 6, pp. 1395–1402, 1995.

[14] S. Judd, H. Qiblawey, M. Al-Marri, C. Clarkin, S. Watson, A. Ahmed, and S. Bach, "The size and performance of offshore produced water oil-removal technologies for reinjection," *Separation and Purification Technology*, vol. 134, pp. 241–246, 2014.

[15] M. Thew, S. Silk, and D. Colman, "Determination and use of residence time distributions for two hydrocyclones," *International conference on Hydrocyclones*, pp. 225–248, 1980.

[16] G. Young, W. Wakley, D. Taggart, S. Andrews, and J. Worrell, "Oil-water separation using hydrocyclones: An experimental search for optimum dimensions," *Journal of petroleum science and engineering*, vol. 11, no. 1, pp. 37–50, 1994.

[17] N. Meldrum, "Hydrocyclones: A Solution to Produced-Water Treatment," *SPE Production Engineering*, vol. 3, pp. 669 – 676, November, 1988.

[18] T. Husveg, "Operational Control of Deoiling Hydrocyclones and Cyclones for Petroleum Flow Control," PhD Thesis, University of Stavanger, 2007.

[19] M. T. Thew, "Cyclones for oil/water separation," in *Encyclopaedia of Separation Science*, 4th ed. Academic Press, 2000, pp. 1480–1490.

[20] P. Durdevic, C. S. Raju, M. V. Bram, D. S. Hansen, and Z. Yang, "Dynamic oil-in-water concentration acquisition on a pilot-scaled offshore water-oil separation facility," *Sensors*, vol. 17, no. 1, p. 124, 2017.

[21] P. Durdevic, S. Pedersen, and Z. Yang, "Challenges in modelling and control of offshore de-oiling hydrocyclone systems," *Journal of Physics: Conference Series*, vol. 783, no. 1, p. 012048, 2017. [Online]. Available: http://stacks.iop.org/1742-6596/783/i=1/a=012048

[22] F. Di Meglio, G. O. Kaasa, N. Petit, and V. Alstad, "Model-based control of slugging: Advances and challenges," *IFAC Proceedings Volumes (IFAC-PapersOnline)*, vol. 1, no. PART 1, pp. 109–115, 2012.

[23] A. Sausen, M. de Campos, and P. Sausen, *The Slug Flow Problem in Oil Industry and Pi Level Control*. INTECH Open Access Publisher, 2012.

[24] S. Pedersen, P. Durdevic, and Z. Yang, "Review of slug detection, modeling and control techniques for offshore oil & gas production processes," *IFAC-PapersOnLine*, vol. 48, no. 6, pp. 89 – 96, 2015.

[25] M. Thew and I. Smyth, "Development and performance of oil-water hydrocyclone separators: a review," 1998.

[26] T. Husveg, O. Johansen, and T. Bilstad, "Operational control of hydrocyclones during variable produced water flow rates—frøy case study," *SPE Production & Operations*, vol. 22, no. 03, pp. 294–300, 2007.

[27] Z. Yang, M. Juhl, and B. Lø hndorf, "On the innovation of level control of an offshore three-phase separator," *2010 IEEE International Conference on Mechatronics and Automation, ICMA 2010*, pp. 1348–1353, 2010.

[28] M. V. Bram, A. A. Hassan, D. S. Hansen, P. Durdevic, S. Pedersen, and Z. Yang, "Experimental modeling of a deoiling hydrocyclone system," in *20th International Conference on Methods and Models in Automation and Robotics*. IEEE, 2015, pp. 1080–1085.

[29] P. Durdevic, S. Pedersen, M. Bram, D. Hansen, A. Hassan, and Z. Yang, "Control oriented modeling of a de-oiling hydrocyclone," *IFAC-PapersOnLine*, vol. 48, no. 28, pp. 291 – 296, 2015.

[30] K. Zhou, J. C. Doyle, and K. Glover, *Robust and optimal control*. Prentice hall New Jersey, 1996, vol. 40.

[31] K. Zhou and J. C. Doyle, *Essentials of robust control*. Prentice hall New Jersey, NJ, 1998, vol. 104.

[32] D. Gu, P. Petkov, and M. M. Konstantinov, *Robust control design with MATLAB®*, 2nd ed. Springer Science & Business Media, 2005.
[33] S. Skogestad and I. Postlethwaite, *Multivariable feedback control: analysis and design*. Wiley New York, 2007, vol. 2.
[34] G. Balas, R. Chiang, A. Packard, and M. Safonov, "Robust control toolbox," *For Use with Matlab. User's Guide, Version*, vol. 3, 2005.
[35] Z. Yang, S. Pedersen, P. D. Løhndorf, C. Mai, L. Hansen, K. L. Jepsen, A. Aillos, and A. Andreasen, "Plant-wide Control Strategy for Improving Produced Water Treatment," *Proceedings of 2016 International Field Exploration and Development Conference (IFEDC)*, 2016.

Part III

Appendix

Pilot Plant Design and Construction

In order to make the results of this study applicable to offshore deoiling facilities, a scaled pilot plant was designed and built to serve as a platform for experimentation. The goal of designing the scaled pilot plant was to scale an offshore de-oiling installation while retaining its key features. The hydrocyclone unit was used as the baseline for design, as scaling it could compromise its separation efficiency due to the complex hydrodynamics which facilitate the separation mechanism. Scaled hydrocyclones were built to enable up-scaling of the platform, but the industrial hydrocyclone were used for efficiency benchmarking to allow for comparison to real hydrocyclones. Thus rest of the units, the pipeline and riser and the gravity separator, were dimensioned according to the hydrocyclone unit. A system to emulate a natural offshore Oil and Gas reservoir was also built as this was important to reproduce the flow conditions that offshore de-oiling facilities endured. The scaled pilot plant included additional transmitters to facilitate various measurements during the experiments. The resulting scaled pilot plant has the ability to emulate offshore scenarios and allows for full user manipulation. The scaled pilot plant can be considered to consist of three main sub-systems: the first sub-system is a pipeline connected to a reservoir, the next is a pipeline riser and the final one being the de-oiling facility, where the de-oiling facility again has two sub-systems, the gravity separator and the hydrocyclone. The uniqueness of the set-up is its versatility, as the individual sub-systems can be coupled together and decoupled thus enabling the investigation of the entire system or the study of individual or combinations of the sub-systems.

1 Water, Oil and Gas Supply system

The supply system consists of a series of tanks, one for water, one for oil and one for gas which in our case is atmospheric air. The water flow is created using a centrifugal pump, shown in figure F.1. The oil is delivered using a diaphragm pump, shown in figure F.1 and the gas is supplied by the building

Fig. F.1: Photo of the set-up showing from left top: Riser platform, Simulink Real-Time target PC interface, reservoir water pump, TD-4100, three phase Gravity separator, oil pump, Coriolis flow meter connected to a valve, PMMA transparent hydrocyclone.

compressor which operates at 8 bars bars. For information about the individual pumps refer to paper E The three phases are combined in a venturi mixer, shown in figure F.3. The venturi mixer is in essence a pipe of varying diameters and operates by using the venturi effect. It is designed to change the velocity profile of the fluids flowing through it by first decreasing and then increasing the pipe diameter. The oil, water and gas mixture is injected into the enlarged section of the pipe and as the mixture flows through, the diameter of the pipe reduces and then increases again inducing a venturi effect, and by doing so it creates vortices which mix the fluids into a homogeneous mixture.

2 Pipeline and Riser

A 25 meter long pipeline transports the liquid/gas mixture from the reservoir to a vertical riser which then raises the mixture onto a gravity separator which is atop a platform that is 6m high. The flow of the mixture can be controlled using a topside choke-valve, V_{topside}. Majority of the pipeline is made from 50mm transparent pipes, which is done to facilitate a visualisation of the flows within the pipes.

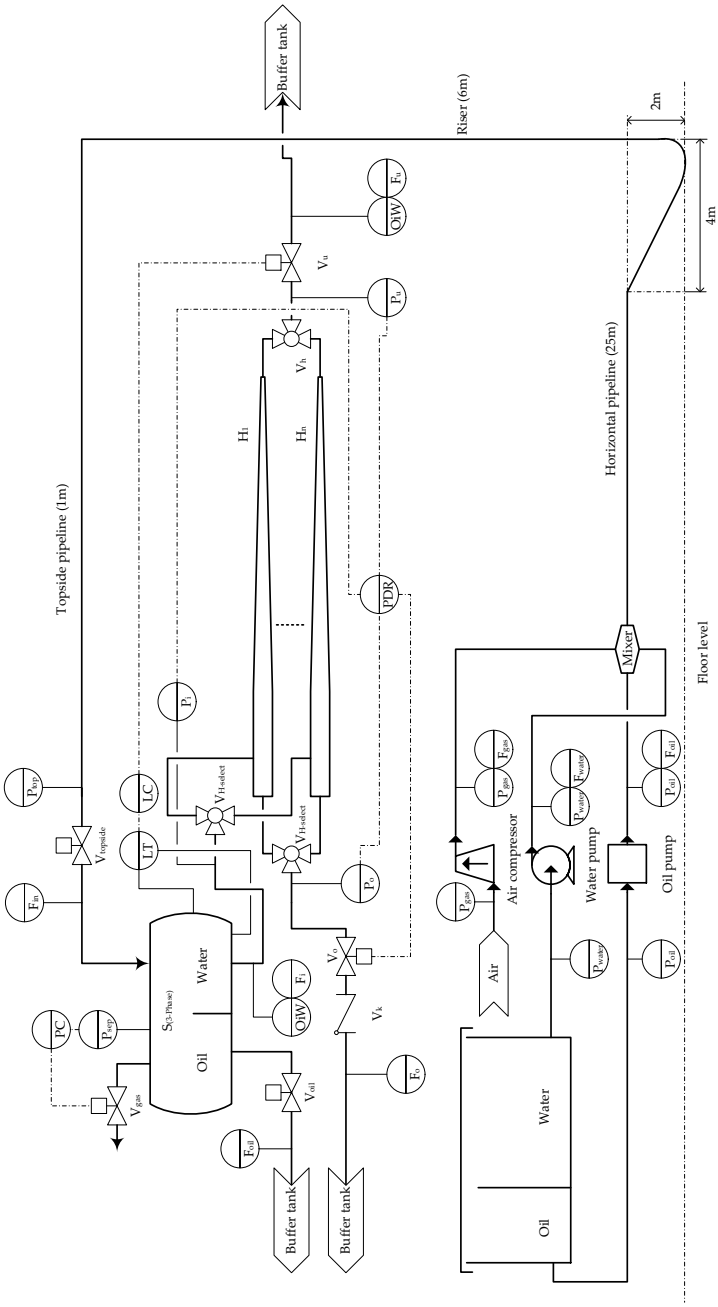

Fig. F.2: Simplified P&ID diagram of the scaled pilot plant. This figure is not to scale.

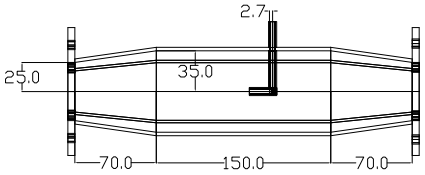

(a) CAD sketch of the oil-water mixer with dimensions, showing the internal workings. This figure is to scale.

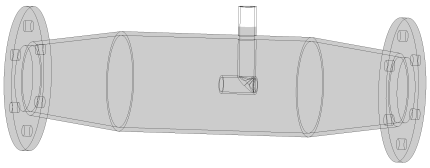

(b) 3D sketch of the oil-water mixer. This figure is to scale.

Fig. F.3: Sketch of the oil, water and gas mixer.

3 Gravity Separator

The three phase gravity separator was designed with a residence time of approximately 3 minutes, following industrial guidelines. The residence time can be changed by altering the height of the interchangeable weir. The separator is equipped with three outlets, one each for water, oil and gas, where the oil outlet is directly connected to the buffer tank, gas outlet is let into the atmosphere. The water outlet is connected to the hydrocyclone, but when required, can be bypassed directly to the buffer tank. The gravity separator was specifically designed and built and the sketch used for the final construction is shown in figure F.4. The gravity separator with all the auxiliaries has been sketched in the P&ID diagram in figure F.2

4 Hydrocyclones

The pilot plant includes two types of de-oiling hydrocyclone separators: one custom built transparent hydrocyclone made of PMMA and two industrial steel hydrocyclone liners manufactured by (Vortoil). A liner is a single hydrocyclone unit, where offshore systems have numerous liners connected parallelly. The transparent hydrocyclone was designed to investigate fluid flows inside the liner, and it was used for the early model development described in paper B and (11). Based on the images attained from the transparent hydrocyclone, refer to figure F.5, it was possible to make an early assessment of the hydrocyclone's performance. This was a preliminary investigation of the system, which involved running the system at different operating conditions i.e observing the air/oil-core created when the centripetal/centrifugal forces are sufficient.

The transparent hydrocyclone has similar dimensions as the industrial hydrocyclone, and was designed based on Coleman and Thew's design, refer to (102), and it is sketched in figure F.6 and a photograph of it can be seen in

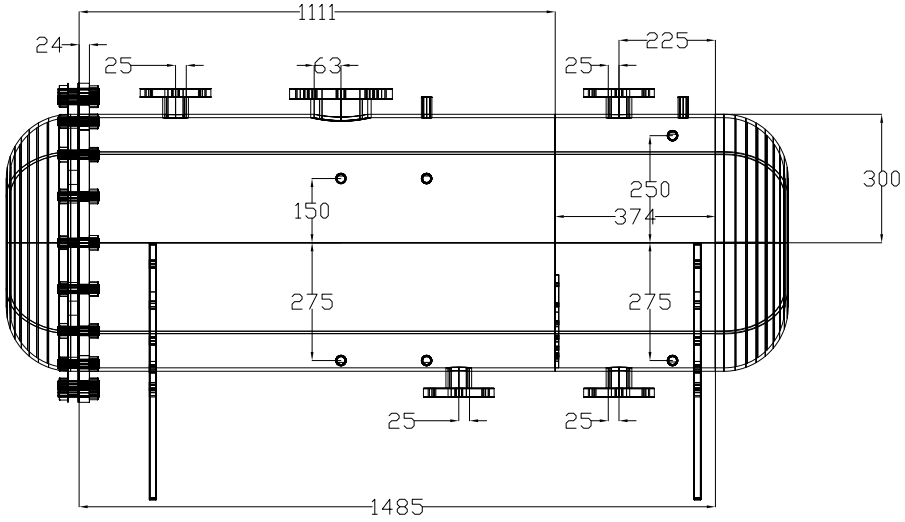

Fig. F.4: Sketch of the gravity separator with dimensions, used for construction. This figure is to scale.

(a) The air-core developed inside the in-house designed transparent hydrocyclone. The experiment was operated at low flow rates as separation of water and air does not require large centrifugal/centripetal forces due to the large density difference.

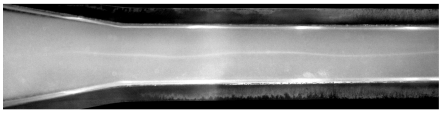

(b) The oil-core developed inside the in-house designed transparent hydrocyclone. The experiment was operated using large quantities of oil such that the oil-core became visible to the naked eye.

Fig. F.5: Development of an air- and oil-core in the transparent PMMA hydrocyclone, the images were captured using commercial image cameras.

figure F.1.

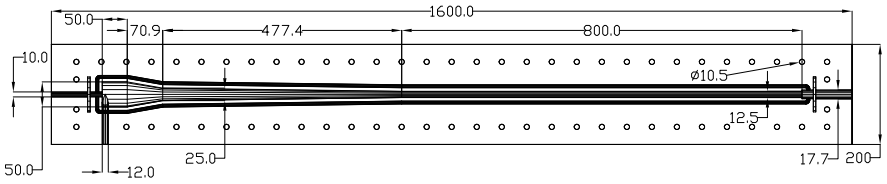

(a) Sketch of the transparent hydrocyclone with dimensions. This figure is to scale.

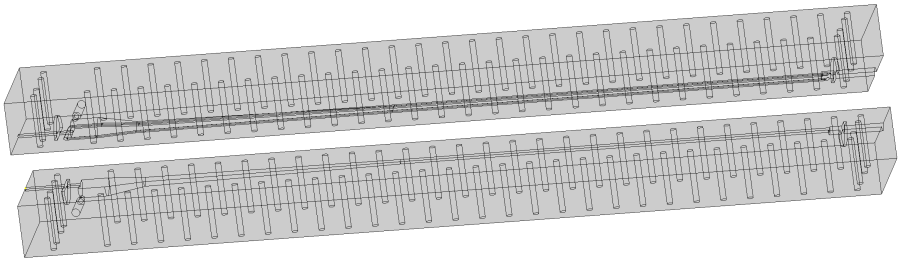

(b) Sketch of the transparent hydrocyclone, showing the two individual pieces of which the final assembly is combined and bolted together. This figure is to scale.

Fig. F.6: Sketch of the transparent hydrocyclone.

The industrial Vortoil hydrocyclones are designed to be placed inside a pressure vessel with 41 stacked hydrocyclones, which operate at a nominal operating pressure of 5.7 bars. The pressure vessel has been scaled for the purpose of the pilot-plant, where each industrial hydrocyclone has one individual pressure vessel, sketched in figure F.7. Thus the industrial hydrocyclone liner is slid into the pressure vessel, which is pressurised by the inlet flow to the hydrocyclone.

All of the mentioned hydrocyclones can be run in parallel, in series or individually and the outlets of the hydrocyclones are directly fed to the buffer tank. The hydrocyclones with all the auxiliaries have been sketched in the P&ID diagram in figure F.2

5 Valves and Actuators

The valves used at the underflow and the overflow are globe valves which use a pneumatic actuator with internal positioning control. This type of valve was chosen due to the relatively high speed and accuracy. The internal controller has been tuned to increase the speed while reducing the overshoot, as the valve is preferred to be ideal, i.e. the input-output dynamics can be ne-

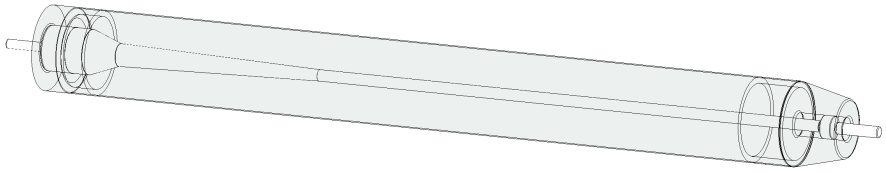

Fig. F.7: 3D sketch of the industrial hydrocyclone liner's casing, the liner is placed inside the casing. This figure is to scale.

glected. This is not fully achievable with any valve available as delay, actuating time and hysteresis induce different dynamics in the valve's input-output performance.

The gas phase valves are magnetically actuated needle type valves with internal volumetric flow rate controllers, which use hot wire anemometers as the feedback signal.

The valves have been sketched in the P&ID diagram in figure F.2

6 Instrumentation

6.1 Pressure Transmitters

The pressure transmitters used on the platform have a piezo-resistive measuring cell using a ceramic diaphragm with a measurement range of 0-16 bars, this range was chosen as the pumps operate at a maximum pressure of 12 bars.

6.2 Water, Oil and Gas-Flow Transmitters

The set-up uses two types of flow transmitter technologies. In the case of oil and water mixtures with 1% or more oil phase, which is the non-conductive fraction of the mixture, coriolis flow meters are used. When the mixture contains 1% or less oil phase, implying that the mixture mainly consists of water fraction which is conductive, electromagnetic flow transmitters are used for measurement. The reason for the distinction is that magnetic flow transmitters, although preferred for their lower price, have a decreased measurement precision with an increase in non-conductive phase, and are thus undesirable anywhere where the water fraction is lower than 99%. The gas phase was measured using hot wire anemometers, which are built into the air valve actuators.

6.3 Level Transmitters

Two types of level transmitters are used: 1) multi level guided radio wave level transmitter which can measure the oil and the interface level between the oil and the water, and 2) a delta pressure transmitter that measures the interface between the liquids. The delta pressure transmitter is the most common offshore method of measuring the level in the gravity separator and thus was chosen for the scaled pilot plant. The multi level transmitter was added as an evaluation and calibration tool for the delta pressure transmitter and in addition to provide precise information about the level of each of the phases.

6.4 OiW Transmitters

Several Oil in Water (OiW) measurement monitors were investigated to measure OiW concentration and oil droplet sizes. Initially, in order to provide an affordable instrument, an OiW monitor based on electric resistant tomography ERT was designed, built and tested, a sketch and a picture of the monitor is shown in figure F.8.

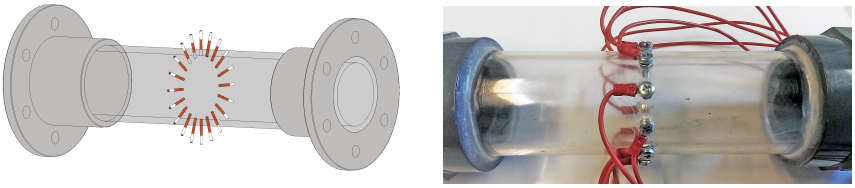

(a) Sketch of the ERT transmitter, the wires and electrical instrumentation is not illustrated. This figure is to scale.

(b) Photo of the ERT transmitter

Fig. F.8: Illustration of the ERT monitor.

The aim of this instrument was to enable fast online measurement of OiW concentrations, and to enable the use of in stream monitoring to reduce delay, for more information refer to paper C. Three commercially available monitors were investigated for the same purposes. For particle sizes a microscopy based monitor was used, the (Jorin, VIPA (VIPA)) which captures images at 30 FPS of the side-stream and analyses the droplet sizes and thus the concentrations of OiW, for reasons described in paper D. For OiW concentration two fluorescence based monitor were used: first the Advanced Sensors EX-1000 and second the (Turner Design, TD-4100XDC (TD-4100)), described in papers D and E. After extensive testing the EX-1000 proved to be less reliable than the TD-4100, which was used through the work for OiW measurements. For

more information about the oil used in the de-oiling experiments, refer to paper E.

The all instrumentation has been sketched in the P&ID diagram in figure F.2

7 Data Acquisition

The control terminal used for the pilot plant uses Simulink real time XPC target interface using National Instruments 6229 I/O cards as the interface between the equipment and the target PC. The data is received and transmitted using 4-20mA and HRAT signals, and all the analogue signals entering the I/O cards are filtered through 1st order 100Hz analogue low-pass filters.

The scaled pilot plant was built on campus at Aalborg University, Esbjerg, and has been used for multiple purposes through this work including process investigation, model development, model validation, controller development and controller performance evaluation.

ISSN (online): 2446-1636
ISBN (online): 978-87-7112-930-4

AALBORG UNIVERSITY PRESS